STUDIES ON *SPIRULINA SPECIES* NCIM 5143 FOR MICROBIAL FUEL CELL APPLICATIONS

A thesis

Submitted by

MOHD. GOLAM ABDUL QUADIR

For the award of the degree

of

Doctors of Philosophy

SCHOOL OF ENERGY SCIENCE AND ENGINEERING

INDIAN INSTITUTE OF TECHNOLOGY GUWAHATI

GUWAHATI-781039, ASSAM, INDIA

OCTOBER 2022

INDIAN INSTITUTE OF TECHNOLOGY GUWAHATI
School of Energy Science and Engineering
Guwahati – 781039

STATEMENT

I do hereby declare that the matter embodied in this thesis is the result of investigations carried out by me in the School of Energy Science and Engineering, Indian Institute of Technology Guwahati, Assam, India, under the guidance of Prof. Pranab Goswami.

In keeping with the general practice of reporting scientific observations, due acknowledgments have been made wherever the work described is based on the findings of other investigators.

October, 2022 Mohd. Golam Abdul Quadir

INDIAN INSTITUTE OF TECHNOLOGY GUWAHATI
Guwahati – 781039

Date: 28.10.2022

CERTIFICATE

It is certified that the work described in this thesis, entitled "Studies on *Spirulina species* NCIM 5143 for microbial fuel cell applications", was done by Mr. Mohd. Golam Abdul Quadir (Roll No. 146151010) for the award of the degree of Doctor of Philosophy is an authentic record of the results obtained from the research work carried out under my supervision in the School of Energy Science and Engineering, Indian Institute of Technology Guwahati, India. The results embodied in this thesis have not been submitted to any other University or Institute for the award of any degree.

October 2022

Professor Pranab Goswami
(Supervisor)
Department of Biosciences & Bioengineering

Professor A. S. Achalkumar
(Co-Supervisor)
Department of Chemistry

ACKNOWLEDGMENTS

I take this opportunity with much pleasure to express my sincere gratitude to all those who have supported me during the course of my Ph.D. I express my sincere gratitude to my supervisor Professor Pranab Goswami for being a considerate teacher and for supporting and encouraging me in my research endeavors during the course of my Ph.D. I thank my co-supervisor Professor A.S. Achalkumar and doctoral committee members Professor Kannan Pakshirajan, Professor Shankar Prasad Kanaujia, and Professor R Anandalakshmi for their valuable feedback and constructive criticism of my work. I especially thank my labmates, Nabajyoti, Khadeeja, Arup, Vinay, Rupam, and Mrinal who supported me by uplifting my morale and professionally during my PhD at various stages. I thank my other lab juniors and seniors Santhosh bhaiya, Reddy bhaiya, Seraj, Naveen, Babina, Priyamvada, Ankana, Phurpa, Kangkana, Malaya, Aparupa, Caroline, Pooja, Priyanki and Smita for their encouraging presence. I thank my friends Krishan, Adnan, Sandeep, Alam, Rajneesh, Rupinder from other labs who made difficult times easy. I thank my parents and sister for being a constant moral support during thisjourney. I thank all the office staff in my department and CIF facility who helped me and have known me during the course of PhD.

M.G Abdul Quadir

October 2022

ABSTRACT

This study utilizes *Spirulina* species NCIM 5143 procured from the National Collection of Industrial Microorganisms, Pune, India. The phylogenetic analysis from 16S rRNA revealed its identity closer to *Spirulina sub salsa* BGLR6. The species wascultured in an inorganic Zarrouk medium supplemented with trace elements in the white light of 2500 lux at a temperature of 32°Cat 180 revolutions per minute. The specific growth rate and doubling time were found to be 0.0771 day^{-1} and 8.98 days respectively. The species was found to be a helical filament in structure with a diameter of 3 µm and a pitch length of 1 µm. It exhibited gliding motility and moved towards light exhibiting the phenomenon of positive phototaxis. This property influences the pattern of biofilm formation by the cyanobacteria and the configuration of filamentous cells within it, depending on the direction of illumination. The static culture always formed a network of filaments on walls that developed into biofilms over time and stuck to the walls. This natural biofilm formation capacity was utilized and the wet weight was inoculated into an H- type biofuel cell setup, leading to the formation of a biofilm over the electrodes. Interestingly, a subpopulation of bacteria was detected in the vicinity of the *Spirulina* filaments, and a few cells were directly attached to the filament structures. This close physical association indicates that crucial metabolite and nutrient exchange might occurbetween the host and bacterial cells. Four distinct heterotrophic colonies were isolated and identified through 16S rRNA sequencing. The strains were *Halomonas saliphila, Halomonas campaniensis, Alcanivorax pacificus,* and *Pelagibacterium lentulum.* We inferred that these pure culture strains were the dominant members of the *Spirulina*-associated bacterial community as theycould form colonies on the Zarrouk medium plate devoid of any organic carbon source, thriving on residual extracellular organic carbon and metabolites exuded by the phototrophic host (*Spirulina*). These associations indicate a copiotrophic habitat typical of a phytoplankton bloom or matured phototrophic biofilm. We believe that this combination of predominant bacterial species isolated by us might be involved in efficient carbon and nitrogen cycling assisting the sustained growth ofthe host cyanobacterium (*Spirulina sub salsa*). A microbial fuel cell with Spirulina species as the anodic catalyst had an oscillating open circuit potential that synchronized with the 12-hour light-dark circadian pattern. However, unlike most of the previous reports, a steep rise in voltage response with the onset of each 12-hour dark phase was observed. Upon checking the contribution of individual anodes and cathodes, it was confirmed that these diurnal variations entrain to the illumination regime and were due to anodic contribution to the total electromotive force. The cathode potential was stable at 270 mV throughout the operation. This observation indicates that more electrons were accumulated over the anode during the dark phase. Next, we focused on elucidating the mechanism behind this phenomenon following the *in-situ* voltammetry in MFC setups. We screened different materials and finally selected graphite plate as the anode considering its conducive nature for forming biofilm and suitable electrochemical behaviors. The voltammetry of biofilms formed over glassy carbon electrodes showed a consistent reversible peak with a formal potential of 0.260 V versus Ag/AgCl and an irreversible oxidative peak with an onset of around 0.6 V versus Ag/AgCl. The photosynthetic production of oxygen was also identified at - 0.25 V versus Ag/AgCl in the voltammogram (oxygen reduction). The redox entity corresponding to the peak at 0.260 V versus Ag/AgCl was present only with the biofilm and absent in the culture supernatant indicating its physical presence in the spaces closely associated with the cell wall. These voltammetry patterns were reproduced over graphite electrodes during in situ electrochemical investigations. From the guiding literature, we presumed that the redox species belong to putative

quinones, flavonoids or temperature-sensitive redox peptides. The magnitude of the irreversible oxidation peak current at ~0.6 V versus Ag/AgCl obtained from the cell-free supernatant increased with the culture age, from 2 µA on day 4 to 42 µA on day 26. This potential was biotic in nature and distinct from the oxidative water splitting reaction identified at ~ 1.15V versus Ag/AgCl as revealed from an extensive electrochemical investigation. The increase in peak current at 0.6V versus Ag/AgCl coincided withthe upsurge of total organic carbon content including proteins, carbohydrates, and phenolic compounds in the supernatant. Based on our results from macromolecular estimation, biofilm microscopy, and electrochemistry we propose a hypothetical model. Firstly, any electron flux emanating out of cells (both cyanobacteria and symbionts) because of the primary metabolic activity like photosynthesis, respiration, or fermentation will first end up with the supramolecular assembly of biofilm matrix containing redox moieties and metabolites interspersed in it. These redox moieties may be diverse and dynamic as these are formed because of microbial metabolic activities, macromolecular degradation, cell lysate recycling, and assimilation and are akin to autochthonous humic and fulvic-like substances in the composition. Further, many unknown exoproteome may also be present in this extracellular compartment with putative redox activity. While these diverse molecules may act as redox buffers storing electrical charges, their interactions with oxygen under oxic conditions may lead to partial electron quenching leading to peculiar voltage modulation patterns observed in our experiment. Further, the voltage output may also be influenced by the presence of artificially introduced redox mediator molecules and their chemical and physical interaction with the biofilm matrix components. The collective electrochemical output of these numerous possible redox reactions within the extracellular matrix and their interaction with oxygen may be responsible for the peculiar increase of anode potential (more negative value) during the dark period observed in our experiment. Secondly, alternate metabolic modes of *Spirulina* and associated symbionts in direct contact with the electrode surface may be directly interacting with the electrodes through an exoelectrogenic process. This study also aimed to investigate the effect of ferricyanide cross-over across the Nafion membrane on the performance of cyanobacterial anodic biocatalysts during the long-time operation of the MFC. These experiments were performed in a specially designed MFC in OCP modes and identified the crossover of ferricyanide from the cathode to the anode chamber. We confirmed that ferricyanide quenches cellular electrons at the biofilm-electrode interface, reducing the anodic redox potential. These conclusions were made on the basis of differences in anodic OCP variations between setups and enhanced magnitude of reductive currents in the Tafel plots. At its high concentration level, the potentiometric response was though enhanced, simultaneously, a toxic effect of this redox mediator on the cells was also confirmed. Thus, the selection of an optimum concentration of the mediator is critical to realize the desired potential benefit in MFC. Moreover, direct contact of cells with the electrode is essential for generating the OCP oscillation between diel cycles and the interaction of ferricyanide with the biofilm matrix induces secretion of an oxidizable entity into the matrix. The results of our study demonstrate the role and associated pros and cons of biofilm extracellular matrix on the electrochemical performance of cyanobacterial biofilm based biophotovoltaic devices. Firstly, the extracellular matrix provides nourishment to cyanobacteria for surviving prolonged dark conditions and harbors symbionts that make the biotic component of BPV resilient and durable for real-time application. Secondly, it provides safety to the cells within it from stressful high mediator concentrations and toxic substances. Thirdly,it may act as a reservoir of endogenously produced or artificially introduced redox molecules enhancing electrochemical performance. On the other side, it is difficult to achieve uniform mediator concentration and predictable control over reaction dynamics within the biofilm matrix

causing unpredictable variations that influence the viability and performance of the BPV system. Moreover, the reaction dynamics within the matrix and metabolic conditions persist within a biofilm also changes with time.

CONTENTS

List of Abbreviations

µA	Microampere
µM	Micromole
µmole	Micromole
µW	MicroWatt
A	Ampere
ARTO	Alternate respiratory terminal oxidase
bEOM	Bound extracellular organic matter
BPV	Biophotovoltaics
CM	Cytoplasmic membrane
COX	cytochrome c oxidase
CV	Cyclic Voltammetry
Cyd	cytochrome bd quinol oxidase
DCMU	((3-(3,4-dichlorophenyl)-1,1-dimethylurea)
dEOM	Dissolved extracellular organic matter
DNA	Deoxyribonucleic acid
EDTA	Ethylenediaminetetraacetic acid
EIS	Electrochemical Impedance Spectroscopy
EMF	Electromotive force
EPS	Extracellular polysachharide
FE-SEM	Field emission scanning emission microscopy
GCE	Glassy Carbon Electrode
ITO-PET	Indium Tin Oxide - Polyethylene terephthalate
LSV	Linear Sweep Voltammetry
MEC	Microbial Electrolytic cell
MFC	Microbial Fuel Cell
MTT	(3-(4,5-Dimethylthiazol-2-yl)-2,5-Diphenyltetrazolium Bromide)
MV	Methyl Viologen
mV	Millivolt
NADH	nicotinamide adenine dinucleotide (NAD) + hydrogen (H)
NADPH	nicotinamide adenine dinucleotide phosphate (NADP) + hydrogen (H)
NDH-1	NADH: plastoquinone oxidoreductase
NDH-2	NADPH:plastoquinone oxidoreductase

NDIR	Nondispersive infrared
OCP	Open circuit potential
OEC	Oxygen Evolving Complex
OM	Outer membrane
OTU	Operational taxonomical unit
PMT	Photomultiplier tube
PS I	Photosystem 1
PS II	Photosystem 2
QIIME	Quantitative Insights into Microbial Ecology
SDH	Succinate: plastoquinone oxidoredutase
SHE	Standard Hydrogen Electrode
TAPS	([tris(hydroxymethyl)methylamino]propanesulfonic acid)
TGP-H-60	Toray Carbon Paper
TM	Thylakoid membrane
V	Volt

R_p	Polarization resistance
A	Ampere
$C_{analyte}$	Concentration of analyte
C_{dl}	Double layer capacitance
D	Diffusion coefficient
E1	Potential at time point 1
E2	Potential at time point 2
E_{anode}	Anodic potential of the anode
$E_{cathode}$	Cathodic potential of the cathode
E_{corr}	Corrosion current at the electrode interface
E_{emf}	Electromotive force of microbial fuel cell
E_p^{ox}	Peak oxidative potential
E_p^{red}	Peak reductive potential
F	Faradays constant
I_{corr}	Corrosion current at the electrode interface
I_1	Current before a potential pulse is applied
I_2	Current before potential pulse goes back to baseline
I_p^{ox}	Peak oxidative current
I_p^{red}	Peak reductive current
mV	MilliVolt
n	number of electrons
R	Universal gas constant
R_{ct}	Charge transfer resistance
R_{el}	Electrolytic resistance
R_{pol}	Polarization resistance
$ß_a$	Anodic slope
$ß_c$	Cathodic slope
T	Temperature

t	Time
v	Scan rate
ΔE	Difference in peak potential
ΔI_{pulse}	Differential current

List of Figures

List of Tables

INTRODUCTION

The quest for sustainable clean energy sources has caused the scientific community to come up with novel, innovative concepts with ambitious objectives. One such line of thought is to view microbial entities as functional materials (Chu et al. 2016). In the year 2015, a new concept was proposed which is envisaged to be a biological counterpart of photovoltaics in near future (McCormick et al. 2015). This concept was called "Biophotovoltaics (BPV)". It is a technology that aims to siphon off electron flux generated by the photolysis of water at photosynthetic reaction centers of phototrophic organisms and utilize it for power generation or chemical synthesis in an electrochemical format (Bombelli et al. 2022; Saper et al. 2018; McCormick et al. 2013). This technology is envisaged to be a substitute for semiconductor-based photovoltaic systems that are costly to synthesize and not environment-friendly. To this end, both subcellular fractions and whole cells have been demonstrated to act as biocatalysts (Quadir et al. 2020). At present, the magnitude of power generation by such devices is not suitable for practical application. Despite this, the prospect of tapping clean energy from self-sustaining biocatalysts and its subsequent development into cheap, standalone power-generating systems in the future has motivated researchers to exert sustained scientific efforts. The prime focus of research has been to (i) enhance biocatalyst-electrode communication (Wenzel et al. 2018a) and (ii) gain better mechanistic insights into the mode of electron transfer across cell walls (Sekar et al. 2018). The methods employed to study cyanobacterial electrochemical behavior in different studies differ on multiple aspects like species, time scale, illumination span, electrodes, reactors, presence or absence of redox mediators, modes of biomass propagation in reactors like (i) planktonic cultures in suspension (Bradley et al. 2013) (ii) naturally formed biofilms on electrodes (Pisciotta et al. 2010) (iii) manually applied biomass on electrodes (Cereda et al. 2014). Because of this, the pattern and magnitude of current generated from different experiments vary between groups, but the phenomenon of light-dependent modulations has been consistently reproduced. The approach of using a specific quantity of inoculum, determined through the estimation of chlorophyll or biomass, does help in correlating the current generated to the number of cells through normalization (Zhang et al. 2018). However, the period of illumination and total span of study in such reports only ranges from a few minutes to hours, not enough for the cells to multiply and form mature biofilms. Zhang and coworkers reported a change in the amperogram pattern due to the extracellular matrix over 5 days. In another study, McCormick and coworkers reported the current profile of *Synechococcus* biofilm in a microbial fuel cell (MFC) for 30 days (McCormick et al. 2011). The current increased until day 19 and declined thereafter. Any realistic application of BPV systems would require standalone operation under static conditions for several months. Under such a condition, the cyanobacteria in direct contact with the electrode surface would gradually form mat like

structure by secreting complex extracellular polysaccharides (EPS) leading to the formation of a thick biofilm matrix containing diverse metabolites, proteins, and complex carbohydrates (Rossi and De Philippis 2015). The thick matured biofilm gradually affects the cell electrode interaction, redox mediator infusibility into the matrix, and light penetration. Mature biofilms also have a steep gradient of parameters like pH, oxygen, ion concentration, light intensity, etc. (David et al 2021). Under such conditions, cells within the biofilm will adopt different metabolic modes like photosynthesis, respiration, and fermentation (Ananyev et al 2012). Examining the electrochemical behavior of cyanobacteria in the context of these metabolicconditions is still a lacuna in BPV research. Next, the current flow needs to pass through a thick insulated cell wall and self-produced biofilm matrix before reaching the electrode. A recent study showed the influence of the peptidoglycan layer on the amperogram of cyanobacteria film formed on the electrodes (Wey et al. 2021). Further, the biofilm matrix of cyanobacteria is known to contain a diverse and dynamic set of proteome and metabolome that is secreted in response to various environmental stimuli and may be involved in metal uptake, remediation, etc (Giner-Lamia et al. 2016; Christie-Oleza et al. 2015). Many of these processes are yet unidentified and may have an influence on the electron mediation process over the long term as indicated in previous studies (Zhang et al. 2018). Moreover, the biofilm formed by a phototroph is a rich source of self-produced complex polysachharides. This reservoir of polysaccharide is under a constant process of synthesis and degradation by the producers themselves and other heterotrophs that form complex relationships during long-term air operation as evident from recent studies (Stuartet al. 2016; P. Bombelli et al. 2022). These factors make BPV systems different from semiconductor photocatalyst that generates exciton upon illumination and can readily transfer electrons or hole to a polarized electrode. The current profiles of any phototrophic biofilm must be interpreted in the context of all aforementioned factors. Thorough time-dependent voltammetry investigations have been reported on many strong and weak electrogens, such that improvement in electrochemical performance correlates with redox metabolite accumulation and growth phase (Modestra and Mohan 2014;Marsili, Baron, et al. 2008;Marsili, Rollefson, et al. 2008). Contrary to this, voltammetry investigations are either absent in earliest studies of BPV or not consistent enough between various reports making it difficult to ascertain the true nature of redox reactions (Gacitua et al. 2020; McCormick et al. 2011; Pisciotta, Zou, and Baskakov 2010).

In this study, we chose a strain of *Spirulina* species (NCIM 5143). This motile strain has a tendency for quick biofilm formation over solid surfaces in a static condition that we exploit by placing a horizontal graphite electrode at the bottom of the MFC setup. We have performed voltammetry and impedance investigation in a time-dependent manner during biofilm maturation, prolonged dark conditions, and resumed illumination. Complementary microscopy, biochemical investigations, metabolomics, and online monitoring of pH, and dissolved oxygen are also performed to validate the inferences made from

electrochemical studies. Our results indicate the formation of a cyanobacterium-dominated biofilm, matured over time adds-on to the complexity of redox processes in the whole-cell biophotoelectrode, resulting in instantaneous electrochemical signals that are net result of all the individual factors at every instant.

OBJECTIVE OF THE STUDY

In the view of above challenges and gaps identified through the literature survey (described in chapter 1) this study aims to delineate the complexity of redox processes occurring at the cyanobacterial biofilm–electrode interface during the process of biofilm formation. To fulfill this aim, the MFC is taken as a device to study the electrochemical behavior of gradually matured biofilms over electrodes. In addition, voltammetry and impedance investigations were carried out in a temporal fashion. Complimentary biochemical assays, microscopy, fluorometry, metagenomics, pH, and dissolved oxygen measurements as described in the following points were carried out to rationalize the inferences of the electrochemical study.

1. Microbiological and Electrochemical characterization of the photosynthetic biocatalyst.
2. Choosing appropriate electrodes and MFC reactors for long-term monitoring and electrochemical investigations.
3. Characterization of biofilms in response to diurnal illumination patterns, prolonged dark periods, and subsequent photosynthetic recovery in a sequence
4. MFC operation in presence of *Spirulina* biofilms following a standardized illumination regime.
5. Time-dependent electrochemical investigations of the MFCs to rationalize the MFC performance.
6. Performance of MFCs under closed circuit operations under versatile metabolic states.

SIGNIFICANCE OF WORK

Biophotovoltaics can be seen both as field fundamental research and as technology. To gain mechanistic insights into the phenomenon of light-dependent current production, many investigations have been reported and are underway that use mutant strains (Sekar et al. 2018; Wey et al. 2021; Kusama et al. 2021a). Such studies interface the cells with electrodes directly and seek to accelerate the electron conduction across the cell-electrode interface (Zhang et al. 2018; Wenzel et al. 2018a; Chen et al. 2022). On the other hand, attempts to introduce cyanobacteria as an electrochemical photocatalyst demonstrating successful real-world application confront us with a real-world scenario where thick organic matter-rich biofilms are formed (Bombelli et al. 2022; Zhu et al. 2019). These biofilms undergo maturation and recruit bacterial communities in the process that undergoes ecological succession with time enhancing the overall

performance and robustness of the system. The study embodied in this thesis work aims to stitch together these two approaches where thorough electrochemical investigations are carried out on a cyanobacteria driven complex multispecies biofilm to gain mechanistic insights and an understanding of possible redox processes at the biofilm electrode interface.

The study embodied in this thesis is categorized into the following chapters.

Chapter 1: **Literature review**

This chapter aims to inform the readers regarding the theoretical basis of the concept of microorganisms as electrochemical biocatalysts. Further, it briefly describes the theory of the electrochemical techniques used to analyze the microorganisms and their biofilms. At last, this chapter contextualizes the concept of electrochemical biocatalyst with respect to the metabolic capacity of cyanobacteria and describes the state-of-the-art development in this field in a concise manner.

Chapter 2: **Materials and Methods**

This chapter lays down the methods optimized and the experimental plans devised to fulfill our objectives in chronological order.

Chapter 3: **Results and Discussions**

This chapter reports the results obtained by the execution of experimental plans. The results are discussed thoroughly and correlated with available literature to the best of our knowledge.

Chapter 4: **Conclusions and Future prospects**

This chapter lays down the key takeaway points that are distilled out of our experiments. It emphasizes the importance of these results for further development of this field and briefly mentions the future prospective research directions to be pursued for the development of Biophotovoltaics.

CHAPTER 1

Literature review

1.1 Microbial cells as electrochemical biocatalysts

Microbial cells have been demonstrated to function as whole-cell biocatalysts driving economically important biotransformation processes and synthesis of value-added fine chemicals in bulk quantities (Ladkau et al. 2014; Wohlgemuth 2010; Beygmoradi and Homaei 2017). A microbial cell harbors a repertoire of enzymes carrying out cascaded metabolic reactions bypassing the problem of poor *ex-vivo* enzyme stability. Integrating this concept with an electrochemical/electrolytic system gives us electrically driven biological technologies that can be used for the biotransformation of cheap products to electrical output or can be used for the synthesis of value-added chemicals through electrical input. The existing terms for these concepts in literature are MFC and microbial electrolytic cells (MEC), respectively (Schröder et al. 2015).

To fulfill the criteria of an ideal electrochemical biocatalyst, the microbial cell must have an intrinsic capacity of electrically communicating with solid electrodes. This intrinsic capacity is bestowed on them by their cellular physiology. Such microbes have been categorized as strong electrogens (Lucinda et al. 2015). Two prime examples are the genera *Geobacter* and *Shewanella* (Marsili et al. 2010; Marsili et al. 2008). These bacteria can be tricked into donating electrons two an electrochemically polarized electrode due to their physiological need of respiring over minerals. On the other hand, these bacteria show a preference for simple carbon sources like acetate and lactate. It would be desirable to explore and include novel bacterial species capable of degrading diverse and complex organic matter with the capacity of turning it into electricity in inventory. Several such investigations have been carried out yielding a vast scientific literature reporting many species from diverse genera capable of producing electricity (Koch and Harnisch 2016). On the other side of the spectrum are weakly electrogenic microbes (Lucinda et al. 2018). These bacteria have been reported to be current producers albeit at a very less magnitude. Nevertheless, studying such microbes may have promising applications in medical, environmental, and other biotechnological applications (Aiyer and Doyle 2022). While strong electrogens have physiological structures involved in electron conduction and secretion of endogenously produced redox molecules, weak electrogens often have to be assisted in their electrical performance by the addition of artificial redox mediators. McCormick and coworkers categorized the method adopted by the pure culture to shuttle electrons to electrodes into four categories: (i) Indirect extracellular electron transfer without recycling. (ii)

Indirect extracellular electron transfer with recycling. (iii) Direct extracellular electron transfer via cell surface entity. (iv) Extracellular electron transfer via nanowire networks (**Figure 1.1**).

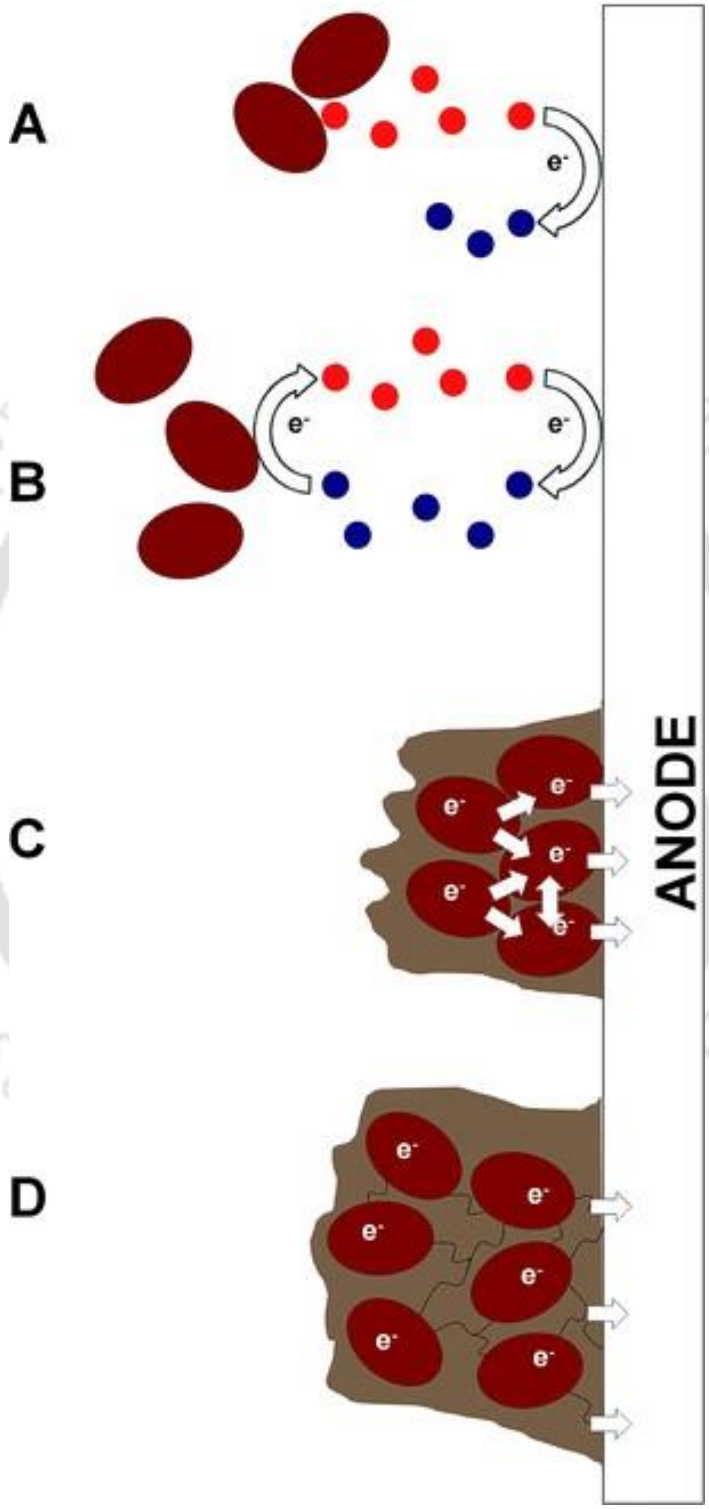

Figure 1. 1. (A) Indirect extracellular electron transfer without recycling. (B) Indirect extracellular electron transfer with redox cycling. (C) Direct extracellular electron transfer. (D) Direct contact by nanowire appendages. (**McCormick et al. 2015**)

1.2 Approaches for mechanistic investigation of microbial electrochemical activity

Electrochemical investigation of any microorganism is reported by using one of the two approaches. (i) A three-electrode system involving a working electrode, reference electrode, and counter electrode (Elgrishi et al. 2018). (ii) A conventional H-type MFC having an anode, cathode operated with or without a fixed resistor (Babauta et al. 2012). (**Figure 1.2**)

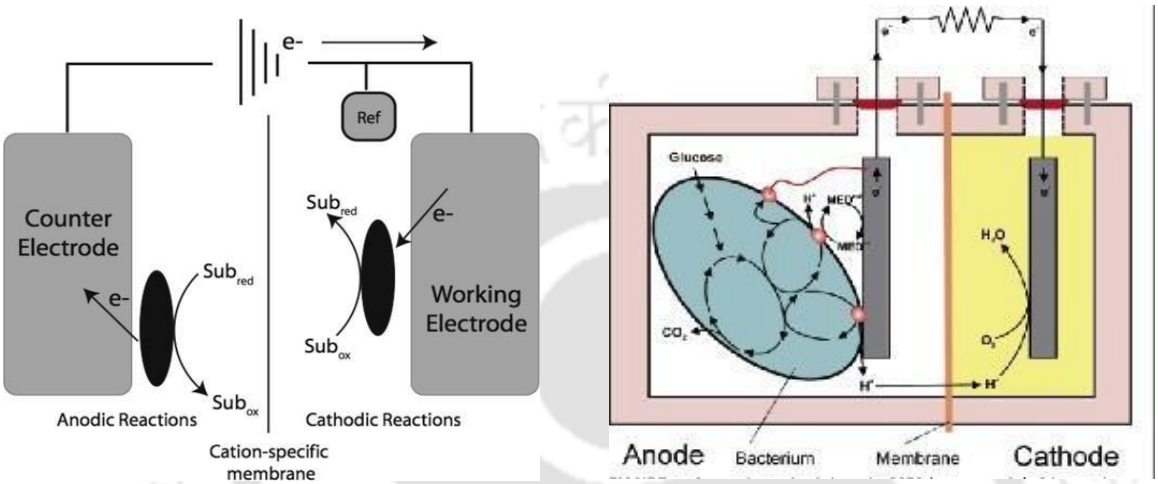

Figure 1. 2. (Left) A three-electrode setup with counter and reference electrodes separated by cation exchange membrane. (Right)A representation of MFC setup with biocatalyst attached to the electrode (**Rabaey and Verstraete 2005**)

Three-electrode setup

In a three-electrode system, the working electrode is polarized at a specific potential with respect to a reference electrode. Usually, the potential magnitude is close to or higher than the redox potential of the molecular entity involved in electron shuttling between microbes and electrodes. Such an approach is very useful when characterizing a strong electrogen whose standard redox potential is well characterized and reported in the literature (Bond and Lovley 2003; Clifford et al. 2021). Many studies have also shown thatbiasing the electrode at a specific potential selects for a specific bacterial population in the vicinity of the electrode (Finkelstein et al. 2006). Studies with pure cultures of strong electrogens have shown that physiological adaptations occur in the cells in response to polarized electrode potentials (Howley et al. 2022). The advantage of a three-electrode system is that we can identify the specific electrochemical potentials of the redox entities involved in electron conduction. The downside of this approach is that the current readings are not reproducible in a fuel cell setup unless the anode is complemented with a high redox potential cathode which is stable with time. For a microbial cell for which the specific redox potential at which the current generation process is not known, researchers investigate the performance by varying the potentials at different magnitudes (Zhang et al. 2018; Saper et al. 2018).

MFC setup

In the H- type MFC setup, the anode, and cathode are complemented across an ion exchange membrane to maintain electrolytic continuity. The anode and cathode can be operated in an open circuit mode or in a closed circuit across a fixed resistor. The anode potential decreases due to electron accumulation when no load (fixed resistor) is connecting the two electrode terminals. When the electrodes are connected through a load, the anode potential becomes less negative and equilibrates with respect to the resistor. The approach of varying fixed resistance magnitude and measuring the corresponding voltage and current of the MFC simultaneously to calculate the corresponding power is used for evaluating the MFC performance (Logan et al. 2006). Such an approach, however, often suffers from operator bias and MFCs have to be operated at a resistor magnitude higher than estimated for sustainable power generation. Watson and coworkers suggested operating an MFC at a fixed resistor for a complete batch cycle thrice before changing the resistor to a lower magnitude (Watson and Logan 2011). This approach of using fixed resistors allowed mixed-species biofilms to adapt and improve their performance. A microbial culture capable of producing current at a high rate will deliver high power density at lower resistance whereas a microbial culture that produces current at a low magnitude will deliver high power density at a resistor of higher magnitude (Menicucci et al. 2006).

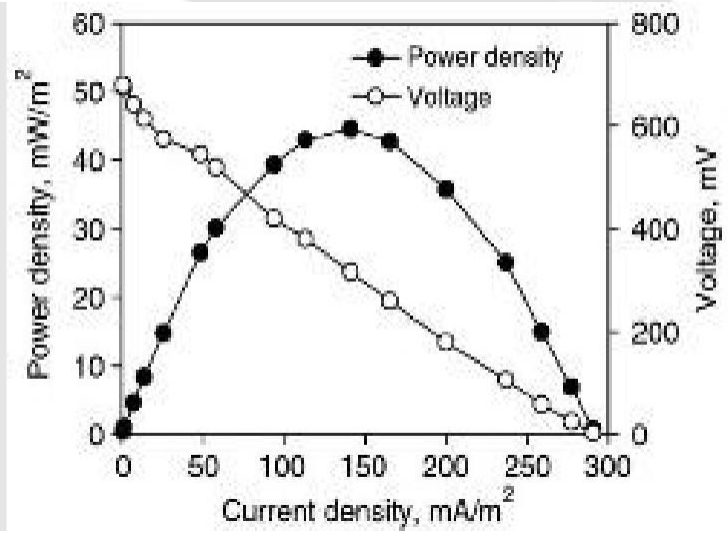

Figure 1. 3. Polarization and Power density curve of a MFC obtained by varying resistance connecting anode and cathode. Corresponding voltage and current are simultaneously measured. Power = Voltage X Current. (**Ichihashi et al. 2011**)

Further, a couple of voltammetric techniques are often used for the analysis of redox reactions occurring at the electrode interface. These techniques include (i) CV and linear sweep voltammetry, (ii) DPV, (iii) Impedance spectroscopy, and (iv) Tafel analysis.

Cyclic Voltammetry

In CV, potential is applied at the working electrode with the help of a potentiostat. The potential is swept linearly from E_1 to E_2 and then returned back from E_2 to E_1. The range of this potential is specified by the operator. However, in the case of linear sweep voltammetry (LSV), the potential is ramped in one direction only, which means either from E_1 to E_2 or from E_2 to E_1. LSV results only in either oxidation or reduction of the analyte depending upon the direction of the potential ramp or sweep. The resulting plot of applied potential vs resulting current is called linear sweep voltommogram (in case of LSV) or cyclic voltammogram (in case of CV). The shape of the CV depends on the nature of electron transfer to the working electrode. If the electron transfer rate is faster than the mass transport rate of the analyte, then the process is termed reversible electron transfer. When both the rates become comparable then it is called quasi reversible electrotransfer process. Again, when mass transport rate of the analyte exceeds the rate of electron transfer rate to the electrode, the process is termed an irreversible electron transfer process. In **Figure 1.4**, potential waveform of CV and the voltammogram of different electron transfer process is shown. The representations E_p^{ox}, I_p^{ox}, E_p^{red}, $_pI^{red}$ are anodic peak potential and anodic current and cathodic peak potential and cathodic current, respectively.

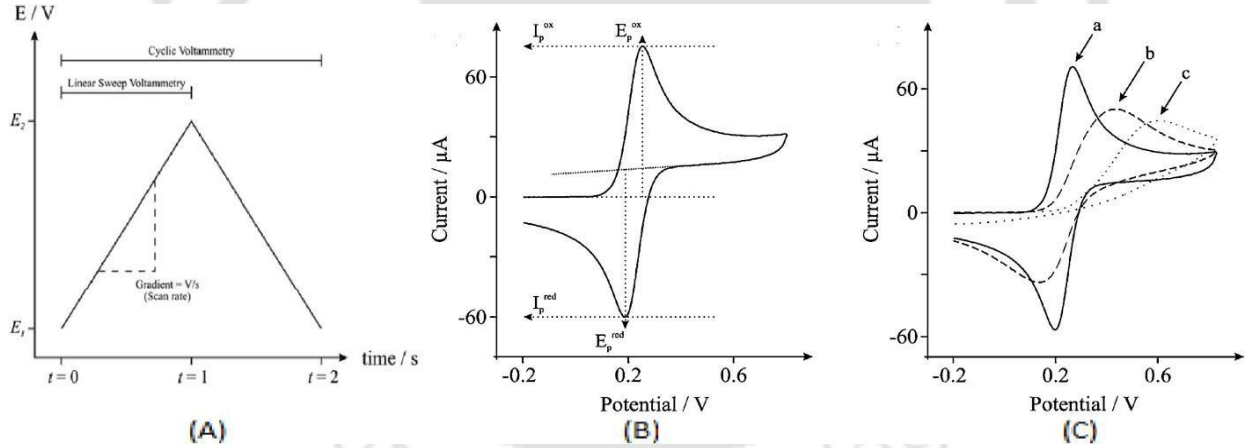

Figure 1. 4. (A) Potential-time profile of CV, (B) peak current and peak potential depiction, (C) typical CV of reversible electron transfer (a), quasi reversible electron transfer,(b) and irreversible electron transfer (c).(**Monk 2001**)

When the peak-to-peak separation ΔE, ($\Delta E = E_p^{ox} - E_p^{red}$) is in the limit of (2.218RT/nF) (where n corresponds to the number of electrons involved in oxidation/reduction), the corresponding process is electrochemically reversible in nature. The ratio of both the peak currents, I_p^{ox}/ I_p^{red} is equal to 1 in such

cases. The peak current increases with increasing the scan rate. The dependence of peak current on scan rate is given by the Randles-Sevcik equation:

$$I_p = 0.4463nFA(nF/RT)^{1/2} D^{1/2}v^{½}C_{analyte}$$

Here, peak current, I_p in a cyclic voltammogram is a function of the temperature T, bulk concentration $C_{analyte,}$ electrode area A, the number of electrons transferred n, the diffusion coefficient D, and the speed at which the potential is scanned v. If the species is freely diffusing, then the above equation shows that for an electrochemically reversible process, a plot of peak current vs. root of scan rate is linear. Deviation from this linearity indicates either a quasi-reversible process or the involvement of surface-adsorbed species. When adsorbed species are involved, the plot of peak current vs. scan rate is linear.

For an electrochemically irreversible process, ΔE is larger than reversible or quasi-reversible reaction couple. The peak position for both the anodic and cathodic peaks, shift with the scan rate. Typical reversible and quasi-reversible voltammograms are shown in figure 1.5.

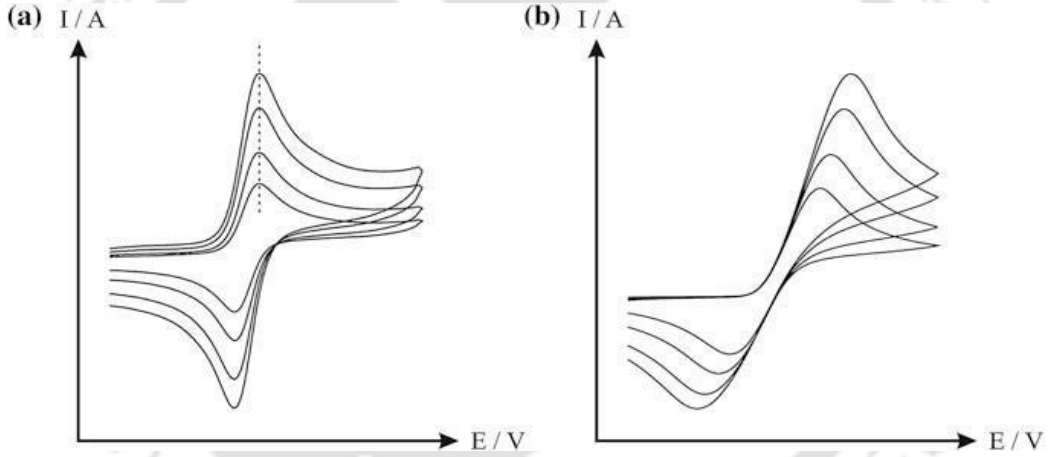

Figure 1. 5. Cyclic voltammogram for reversible (a) and quasi-reversible(b) electron transfer process (**Monk 2001**)

Differential Pulse Voltammetry

When the analyte concentration is very less, it is difficult to detect through a classical CV. The current arising from non-faradaic processes causes such difficulty. This reduces the limit of detection. Limit of detection can be increased by using the pulse method. When a pulse is applied to the working electrode, faradaic current due to the analyte decreases as a function of $t^{-1/2}$. While the non-faradaic current decreases exponentially. Thus, at the latter pulse life, the amount of non-faradaic current decreases significantly more than that of the faradaic current. This is shown in **Figure 1.6**. Thus, by using the pulse method sensitivity can be improved significantly. Differential Pulse Voltammetry (DPV) is a commonly used pulse voltammetric technique.

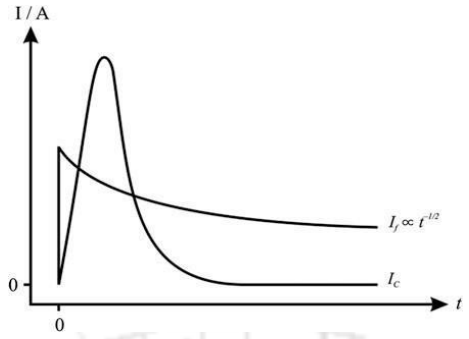

Figure 1. 6. Effect of non-faradaic and faradaic current following the application of a potential step (**Monk 2001**)

In DPV, a linear potential ramp of dE/dt with succession of fixed magnitude of pulses is applied at the working electrode. The value of current is measured twice: a. just before the potential rise when a pulse is applied (I_1) and b. just before the potential decreases back to baseline (I_2). The difference between the two currents, $\Delta I_{pulse}= I_2 - I_1$(differential of current) is plotted against applied potential. This typical plot is called a differential pulse voltammogram. In **Figure 1.7,** the DPV waveform along with ΔI vs. potential plot is shown.

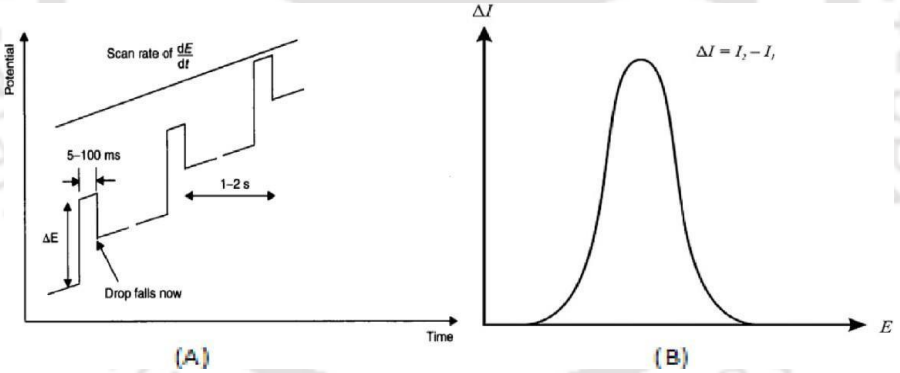

Figure 1. 7. (A) The potential waveform of DPV (B) a typical DPV plot (**Monk 2001**)

Electrochemical Impedance spectroscopy

In impedance spectra, the voltage across a working electrode is varied in a sinusoidal waveform from higher frequency to lower frequency. The amplitude for biofilm systems is ±10 mV. The corresponding current response also emerges in a sinusoidal waveform. Due to the impedance, there is a phase difference between the voltage stimulus and the current response. Upon representing the sinusoidal data, as a complex number, real and imaginary components are resolved. Plotting these components in the x-y axis yields a Nyquist plot as shown in (**Figure. 1.8a**). The real component that is represented on the x-axis is the resistance.

and the imaginary component represented on the y-axis is capacitance. In the context of biofilm electrodes, R_{el} represents electrolytic resistance, R_{pol} represents the polarization resistance of the electrode. Deduction of R_{el} from R_{pol} gives us the charge transfer resistance (R_{ct}) of the redox species present at the electrode interface. C_{dl} represents the electrical double layer of the biofilm-electrode interface. The data are alwaysfitted to validate equivalent circuits and figures are reported. Another way of representing these data is the Bodes plot (**Figure. 1.8 b**). In this representation, change in total impedance and phase angle with frequency is plotted. Due to the complexity and heterogeneity of the biofilm systems, accurate equivalent circuits that resolve all the impedance factors have been validated only for *Geobacter* species (Babauta and Beyenal 2014; Kretzschmar and Harnisch 2021). For our investigative purpose, we estimate the R_{ct} for ferricyanide species present at the electrode interface.

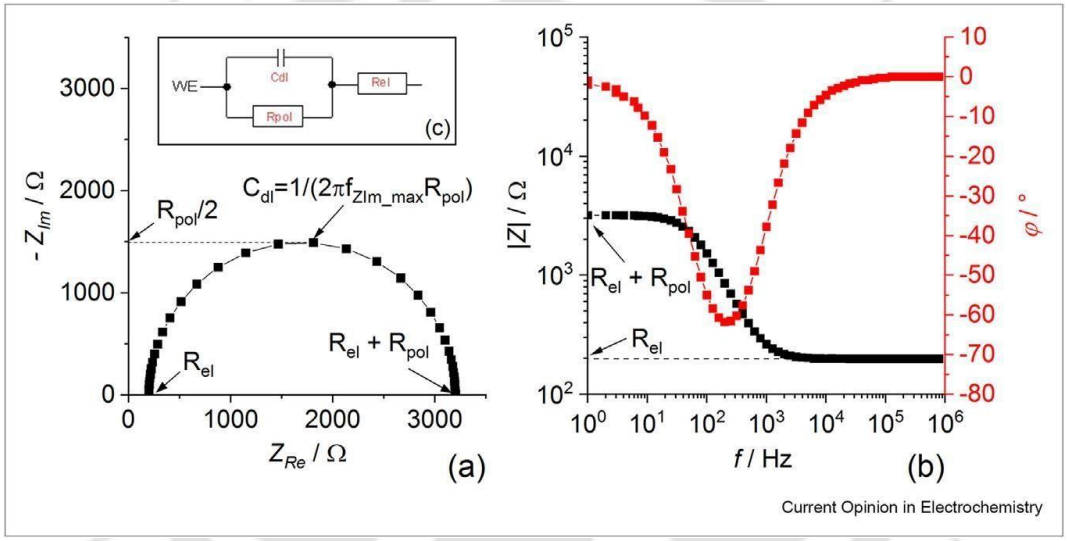

Figure 1. 8. Representational styles of impedance spectroscopy. (a) Nyquist plot. (b) Bodes plot. (c) Equivalent circuit. (**Kretzschmar and Harnisch 2021**)

Tafel analysis

Briefly, representing an LSV graph which is represented as potential vs current, in the format of Log (I) vs E, gives us a Tafel representation of the LSV data. A researcher can analyze the data visually by observing the point of steady state potential and current i.e. E_{corr} and I_{corr}. Further, fitting the slopes within ±120 mV with any vendor-specific software yields values like (anodic slope) $ß_a$, (cathodic slope) $ß_c$, (Polarization resistance) R_p, (Corrosion potential) E_{corr}, (Corrosion current) I_{corr}. These values allow us to estimate the electrochemical conditions prevalent at the electrode interface during steady-state conditions.

1.3 Cyanobacteria as electrochemical biocatalyst

The organisms in phylum cyanobacteria are highly preferred in biophotovoltaic research. The prokaryotic structure of these organisms simplify the pathway of electron transfer across the cell wall. It has been suggested that these organisms were responsible for great oxidation event on earth that paved way for evolution of multicellular life forms. These organisms form a major part of marine phytoplankton across the globe and contribute to net global oxygen production. They play role of primary producers in microbial ecology and act as hosts of self-sustaining microbial communities. Their enzyme repertoire includes photosystem enzyme complexes (PS II and PS I). These enzymes are present in the thylakoid membrane of the cyanobacteria and collaborate in a Z scheme to transfer electrons generated from water splitting at the oxygen-evolving complex (OEC) of PS II to redox cofactor NADPH passing through a series of membrane-bound protein complexes present in the thylakoid membrane (TM) (Fig. 1.9). Further, it is also a fact that in cyanobacteria, plastoquinone pool is shared by both respiratory and photosynthetic pathway. The respiratory pathway proteins like NADH: plastoquinone oxidoreductase (NDH-1), NADPH: plastoquinone oxidoreductase, (NDH-2), and Succinate: plastoquinone oxidoredutase (SDH) are present in both cytoplasmic membrane and thylakoid membrane. Oxygen-reducing proteins like cytochrome c oxidase (COX), cytochrome bd quinol oxidase (Cyd), and alternate respiratory terminal oxidase (ARTO) are also interspersed between thylakoid and cytoplasmic membranes. In a physiological state, the redox potential generated in the form of NADPH is assimilated for biosynthetic pathways including the carbon fixation pathway. However, it has been observed that upon interfacing these cyanobacteria with electrodes, a light-dependent increase in current can be observed. This observation has been the basis of its use as a photobiocatalyst in electrochemical cells and the emergence of the cellular biophotovoltaics (BPV) concept.

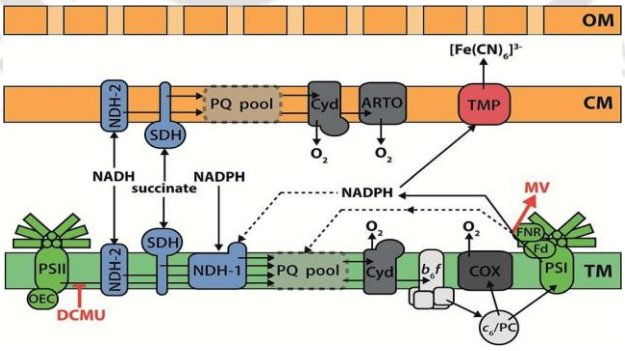

Figure 1. 9. Schematic representation of the electron transfer pathways in a cyanobacteria. OM (Outer membrane), CM (Cytoplasmic membrane), TM (Thylakoid membrane), TMP (Transmembrane protein), ARTO (Alternative respiratory terminal oxidase), Cyd (Cytochrome bd quinol oxidase), COX (Cytochrome c oxidase), PQ Pool (Plastoquinone pool), PS1 (Photosystem 1), PS2 (Photosystem 2), OEC (Oxygen evolving complex), Fd (Ferredoxin), FNR (ferredoxin:NADPH oxidoreductase), NDH-1 (NADH: plastoquinone oxidoreductase), NDH-2 (NADPH:plastoquinone oxidoreductase), SDH (Succinate: plastoquinone oxidoreductase), b6f (cytochrome b6f complex), c6/PC (cytochrome c6/plasticyanin), MV (Methyl Viologen), DCMU ((3-(3,4-dichlorophenyl)-1,1-dimethylurea) ; (**McCormick et al. 2015**)

1.4 Current state of research on cyanobacterial electrogenicity.

The earliest reports on the electrochemical behaviour of cyanobacterial cells were by Japanese researchers in the 1980s and 90s (Yagishita et al. 1999; Yagishita et al. 1997; Yagishita et al. 1993). These researchers demonstrated current production in both light and dark metabolic modes. The electrochemical systems used in the study were mostly fuel cell systems and a few employed three-electrode systems in their study. The drawback of these reports was that most of them used quinone-based artificial chemical mediators to demonstrate current production. Thus, this research was largely limited to lab-based demonstration of the phenomenon. In the absence of a pressing demand for sustainable energy generation, this field of research was largely forgotten. After a brief hiatus, interest in the field was resumed by the report of Pisciotta et al (2009), who reported light dependent current production from a photosynthetic consortium dominated by cyanobacteria (Yongjin et al. 2009). The key aspect of this report was that no artificial redox mediator was introduced into the fuel-cell system. In their subsequent study, it was demonstrated that this phenomenon of light dependent current production due to photosynthesis is a widespread phenomenon observed across diverse species of phylum cyanobacteria (Pisciotta et al. 2010). The group also tried to deduce the possible pathway of electron flux across the cellular system by using specific metabolic inhibitors and emphasized that the electron leaks out of the plastoquinone pool and is conducted out of the cell through quinol bd1 oxidase (Pisciotta et al. 2011). On the other hand, a group at Cambridge University headed by Professor Christopher Howe published two research articles on biophotovoltaics in the year 2011. In their first report, they focused on two aspects i.e. cell-redox mediator interaction kinetics with ferricyanide as redox mediator and pathway of electron movement outside the cellular structure (Bombelli et al. 2011). As opposed to Pisciotta et al, they proposed the pathway of electron extrusion out of the photosynthetic system to be from the reducing end of photosystem 1 via some unidentified transmembrane protein on the cell wall. The same year, the group also demonstrated current production from multiple species of cyanobacteria and eukaryotic algae biofilms in an MFC setup containing a platinum-based air cathode (McCormick et al. 2011). The biofilms were artificially formed over ITO-PET sheets by settling due to gravity. The group also demonstrated the operation of a small digital clock by connecting their devices in a parallel configuration. The group further tried different approaches for improving the performance by testing various electrodes (Bombelli et al. 2012), mutating the cyanobacterial terminal oxidases (Bradley et al. 2013), adapting the system into a microfluidic configuration (Bombelli et al. 2015) and consistently reported light dependent current production. One of the studies during this period also demonstrated the application of cyanobacteria in an electrolytic cell for hydrogen production (McCormick et al. 2013). Ultimately, in 2015 they coined the term "Biophotovoltaics" (BPV) and proposed a concept where they clearly classified MFC systems into (i) MFC, (ii) Photosynthetic MFC, (iii) Complex MFC and (iv) Biophotovoltaic cell (McCormick et al. 2015).

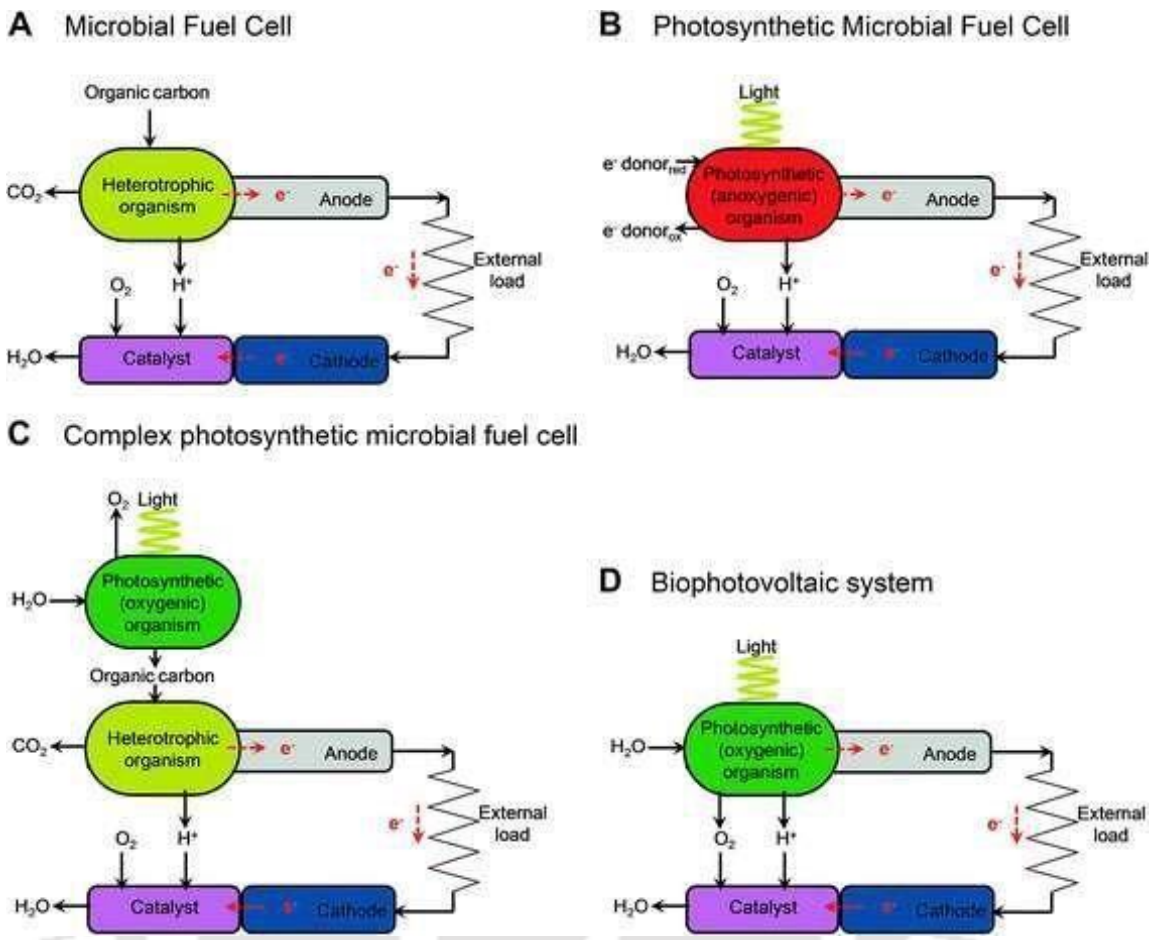

Figure 1. 10. Classification of bioelectrochemical system according to the nature of biocatalyst employed in the system.(A) Microbial Fuel Cell. (B) Photosynthetic MFC. (C) Complex photosynthetic MFC. (D) Biophotovoltaic system. (**McCormick et al. 2015**)

The group has been consistently working on this concept for its improvement and development through approaches like electrode microstructuration (Chen et al. 2022; Wenzel et al. 2018a), developing microfluidic BPV (Saar et al. 2018a), developing paper-based BPV (Sawa et al. 2017), genetic engineering of cyanobacteria for inclusion endogenous mediators (Clifford et al. 2021), etc. In one of their recent studies, they integrated cyanobacterial biocatalyst into an aluminium air battery and demonstrated the steady operation of a microprocessor powered by it for more than 4 months. This study has been a breakthrough in the field (Bombelli et al. 2022). In spite of this, we must point out that this device was not entirely powered by photosynthetic metabolism but was also dependent on the alkaline microenvironment produced by the cyanobacteria that enhanced the rate of aluminium oxidation at the anode. The authors have

not been able to differentiate the individual contribution of the two distinct processes. Further, many different groups have been consistently working for improving the mechanistic understanding and performance of BPV devices. A group of A.K. Jones at Arizona state university demonstrated current production from *Synechocystis* by mutating functional photosystem 2 reaction centers (Cereda et al. 2014). Further, they also demonstrated that cyanobacterial pili do not contribute to electrogenicity (Thirumurthy et al. 2020). A group at Technion-IIT headed by Naom Adir has demonstrated that partial fluidization of cyanobacteria increases the magnitude of photocurrent, possibly due to better access of intracellular metabolites to the electron harvesting anode (Saper et al. 2018). The group also demonstrated that the application of electrochemical bias may lead to the secretion of reduced NAD cofactors out of the cellular structure (Shlosberg et al. 2021). Though they proposed a mechanism through schematics, no biological deduction or proof was furnished. A group at the University of Georgia, headed by R.P. Ramasamy demonstrated that the inclusion of metal-respiring outer membrane proteins into the cell wall of cyanobacteriathrough genetic engineering enhanced the magnitude of current (Sekar et al. 2018). The same group also reported that knocking out terminal respiratory oxidases significantly enhanced the extracellular electron transfer property of cyanobacterium (Sekar et al. 2016). The group of Shuji Nakanashi at Osaka university demonstrated that treating cyanobacterial cells with a membrane-permeable artificially synthesized redox mediator molecule poly(2-methacryloyl oxyethyl phphosphoryl choline o-vinyl ferrocene) can help in detection of intracellular circadian rhythm through electrode (Nishio et al. 2014). Using the same approach, the group demonstrated that it was possible to electrochemically tune the intracellular circadian rhythm of cyanobacteria by controlling the electrochemical potential of an electrode (Lu et al. 2014). The same group also reported recently that the current production capacity of *Synechocystis* species is closely related to extracellular metal reduction capacity (Tanaka et al. 2021). A recent study from the lab of Stefano Freguria demonstrated that for the cyanobacteria species, *Microcystis aeruginosa*, the current generated was not dependent on the intensity of light, but rather was influenced by the pH of the medium (Lemos et al. 2021a). This report stands in direct contradiction to other BPV-related reports. A number of groups have also reported various fabrication strategies to enhance the rate of electron transfer between cyanobacteria and electrodes. Studies from the group of S. Freguia and Lo Gorton have demonstrated the wiring of cyanobacterial cells to the electrodes through immobilized redox polymers containing osmium complexes (Darus et al. 2017). A recent study by S Choi's group demonstrated that naturally formed gold nanoparticles in cyanobacteria enhanced the rate of current production from a cyanobacterium (Liu and Choi 2021). Research published from our lab at IIT Guwahati also reported significant improvement in current production as a result of graphene nanoplatelet-based fabrication (Kaushik and Goswami 2018). Further, a conductive polymer entrapped magnetic nanoparticle-based fabrication was also shown to enhance the rate of current production significantly while remediating toxic dyes in synthetic wastewater

(Kumar et al. 2018). Despite of this volume of work by different groups, there is a lack of standardization of methods between different groups making it difficult to compare and assess these works. Moreover, there is a need for molecular-level investigation in the context of biophotovoltaics in order to improve the mechanistic insight of the phenomenon.

1.5 Research gap and motivation of study

Since BPV is a field requiring an interdisciplinary approach, different research groups have been pursuing this field in their own way. Each developing and standardizing their own procedures for studying cyanobacterial exoelectrogenicity. Thus, there is a lack of standardization making it difficult to compare the results from different groups.

1. Researchers use either a fuel cell or a three-electrode setup for analyzing the electrochemical behavior (McCormick et al. 2011; Zhang et al. 2018). The final result is expressed as power density normalized to electrode surface area or current density normalized to electrode surface area. Since there is no consensus on the magnitude of the resistor to be used, duration of stabilization, and the magnitude of electrochemical bias to be applied in chronoamperometry, the results are difficult to compare for evaluating the performance of biocatalysts between various reports.
2. Electrodes used range from flat ITO sheets, microporous ITO, nanostructured electrodes, Toray fiber paper, carbon cloth, graphite, platinum electrodes, and a conductive polymer. Further, the electrodes can also be categorized as unmodified, immobilized through redox polymer, or containing redox mediator. These different electrodes, result in different levels of cell-electrode interactions resulting in different patterns of current profile (Tschörtner et al. 2019).
3. Complete absence of voltammetry investigations or inconsistent voltammetry results between groups with attributions without proper molecular identification, obscure the mechanistic understanding (Zhang et al. 2018).
4. Differences in the nature of attachment between cells and electrodes, which may be (i) spontaneously formed mature biofilms (Pisciotta et al. 2010), (ii) artificially immobilized cell biomass (Cereda et al. 2014), (iii) Planktonic biomass settled through gravity (Saper et al. 2018), (iv) Stirred biomass in suspension communicating with electrode through an endogenous or artificially added mediator (Lai et al. 2021).
5. Difference in the pattern, duration, and intensity of illumination (Darus et al. 2017) (Wenzel et al. 2018b).
6. Difference in the cyanobacterium species used each having its unique physiology. For instance,

(i) At least two reports on *Spirulina* species differed from conventional BPV responses (Fu et al.

2009)(Fu et al. 2010) (ii) *Microcystis aeruginosa* did not show light dependent modulations (Lemos et al. 2021b). In some cases, researchers have also utilized mixed consortiums dominated by cyanobacterium, increasing the complexity and making it difficult to explain the mechanism of the current generation (Zou et al. 2010).

Moreover, points 4, 5, and 6 mentioned above, i.e. the nature of biofilm attachment to the electrode, pattern and time duration of illumination, and the nature of biocatalyst used, together make the biofilm-electrode interface, more and more complex with time due to secretion and accumulation of extracellular polysachharides in the biofilm matrix (Pereira et al. 2009). The carbon reserves stored in the extracellular space also invite heterotrophs to establish complex interactions with time, leading to the formation of a mat-like structure in long run. Any real-world standalone operation of a BPV device would require a continuous open-air operation for months, causing an ideal BPV system to form biofilms in a photosynthetic MFC. This proposition was further verified by recent breakthrough research by Bombelli et al (2022). In which a microprocessor was powered by a BPV device inoculated with axenic culture, at the end of an operation that was found to be harboring symbionts like *Halomonas* and *Pseudomonas* in the thick matrix-like structure **Figure 1.11**. However, even this study did not carry out a thorough *in-situ* time-dependent electrochemical investigation coinciding with the progression of biofilm formation.

Figure 1. 11. Thick matrix formation on aluminium filament electrodes. (**Bombelli et al. 2022**)

These factors motivated us to perform a time-dependent *in-situ* electrochemical investigation during the progression of biofilm formation on a stable, non-corrosive electrode and to further perform biochemical, physiological, and microscopic investigations to rationalize those electrochemical results. Our choice of species was *Spirulina* species (NCIM 5143) procured from NCL Pune. We chose this organism because contradictory reports were present for *Spirulina* species, which showed enhanced current production in dark conditions. Moreover, it is also species of high commercial value with a well-established market and

procedures for open-air cultivation. This makes it suitable for a standalone BPV application. *Spirulina* species have also been reported to adopt versatile metabolic modes like photosynthesis, respiration and auto-fermentation making it possible to study prolonged dark conditions in the context of electrochemical performance (Ananyev et al. 2008). Moreover, there are also reports of *Spirulina*-based phototrophic mats in shallow sublittoral regions of the Baltic sea (**Figure 1.12**) (Włodarska-Kowalczuk 2014).

Figure 1. 12. Spirulina-based mat at the shallow regions of the Baltic sea.

CHAPTER 2

Materials and Methods

2.1. Characterization of the biocatalyst

The *Spirulina* species (accession number 5143) was procured from the National Collection of industrial microorganisms, Pune, India, and cultured in the recommended inorganic growth medium. The medium composition was 119 mM $NaHCO_3$, 29.4 mM $NaNO_3$, 17.1 mM NaCl, 2.87 mM K_2HPO_4, 5.73 mM K_2SO_4, 0.811 mM $MgSO_4.7H_2O$, 0.36 mM $CaCl_2$, 36 µM $FeSO_4.7H_2O$ and one µM $NiCl_2$ at pH 9.8. The medium was prepared by separately autoclaving the sodium bicarbonate salt at 15 lbs for 20 minutes. The organism was cultivated in narrow-mouthed 250 ml conical flasks kept in Orbitek-LT (Scigenics) shaker incubators maintained at 30°C at 180 rpm. The cultures were illuminated at a light intensity of 2500 lux as measured by a lux meter.

Growth kinetics measurement of the culture was performed by measuring optical density (O.D.750), chlorophyll concentration, and biomass (both wet and dry). The sampling was done by using cut tips to prevent errors due to biomass aggregation. The optical density method of measuring growth kinetics was found to be unsuitable for this strain due to its filamentous nature and tendency of rapid aggregate formation in a cuvette causing statistically significant variations both while sampling and optical density readings. For biomass measurement methods prescribed by Lee and coworkers were followed (Lee and Shen 2004). 2.5 ml aliquots of suspension culture withdrawn with cut tips were washed with distilled water and vacuum filtered through pre-heated and pre-weighed 0.45µ (Axiva) nylon membrane filters. The weight was measured on a Sartorius analytical weighing balance BSA224S-CW with an accuracy of 0.1 mg to obtain wet biomass. Filters were then dried at 60°C and measured until a constant weight was obtained. For chlorophyll estimation, wet biomass pellets were suspended in 90% methanol overnight and absorbance was measured at 665 nm and 650 nm. Pigment concentration was estimated by formula: Chlorophyll (mg/L) = (16.5 X A_{665}) - (8.3 X A_{650}) as mentioned in (Qiang et al. 1996)

16S ribosomal RNA sequencing was done using cyanobacteria-specific primers cya106F and cya1281R by NCIM, Pune (Nübel et al.1997). The sequences of the primers were (5' - CGG ACG GGT GAG TAA CGC GTG A – 3') and (5'- GCA ATT ACT AGC GAT TCC TCC -3'). These primers are useful for amplifying 16S sequences of cyanobacteria from unialgal non-axenic cultures. The analysis of the sequences through BLAST revealed maximum identity to *Spirulina subsalsa* BGLR6. Phylogenetic

dendrograms were constructed with MEGA6 software by using the Neighbor-joining method (Saitou and Nei 1987).

Biofilm cultures submerged under a water column were initiated by using a photosynthetically active 12-day-old *Spirulina* suspension culture having chlorophyll concentration ~ 1.9 mgL^{-1}. Plates were exposed to 2500-lux illumination from white fluorescent lamps in two configurations i.e. (i) illuminated from above (ii) illuminated from the bottom at ambient room temperature (**Fig. 2.1**). The growth of the biofilm was monitored by measuring the wet weight of the biofilms in triplicate. Biofilms were allowed to mature for 20 days in photosynthetic mode. A period of dark metabolism was deliberately induced by placing matured biofilms in continuous dark conditions for 9 days. Thereafter photosynthetic growth was again resumedfor a period of 11 days.

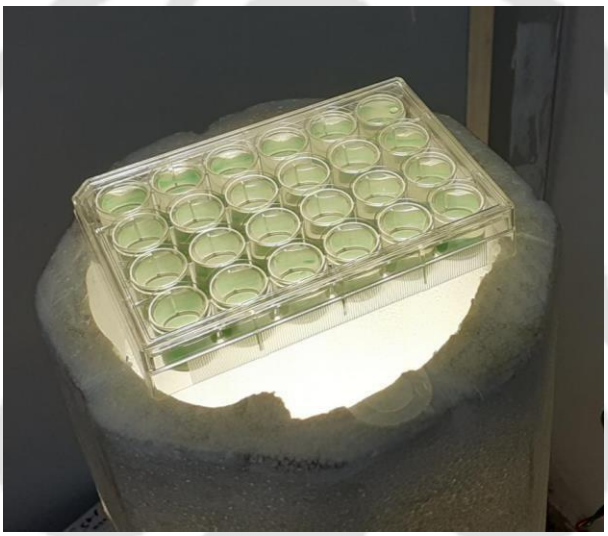

Figure 2. 1. A 24-well plate illuminated from below.

2.2. Axenic culture treatment methods

The *Spirulina* suspension culture was examined under the dark field microscope to detect the presence of a closely associated bacterial population. This observation was also made in the cell mass isolated from the surface of the newly procured agar slants from the repository. Axenic *Spirulina* monocultures were prepared by sequentially subjecting the cultures to *ß*-lactam antibiotic cocktail treatment, filter washing, serial dilution, and micromanipulation. The approach for antibiotic treatment was adapted from literature (Vaara et al.1979; Castenholz et al. 2015; Ferris and Hirsch 1991; Sena et al. 2011). In the presence of a cocktail of *ß*-lactam antibiotics, the rapidly dividing contaminated bacterial cells will be eliminated. For antibiotic cocktail treatment, specific wet biomass of *Spirulina* culture was resuspended in sterile

Zarrouk medium and kept in dark for 12 hours at ambient temperature to starve it of intracellular carbon reserves. The cultures were then washed and resuspended in fresh 10 mM bicarbonate buffer. This suspension was mixed with autoclaved Soyabean casein digest medium (Himedia M011) prepared in bicarbonate buffer in a 1:10 (volume/volume) ratio and allowed to grow in dark at 37°C, 180 rotations per minute. The cultures were observed under a dark field microscope every hour. An antibiotic cocktail with the composition of (100 µg ml^{-1} Meropenem, 100 µg ml^{-1} Imipenem, 100 µg ml^{-1} Carbapenem, and 100 µg ml^{-1} Ampicillin final concentration) was introduced into this culture once the bacterial load was observed to increase under a microscope. Aliquots were collected every 2 hours and washed thrice with 100 mM bicarbonate buffer before spreading on a Tryptic soy agar plate. The plates were kept under illumination at 30°C. The plates which showed growth of *Spirulina* mat-like colonies without the presence of bacterial colonies were selected for further steps.

The mats like colonies of *Spirulina* were collected in Eppendorf tubes and were subjected to mechanical shearing with a micro pestle in the presence of bicarbonate buffer. The obtained suspension was again washed with the bicarbonate buffer and serially diluted before spreading on inorganic Zarrouk medium agar plates. The *Spirulina* mats grown over agar plates were again collected, sheared, washed, and diluted before spreading on Zarrouk medium plates. This process of repeated subculturing and dilution was done four times.

In the final step, the obtained mats were sheared and diluted. Attempts were then made to capture single filaments from the diluted suspensions through the capillary action of sterilized glass capillaries (Z114960 Sigma). These single filaments were observed under a stereomicroscope and were used for initiating monoclonal *Spirulina* suspension cultures.

2.3. Isolation and characterization of pure cultures of symbionts.

The bacterial load reappeared in the late log phase of cyanobacterial suspension cultures initiated from a single filament obtained through micromanipulation. It was observed that the colony characteristic of the bacteria from freshly procured agar slants and antibiotic-treated *Spirulina* cultures were similar (**Fig.2.2**). Thus, the colonies were picked up and cultured in the soybean casein digest agar medium (Himedia M011). The growth was monitored by measuring optical density at 600 nm. Optimum growth conditions were determined by measuring the specific growth rate and doubling time at various temperatures (4-45°C), salinity (0.5-10%), and pH (7-10) conditions.

Figure 2. 2. Bacterial colonies obtained with Spirulina mat-like colonies on Zarrouk medium plate.

16S molecular DNA-based identification of pure isolated cultures was carried out by Eurofins Scientific. The primers used were 27F having sequence (5′-AGAGTTTGATCCTGGCTCAG-3′) and 1492R having sequence (5′-GGTTACCTTGTTACGACTT-3′). The following procedure was followed: -

1. DNA was isolated from the pure cultures. Its quality was evaluated on 1.0% Agarose gel, and a single band of high-molecular-weight DNA has been observed.
2. Fragment of 16S rDNA gene was amplified by 27F and 1492R primers. A single discrete PCR amplicon band of 1500 bp was observed when resolved on Agarose gel.
3. The PCR amplicon was purified to remove contaminants.
4. Forward and reverse DNA sequencing reaction of PCR amplicon was carried out with forward primer and reverse primers using BDT v3.1 Cycle sequencing kit on ABI 3730xl Genetic Analyzer.
5. Consensus sequence of the 16S rDNA gene was generated from forward and reverse sequence data using aligner software.
6. The 16S rDNA gene sequence was used to carry out BLAST with the database of NCBI Genbank database. Based on the maximum identity score first ten sequences were selected and aligned using the multiple alignment software program Clustal W. Distance matrix was generated and the phylogenetic tree was constructed using MEGA 7.

2.4. Microscopy and imaging

The optical microscopy was conducted on biofilms cultured in 24 well plates and electrodes retrieved from the half-cell setup. An inverted microscope of model Eclipse Ti-U (Nikon) was operated in

brightfield at 20x (S Plan Fluor ELWD 20x) objective and 10x (Plan Fluor 10x) objective. Images and videos were captured through a Nikon DS-Ri1 camera both in a focal plane and through the bulk of biofilm by gradually rotating course adjustment. Biofilms formed on opaque graphite electrodes were imaged with a Zeiss Axio Scope A1 microscope operated in reflected mode. Images were captured with 20x ZeissEC Epiplan objective with a Zeiss axiocam 503 color camera in both darkfield and fluorescence. Olympus SZX16 microscope was used while micromanipulations of *Spirulina* filaments.

FE-SEM imaging was done for studying the surface morphology of electrodes, microbes (both cyanobacteria and heterotrophs), and multispecies biofilm structures. The FE-SEM used was Model: Sigma300, Make: Zeiss. The electrodes were used directly for imaging. Biological samples like microbes and biofilms were washed in deionized water followed by fixing in 2.5% glutaraldehyde. The time for fixing bacterial cultures was 30 minutes and for fixing *Spirulina* multispecies biofilms was 3 hours. Glutaraldehyde was washed away repeatedly after fixing with deionized water. The samples were dehydrated by using gradient alcohol series of 30, 40, 50, 60, 70, 80, 90, and 100 (%). After vacuum drying, samples were mounted on stubs and puttered with gold before imaging. Images were collected at magnifications of 1900x, 5000x, and 10000x.

2.5. Dissolved oxygen and pH monitoring

The dissolved oxygen in the MFC setups was monitored by using a handheld Extech DO700 dissolved oxygen probe (Range: 0 to 200%). Further, in order to monitor the variation in concentration of dissolved oxygen and pH within a volume 250 ml container, biofilm cultures were established in conical flasks at an illumination of 2500-lux intensity. This mimicked the conditions in 250 ml volume anodic chambers used in subsequent experiments. A dissolved oxygen probe (VisiFerm DO Arc 325 H0, HAMILTON) and pH probe (EasyFerm Plus PHI Arc 325, HAMILTON) connected to minifors2 bioreactor (INFORS HT), recording online parameters of the system through bioprocess platform software (eve ®) were placed at the center of a flask with the help of biuret stand.

2.6. Extraction of extracellular polysaccharide matrix and its fluorescence spectroscopy.

Suspension cultures of *Spirulina* species cultured under high rpm exude out a lot of organic matter in the extracellular space (Mouhim et al. 1993). Some of it is also retained on the aggregated cell flocs. The part that is exuded in the supernatant is called dissolved extracellular organic matter (dEOM) and the part that is retained in the aggregated flocs is called bound extracellular organic matter (bEOM). dEOM was obtained by subjecting 5 ml aliquots of *Spirulina* suspension culture to centrifugation at 4000 rpm for 15 minutes and passing the supernatant through a 0.45 µ syringe filter (AXIVA) (Korak et al. 2015). The biomass pellet was further resuspended in 5ml of 0.6% NaCl solution and vortexed at room temperature.

The suspension was further centrifuged at 10000 rpm for 15 minutes and the supernatant was filtered through a 0.45 µ syringe filter (AXIVA) to obtain bEOM. Sampling was done six times during the course of one growth curve from early log phase to early stationary phase. The total organic carbon content was determined on Analytik Jena multi N/C 2100S equipped with an autosampler and NDIR detector.

Undiluted dEOM and bEOM were subjected to fluorescence spectroscopy in a 1cm path length cuvette using Fluoromax-4C (HORIBA Scientific). Readings were collected with PMT detector voltage set at 900 V with excitation and emission slit width set at 10 nm. Excitation spectra were collected from 200 nm to 500 nm with 1 nm increments. Emission spectra were in the range of 200 nm to 700 nm with 1 nm increments.

2.7. Extraction and estimation of extracellular polysaccharide matrix from biofilm cultures.

The extracellular matrix of the biofilms was extracted by a modified method adopted from earlier reports that ensured minimal cell lysis (Stuart et al. 2016; Mouhim et al. 1993). Briefly, biofilms were vacuum filtered on 0.45µ nylon membrane filters. The wet biomass was measured over a weighing balance. The biomass obtained was homogenized gently in 50 mM TAPS buffer (pH 9) containing 25 mM EDTA through a Tarson micropestle. Finally, a 2 ml volume of the homogenate was incubated at 40°C at 180 rpm in a shaker incubator overnight. The suspension was centrifuged at 5000xg and the supernatant obtained was filtered through 0.45µ nylon syringe filters. The filtrate obtained contained bound extracellular polysaccharides of biofilm. The trichomes were checked for cell lysis through microscopy. All samples were stored at 4°C until further biochemical analysis. The macromolecular estimates obtained for biofilms at each stage were normalized to the corresponding wet weight of the biofilm.

2.8. Biochemical characterizations

Total carbohydrate estimation was done by phenol-sulfuric acid method using glucose as standard in the concentration range of 0 to 60 µg ml^{-1}. Total protein was estimated by Bradford method by using protein as standard in the range of 0 to 1 mg ml^{-1}. Total phenolics were estimated by Folin-Ciocalteau reagent by the method of Ainsworth that used gallic acid as standard in the range of 0 to 500 µmole.

25-day-old matured biofilms were harvested for glycogen and NAD(P)(H) analysis. Glycogen estimation was performed by the method of (de Porcellinis, et al. 2017). Briefly, biofilm pellets were washed and suspended in 50 mM TRIS-HCl buffer. The suspensions were lysed through sonication at 4°C. The lysate obtained was centrifuged at 6000xg for 10 minutes at 4°C. The glycogen in the supernatant was further precipitated with 96% ethanol in a ratio of 1:9 (lysate: 96% ethanol). The mixture was further heated at 90°C for 10 minutes and incubated on ice for 30 minutes. The centrifugation at 20000xg, 4°C for 30

minutes yielded a translucent pellet that was dried at room temperature. The enzymatic degradation with amylase (2 Unit/ml) and amylopectin (8 Unit/ml) in sodium acetate buffer (pH 5) at 25°C overnight was performed. The glucose solution obtained was quantified using Sigma GAGO20-kit based on a colorimetric reaction involving glucose oxidase-peroxidase and o-dinasidine, following the protocol given by the manufacturer.

NADH/ NAD^+ and NADPH /$NADP^+$ ratios were determined by enzymatic cycling-based colorimetric assay (Kern, Price-whelan, and Newman, ND et al. 2014). Briefly, biofilms harvested from wells were obtained as pellets by centrifugation at 21000xg for 2 minutes. Pellets were suspended in 600 µl of 0.2 M HCl (for NAD^+ and $NADP^+$) and 600µl of 0.2 M NaOH (for NADH and NADPH). After incubation at 55°C for 10 minutes, the samples were chilled on ice. This followed neutralization drop-wise addition of 600 µl of 0.1M NaOH (for NAD^+ and $NADP^+$) and 600 µl of 0.1M HCl (for NADH and NADPH) while vortexing of samples. The supernatant obtained by centrifugation at 21000xg for 5 minutes was further stored at -80°C or used for colorimetric analysis right away. The reaction was driven by alcohol dehydrogenase (for NAD/NADH) and glucose-6-phosphate dehydrogenase (for NADP/NADPH). Phenazine ethosulfate was used as a chemical mediator between analyte and MTT. The colorimetric reaction was based on MTT with signal at 570 nm detected by Thermo scientific multiscan sky-high microplate spectrophotometer.

2.9. 16S ribosomal RNA-based community analysis

50 days matured biofilm culture (volume 250 ml), which had undergone a 9 days period of prolonged dark induction followed 1-week photosynthetic revival, was used for extraction of the extracellular matrix as described above. The extracellular matrix content was filtered through a 0.2 µm nylon membrane filter to collect bacterial population over it. The filters were then stored at 4°C in falcon tubes and sent for community analysis to Eurofins Scientific.

2.9.1. Metagenomic DNA Isolation, Qualitative and Quantitative analysis

Metagenomic DNA was isolated from the received bacterial culture sample using Quick-DNA Miniprep Plus Kit (Zymo Research) as per the kit protocol. The quality of the isolated metagenomic DNA sample was quantified using NanoDrop.

2.9.2. Preparation of 2 x 300 MiSeq library

Amplicon libraries were prepared using Nextera XT Index Kit (Illumina inc.) as per the 16S Metagenomic Sequencing Library preparation protocol (Part # 15044223 Rev. B). Primers for the amplification of the bacterial specific region were designed and synthesized at Eurofins Genomics Lab.

Amplification of the bacterial 16S region was carried out. 3 µl of PCR product was resolved on 1.2% Agarose gel at 120V for approximately 60 min or till the samples reached 3/4th of the gel. The sequence of the primers used were Forward primer (5'- GCCTACGGGNGGCWGCAG – 3') and Reverse primer (5' - ACTACHVGGGTATCTAATCC – 3'). The QC passed amplicons with the Illumina adaptor were amplified using i5 and i7 primers that add multiplexing index sequences as well as common adapters required for cluster generation (P5 and P7) as per the standard Illumina protocol. The amplicon libraries were purified by AMPure XP beads and quantified using Qubit Fluorometer.

2.9.3. Quantity and quality check (QC) of library on Agilent 4200 Tape Station

The amplified library was analyzed on a 4200 Tape Station system (Agilent Technologies) using D1000 Screen tape as per manufacturer instructions.

2.9.4. Cluster Generation and Sequencing

After obtaining the mean peak size from Tape Station profile, library was loaded onto MiSeq at appropriate concentration (10-20 pM) for cluster generation and sequencing. Paired-End sequencing allows the template fragments to be sequenced in both the forward and reverse directions on MiSeq. The kit reagents were used in binding of samples to complementary adapter oligoes on paired-end flow cell. The adapters were designed to allow selective cleavage of the forward strands after re-synthesis of the reverse strand during sequencing. The copied reverse strand was then used to sequence from the opposite end of the fragment.

2.9.5. Bioinformatics Analysis

The comprehensive software, QIIME was used for bioinformatics analyses. It comprises tools and algorithms such as FastTree for heuristic based maximum-likelihood phylogeny inference (Price et al., 2010), the RDP classifier for the assignment of taxonomic data using a naïve Bayesian classifier (Wang et al., 2007) and others. This allows QIIME, which continues to undergo development, to easily and relatively adapt novel standalone tools, and thus improve in step with advances in the field of microbial community ecology. The bioinformtics works flow is depicted in **fig 2.3**.

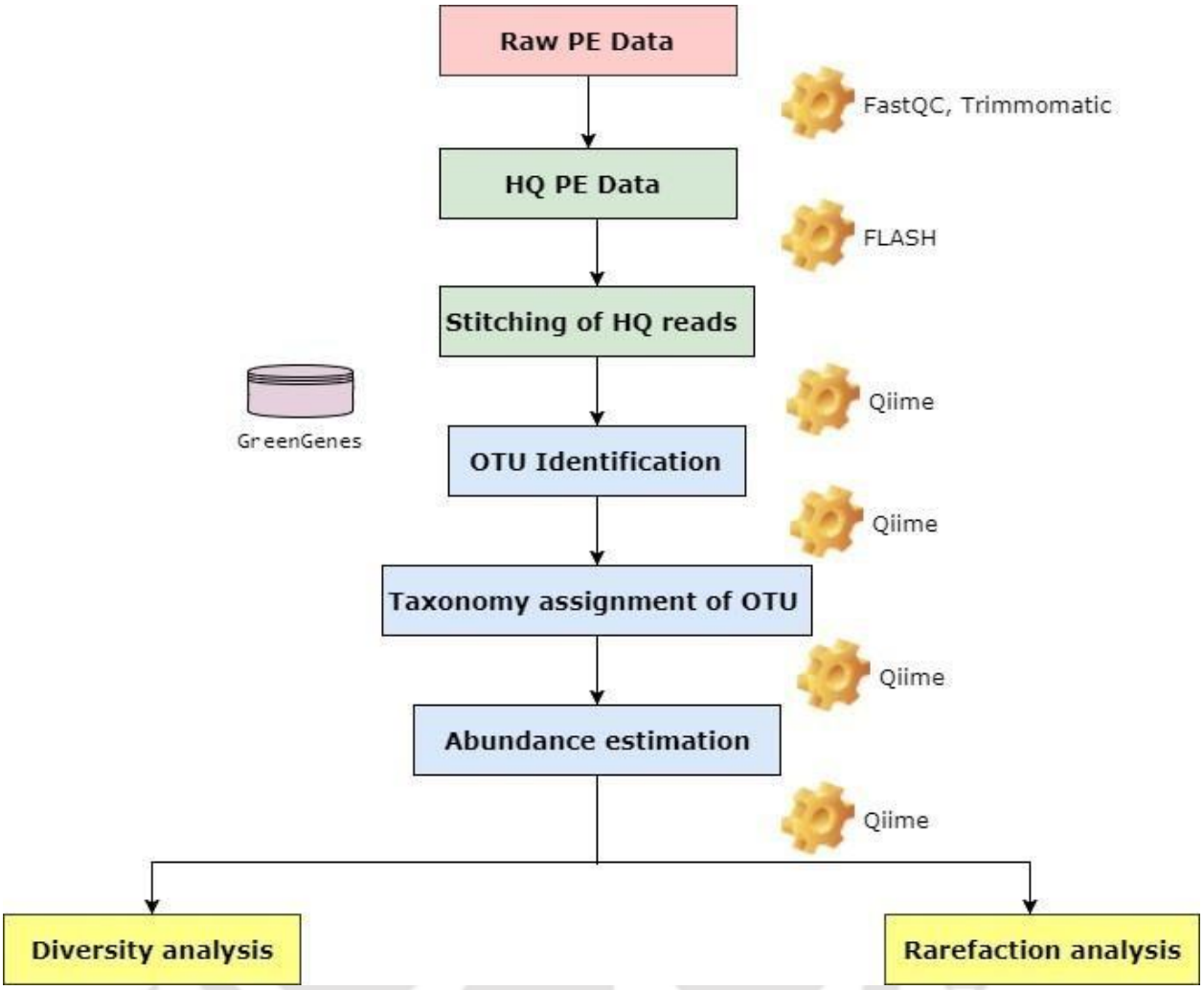

Figure 2. 3. Bioinformatics workflow for 16S community analysis.

To process the data of one 16S samples the following steps were performed:

1. High quality clean reads were obtained using Trimmomatic v0.38 to remove adapter sequences, ambiguous reads (reads with unknown nucleotides "N" larger than 5%), and low-quality sequences (reads with more than 10% quality threshold (QV) < 20 phred score) along with a sliding window of 10 bp and a minimum length of 100 bp.
2. Stitching the PE data into single end reads.

3. Picking Operational Taxonomic Units (OTUs) based on sequence similarity within the reads and picks a representative sequence for 16S bacteria from each OTU against Greengenes database (version 13_8).
4. Assigning the OTU to a taxonomic identity using reference databases.
5. Calculated diversity metrics for each sample and compared the types of communities, using the taxonomic assignments.
6. OTU-picking identifies highly similar sequences across the sample and provides a platform for comparisons of community structure. All the sequences from the samples were clustered into OTUs based on their sequence similarity. OTUs are clusters of sequences, frequently intended to represent some degree of taxonomic relatedness done using UCLUST at 97% sequence similarity and each resulting cluster typically represents a species. Since each OTU may be made up of many sequences, a representative sequence for OTU is picked for downstream analysis. This representative sequence was used for the taxonomic identification of the OTU. This results with the different chart figures at different taxonomical levels. The graph corresponding genus is shown inresults section.

2.10. Assembly and operations of electrochemical reactors

A number of different combinations and configurations of electrodes with MFC setups were used until a combination was judged to be suitable for long-term electrochemical investigation during the course of biofilm formation.

2.10.1. Electrodes

For the purpose of electrochemical investigation of *Spirulina* biofilms within H-type MFC reactors, Indium Tin Oxide (ITO) coated Polyethylene Terephthalate sheets (Sigma 639303) and Toray carbon paper (TGP-H-60) were used in the preliminary experiments. Further, Isomolded graphite electrodes (Graphitestore) were also included in the study. Based on the durability and reproducibility of electrochemical data obtained from the electrodes, Isomolded graphite electrode was chosen for further experiments as described below.

In three-electrode format Ag/AgCl reference electrodes (Metrohm), Pt-rod counter electrodes (Metrohm) and Glassy carbon electrode (GCE) tip (Metrohm) working electrodes were used for analyzing redox properties of bacterial biomass and supernatant. While evaluating the electrochemical surface area of 1-cm^2 electrodes (graphite, Toray paper, carbon cloth, ITO) with ferricyanide, the working electrode of three- electrode configuration was substituted by the electrode under investigation.

2.10.2. Devices

Autolab PGSTAT302N, Netherlands potentiostat with Frequency Response Analyzer was used for all electrochemistry analysis. For long-term monitoring of voltage and current response of an MFC, Agilent 34972A LXI, USA with copper crocodile clips were used. Data were collected in 10 seconds intervals.

2.10.3. MFC construction and operation

Dual-chambered MFC setups were assembled by cutting open a 4 x 4 cm window on the walls of two T75 cell culture flasks (Thermo Fischer Scientific) (**Fig. 2.4 a**). A 5 x 5 cm piece of protonated Nafion 117 membrane (Sigma) was sandwiched between two square silicone gaskets, exposing the membrane from two sides. This sandwich assembly was placed between the two T75 flasks such that the membrane face was exposed through cut-out windows on both sides. The system was made leak-proof by using waterproof silicone glue at the joints. The flasks were held together tightly by wrapping transparent duct tape around them. The silicone glue, duct tape, and silicone gaskets were procured from the local market. Nafion membranes were prepared by lightly boiling them in 3% H_2O_2 for an hour. Further protonation of membranes was done by boiling them in 0.5M H_2SO_4 for an hour. Rectangular pieces of graphite (Isomolded graphite electrode, Graphitestore) were used as electrodes on both anodic and cathodic sides. Dimensions of electrodes were 2 cm x 5 cm for the anodes and 2.5 cm x 7 cm for the cathodes. The electrodes were connected using titanium wires and placed at the bottom of the setup in a horizontal orientation. The electrodes were fastened to a plastic raft with cotton threads, which were stuck to the base of the T75 flask (standing in a vertical orientation). This configuration maximized the interaction between electrodes and mat-like biofilms formed by filamentous trichomes while minimizing the risk of physical disturbance due to shear stress during potentiostatic analysis, probe, or reference electrode dipping. The final distance between the centers of the horizontally placed electrodes was approximately 4 cm. The anolyte used for this study was the inorganic growth medium mentioned above and the catholyte used was 100 mM phosphate buffer (pH 8) with 80 mM potassium ferricyanide. The T75-based MFC setups were also installed with MF-2052 Ag/AgCl reference electrodes enclosed in a salt bridge for continuous monitoring of individual electrodes. Similar setups were also assembled from T25 culture flasks with rectangular strips of Toray carbon paper and ITO- PET sheets (2 cm X 10 cm) stuck to the walls of the flask for preliminary experiments. The final distance between the centers of the horizontally placed electrodes was approximately 3.4 cm in this case.

All setups were loaded with 10-day old photosynthetically active suspension culture equivalent to 1.1gm wet weight at pH 9.3 having chlorophyll concentration of 1.8 mg/L (approx.). The volume of each anodic and cathodic chamber was 250 ml. Similarly, for T25 flask based MFC setups with a 50 ml

volume, culture equivalent to 200 mg wet weight was used for inoculation. Current-Voltage data collection of the setups was done using a data-logger model (Agilent 34972 A LXI) in 10 seconds intervals. The reductive reaction in the cathode is driven by a single electron reductive reaction of ferricyanide on the electrode surface to ferrocyanide. The anodic reaction was driven by microbial metabolism of the Spirulina filaments and associated microbial community as described in Results and Discussions.

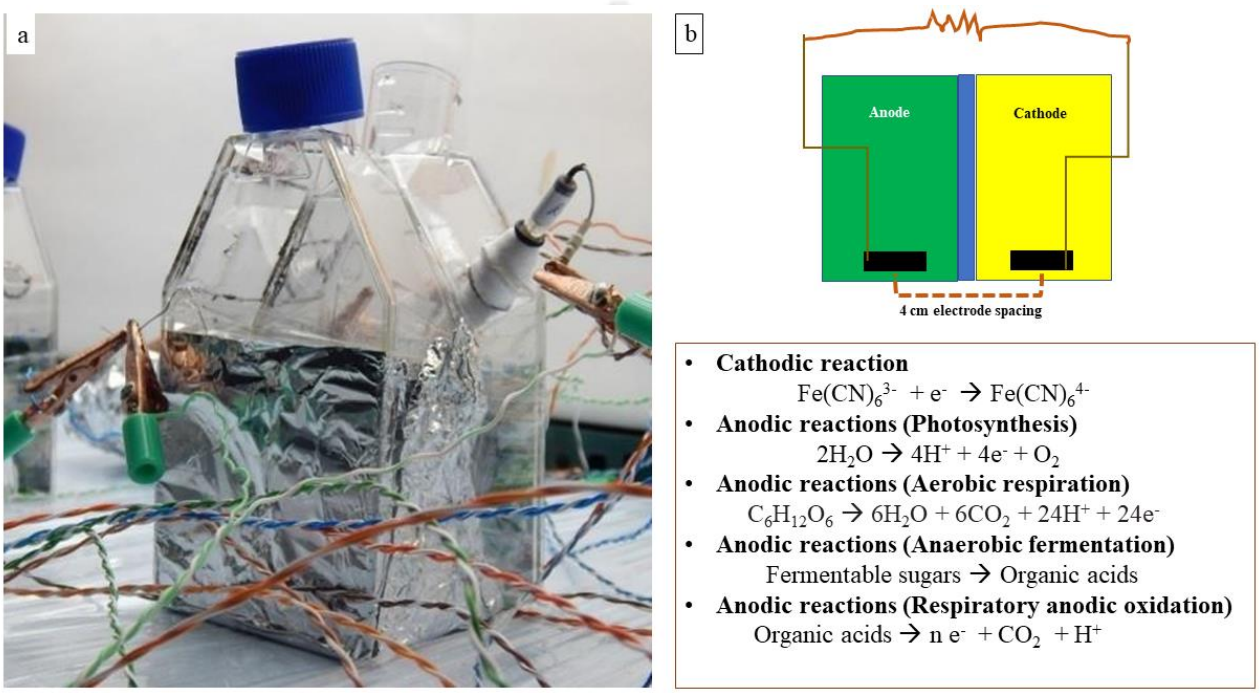

Figure 2. 4. (a) Image of a constructed MFC with reference electrode installed with a salt bridge. (b) Pictorial representation of electrode placement in the reactor and putative chemical reactions operational at anode and cathode electrodes.

2.10.4. MFC configurations and electrochemical experiments

Five independent experiments were performed, two in open circuit and three in closed circuit configurations. The first experiments were preliminary in nature and involved T25 flask-based MFC setups operated in open circuit mode. Voltage was recorded in an 8-hour/16-hour light-dark cycle until the signal magnitude subsided. These setups contained ITO and Toray strips as electrodes. A control was also operated for each category, which had an inorganic growth medium devoid of biomass (**Figure 3.11 in the next chapter**).

The second experiment involved five setups i.e. two sets of duplicate setups with an additional half-cell setup containing only an anode (**Figure 3.27-28 in the next chapter**). The setups were operated in open circuit mode. Reference electrodes (MF-2052 Basi) were placed in anodic chambers of one setup each duplicate set and the half-cell setup. These were used to measure the electrochemical open circuit voltage potential (OCP) profiles of individual electrodes. The other setup in each duplicate set and the same half-cell setup were used for time-dependent electrochemical analysis. One set of duplicates had the anode enclosed within dialysis bags, with a molecular weight cut of 14000 daltons (Sigma D9527), to prevent biofilm formation over the anodes. These were named MFC-1. The other set of duplicates with bare anodes was called MFC-2. The reactors were operated temporally following a specific regimen of 40 days blank operation (control) → 12-hour/12-hour light-dark cycle for 20 days with photosynthetic biomass → 9 days continuous dark → resumption of 12-hour/12-hour light-dark cycle illumination pattern indefinitely. The polarization curve was generated by applying variable resistors in the range of 3 Megaohm to 1.2 ohms. The corresponding current was calculated by using ohms law (Voltage = Current X Resistor). Power calculations were derived by the formula (Power = Voltage X Current). The current and power values were normalized to electrode surface area and expressed as per cm^2. The electrochemical investigation was carried out on one setup of each duplicate set and half-cell setup during the MFC operations at different time points as described below in the electrochemistry section.

The third experiment involved six MFC-2 setups operated in closed circuits with resistors of magnitude 330 kiloohm, 10 kiloohms, 1 kiloohm, 327 ohms, 220 ohms, and 1.2 ohms. The temporal regime followed in this experiment was 2 days blank (control) → 25 days of biofilm formation without data logging → 8 days respiratory/autofermentative biomass → a 4-day interruption of data logging → 12-hour/12-hour light-dark cycle for 3 days (**Figure 3.42, 3.44 in the next chapter**).

The fourth experiment involved seven MFC-2 setups operated in closed circuits with resistors of magnitude 330 kiloohm, 200 kiloohms, 145 kiloohms, 78 kiloohms, 10 kiloohms, 1kiloohm plus a setup operated in an open circuit. The temporal regime followed in this experiment was 5 days blank (control)

→ 25 days photosynthetic regime in 12hr/12hr light-dark cycle → 9 days dark metabolism → resumption of 12hr/12hr light-dark cycle. Biomass had to be replaced in setups OCP, 200 kiloohm, 77.8 kiloohm on day 13 due to excessive cross-over inhibiting photosynthesis. Zarrouk medium was replaced in setup 10 and1 kiloohm on day 24 to minimize the toxic effect of ferricyanide. Pulse voltammetry was carried out at the end of the MFC operation for all the setups as described below in the electrochemistry section (**Figure 3.45 in the next chapter**). A fifth short experiment was performed with one MFC-1 and one MFC-2 set up in order to identify the importance of direct biofilm contact with the electrode for current generation (**Figure 3.50** in the next chapter).

2.10.5. Electrochemical techniques and parameters

First, for evaluating the electrochemical behavior of *Spirulina* cultures in suspension culture, the CV of biomass pellet and supernatant at 1 mV/sec was performed in the potential window of -1 to 1 V. To differentiate the independent behavior of water splitting from the biotic irreversible oxidative reaction, the range was extended from -1 to 1.5 V at a scan rate of 5 mV/sec. The system was purged with Argon in order to eliminate dissolved oxygen.

Second, for evaluating the electrochemical surface area of the electrodes in the ferri-ferro couple, the CV was performed at various scan rates ranging from 1, 5, 10, 20, 40, 50, 70, 80, 90, and 100 mV sec^{-1} . Peak currents and peak potentials were obtained by fitting and used for analyzing the ideal behavior of ferricyanide on respective electrodes.

Third, electrochemical analysis of the biofilm- electrode interface was carried out at different time points during operation for open circuit MFC setups. Closed-circuit setups were analyzed at the end of operation only once. The anode was connected to the working electrode, the cathode to the counter electrode, and an Ag/AgCl Metrohm reference electrode to the reference wire of the potentiostat. The reference electrode was placed in the anodic chamber, close to the anode. The electrochemical analysis was carried out in sequential order of impedance spectra, CV, and pulse voltammetry. Electrochemical Impedance Spectroscopy (EIS) was performed in the range of 100000 Hz to 0.1 Hz, with an amplitude of 10 mV with 50 data points. DPV (DPV) was scanned in the range of -1 V to 1 V. The parameters were: step potential 5 mV, modulation amplitude 50 mV, modulation time 0.3 seconds, and interval time 5 seconds. Three cycles of CV were carried out at 5 mV/sec in the range of -1 to 1 V (vs Ag/AgCl). The tafel slope was derived from the anodic sweep of CV from -1 V to 1 V. Slopes were fitted in the pre-Tafel region (+/- 120mV) and parameters derived from it were anodic slope, cathodic slope, polarization resistance, corrosion current, and corrosion potential.

CHAPTER 3

Results and Discussions

Overview of the chapter

Broadly, this chapter is divided into five sections. The first section (**Section 3.1**) describes the experiments carried out for the thorough characterization of the biocatalyst to be employed for driving the microbial fuel cell system. The section starts with 16S-based molecular characterization and other growth-related characterization of the cyanobacterial strain. The species of Spirulina is identified to be *Spirulina subsalsa*. The species is found to be growing with a specific growth rate of 0.0771 day^{-1} and a doubling time of ~ 8.98 days. Next, the spirulina species is found to be hosting a stable microbial consortium that is robust and resilient to antibiotic-based cleaning procedures and other procedures like serial dilution, subculturing, microfiltration etc. The microbial composition hints presence of a symbiotic community thriving in the copiotrophic extracellular microenvironment. Biochemical and Spectroscopic characterization of the extracellular exudate indicates the presence of a rich copiotrophic environment that is undergoing recycling by the associated microbial community. Isolation and 16S characterization of recurrently occurring microbial colonies from the Zarrouk plate confirmed the results of the 16S community analysis. Under the static condition, the culture configures itself into a two-dimensional biofilm-like structure that sticks on flat surfaces. The biofilm structure is thick enough and contains Spirulina filaments and associated microbes embedded in biofilm matrix.

In **Section 3.2**, preliminary electrochemical readings of the spontaneously formed biofilm, interfaced with the electrodes is observed and verified for its reproducibility. Next, characteristic voltammetric peaks for the biomass and associated supernatant are identified by ensuring reproducibility on standard glassy carbon electrodes. Next, suitable electrodes and biofuel cell reactors capable of withstanding repeated voltammetric investigation for a prolonged time period are chosen. In **section 3.3**, the influence of illumination direction on biofilm structure was investigated. Further, the influence of 9 days long dark starvation period on the biofilm structure was investigated for change in terms of, microbial population composition, metabolic state, microenvironment, biochemical composition, redox state, during biofilm formation, maturation, dark starvation, and photosynthetic recovery. Additionally, the effect of ferricyanide exposure to matured biofilm is evaluated using a dissolved oxygen probe and microscopy.

In subsequent **sections 3.4** and **sections 3.5**, Spirulina biofilms are evaluated for their electrochemical performance in both open-circuit and closed-circuit modes in microbial fuel cell setup. Corresponding results of voltammetric and impedance spectroscopy are also reported in these sections. The results give insight into the complex interplay of ferricyanide, dissolved oxygen, extracellular organic matter, and polarization magnitude on the electrochemical performance of the biofilm-electrode composite under versatile metabolic modes.

3.1 Characterization of photosynthetic bacteria

Spirulina species NCIM 5143 received from NCIM, Pune, India, and used in the current study showed the closest homology to *Spirulina subsalsa* species upon phylogenetic analysis through 16S rRNA sequencing (**Figure 3.1a**). The species has been reported to be present as sublittoral phototrophic mats and biofilms formed over anthropogenic plastic substrates in the marine environment (Włodarska-Kowalczuk 2014) (Ryabushko et al. 2021). The strain was cultured in phototrophic mode and exhibited gliding motility under the microscope. Upon inoculation into the Zarrouk medium and cultivation under illuminated shaking conditions (180 rpm, 2500 lux), the biomass increased with a specific growth rate of 0.0771 day^{-1} and a doubling time of ~ 8.98 days (**Figure 3.1b**). The increase in biomass was accompanied by the gradual increase in pH of the suspension culture due to the involvement of the active carbon concentrating mechanism of the alkaliphilic cyanobacteria (Klanchui et al. 2017). A linear correlation was found between the harvested wet biomass and dried biomass (**Figure 3.1c**). Normalized values of chlorophyll content with corresponding dried biomass indicated an increase in chlorophyll content up to 13 mg gm^{-1} until day 30. Thereafter the chlorophyll content per unit biomass decreased in the late log phase (**Figure 3.1d**). This decrease in chlorophyll content could be due to physiological changes entailing the self-shading effect, *Spirulina* filament flocking or bicarbonate depletion (Schuurmans et al. 2017).

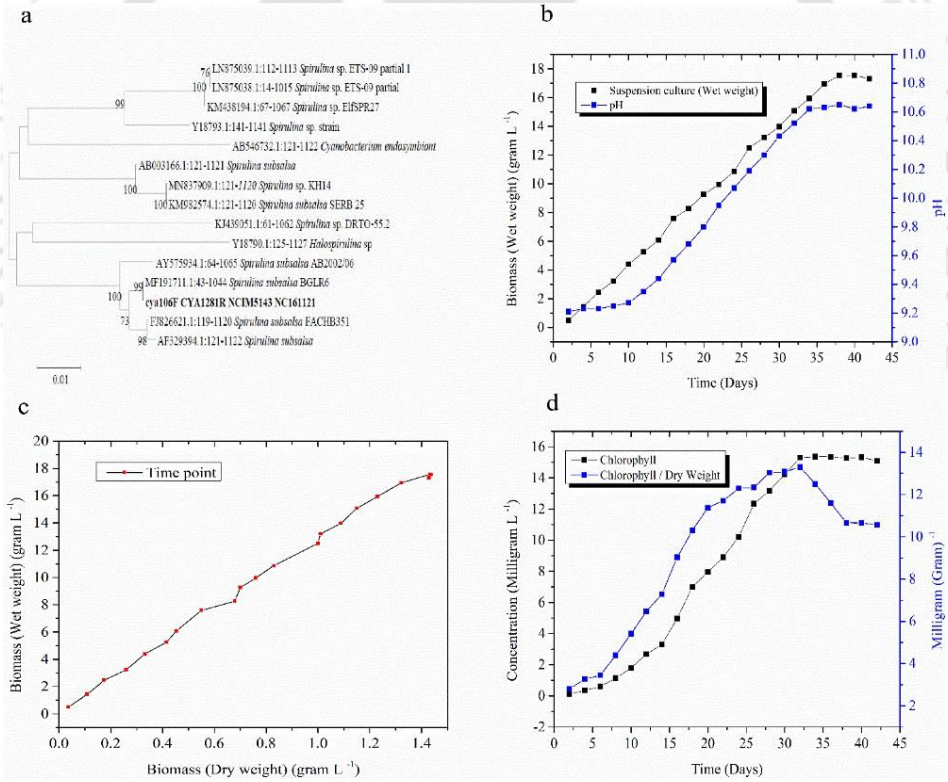

Figure 3.1. Phylogenetic analysis and growth kinetics of *Spirulina* NCIM 5143. (a) Phylogenetic analysis of *Spirulina* NCIM 5143 for its closest species. (b) Growth curve of *Spirulina* NCIM 5143 (■) and corresponding pH change in the culture broth

(■). (c) Correlation between the *Spirulina* wet-weight biomass and dry cell weight. (d) Quantification of chlorophyll content of the *Spirulina* biomass in terms of weight/volume (w/v) (■) and weight/weight (w/w) (■) in the suspension culture during the growth.

Spirulina NCIM 5143 was propagated through regular sub-culturing on agar plates and did not resuscitate upon long-term cryopreservation (Prasad et al. 2013). A significant bacterial population was observed under dark field microscopy in suspension cultures initiated from freshly prepared agar slants upon reaching the late log phase (**Figure 3.2a**). Procedures for obtaining axenic cultures were followed by culturing the biomass in dark with *ß*- lactam antibiotic cocktail in presence of soybean casein digest at 37°C for 48 hours. Periodically harvested (at 2-hour intervals) aliquots were washed with sterile bicarbonate buffer and plated on soybean casein digest medium. *Spirulina* mats, seemingly devoid of bacterial colony growth could be obtained between eight to twelve hours following antibiotic treatment (**Figure 3.2b**). The *Spirulina* mat colonies were repeatedly filter-washed with sterile bicarbonate buffer and again cultured in a Zarrouk medium. A significant bacterial load reemerged in the cultures as the biomass density increased and the cultures entered the stationary phase (**Figure 3.2c-e**). The bacterial load was temporarily reduced upon repeated washing with a sterile buffer followed by micro isolation of single filaments with sterilized glass capillaries under a stereomicroscope. The single filaments were used for establishing new cultures in test tubes. However, the associated bacterial load reemerged upon the increase in biomass. As observed in **Figure 3.2f-h** insets, a subpopulation of bacteria was detected in the vicinity of the *Spirulina* filaments, and a few cells were directly attached to the filament structures. This close physical association indicates that crucial metabolite and nutrient exchange might occur between the host and bacterial cells. Additionally, the epiphytic bacterial subpopulation might also be closely associated with cyanobacterial flocs. In nature, bacterial communities thrive in close association with phytoplankton forming symbiosis or commensalism. These communities are often co-isolated with the cyanobacterium (Zhu et al. 2016; Halary et al. 2022; Nair et al. 2022).

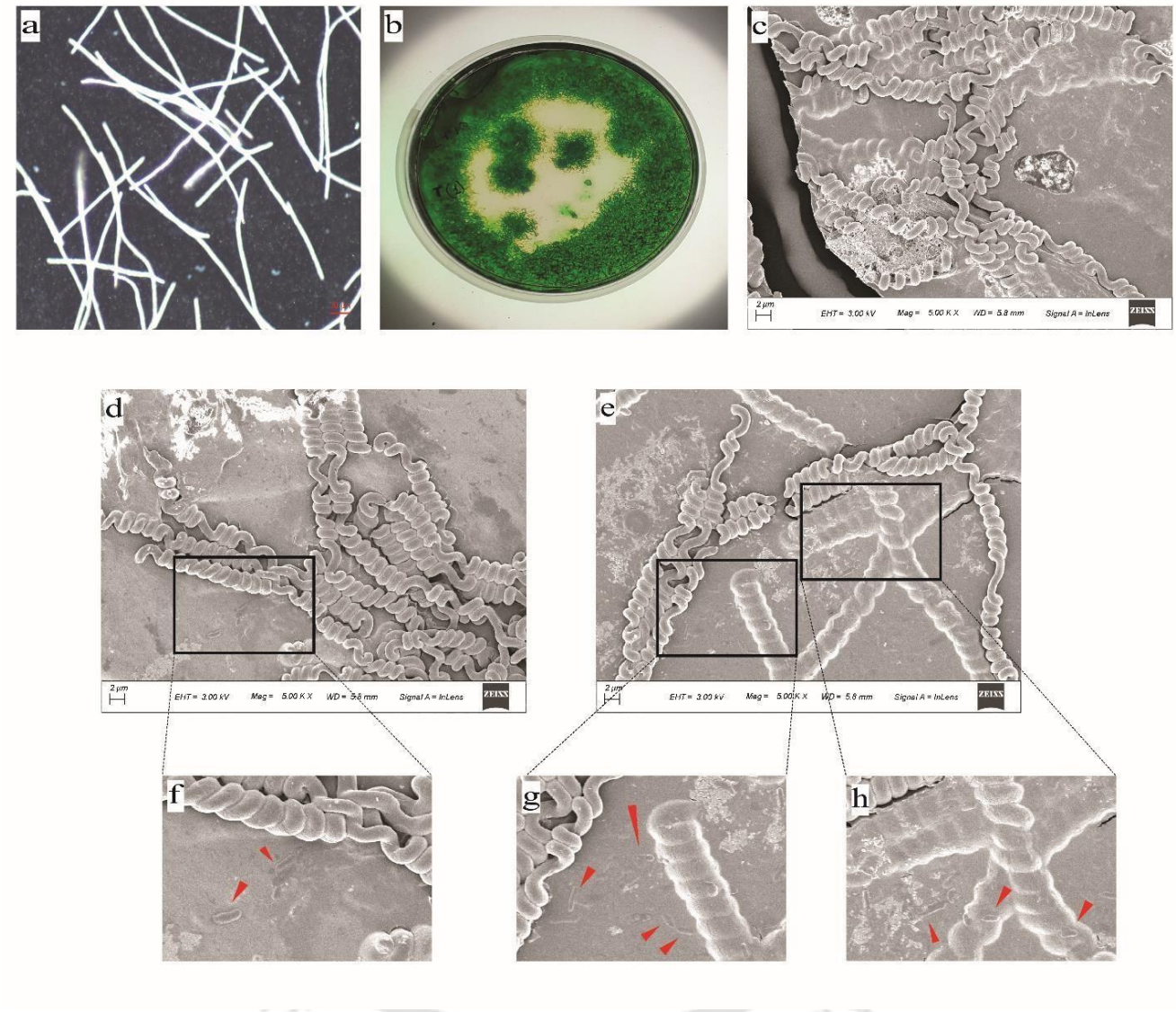

Figure 3. 2. Microscopic characterization of *Spirulina* NCIM 5143. (a) Darkfield microscopic image of 40 days old stationary phase *Spirulina* culture at 50X magnification. White dots around the filaments are heterotrophic bacteria. (b) Mat-like colonies of *Spirulina* spread over a soybean casein digest agar plate. FESEM images of *Spirulina* culture at 5000x magnification (c) from early log phase culture, 15 days old (d) late log phase culture, 25 days old, and (e) stationary phase culture, 40 days old. Magnified areas of (f) figure d showed epiphytic bacteria in the vicinity of *Spirulina* filaments; and magnified areas of fig e showed epiphytic bacteria in the vicinity of *Spirulina* filaments (g) and in direct contact with *Spirulina* filaments (h). Red arrows indicate bacterial cell locations

The observed increase in bacterial load with the increase in cyanobacterial biomass is like the phytoplankton bloom-associated microbial community in natural water bodies. The abundantly exuded phytoplankton organic matter in the extracellular space is degraded and recycled by the bacterial

community (Huisman et al. 2018; Buchan et al. 2014). Thus, to verify this aspect, the macromolecular estimation and spectroscopic analysis of the supernatant were carried out. A gradual increase in carbohydrate (150 mg/L), protein (8 mg/L), phenolic (12 µmole), and total organic carbon (140 mg/L) contents in the supernatant with the increase in biomass was detected, and the amount increased after 40 days of cultivation are shown in the parentheses (**Figure 3.3 a, b**). Further, excitation-emission spectra of the supernatant indicated three distinct regions of fluorescence excitation-emission at wavelengths 275/325 nm, 250/460 nm, and 350/460 nm corresponding to a protein-like material, humic acid-like material, and fulvic acid-like material (Chen et al. 2003; Jiang et al. 2019). The intensity in these three regions was absent in the Zarrouk medium (**Figure 3.4a; 3.5a**). However, the intensity in these regions increased with time as the organic matter accrued in the culture supernatant (**Figure 3.4b-d; 3.5b-d**). This increase in intensity indicates constant recycling and remineralization of the exuded organic matter by the associated microbial flora and possibly cyanobacteria itself leading to the accumulation of refractory fluorescent humic and fulvic-like materials (Romera-Castillo et al. 2010; Coble 1996; Li et al. 2015; Parlanti et al. 2000).

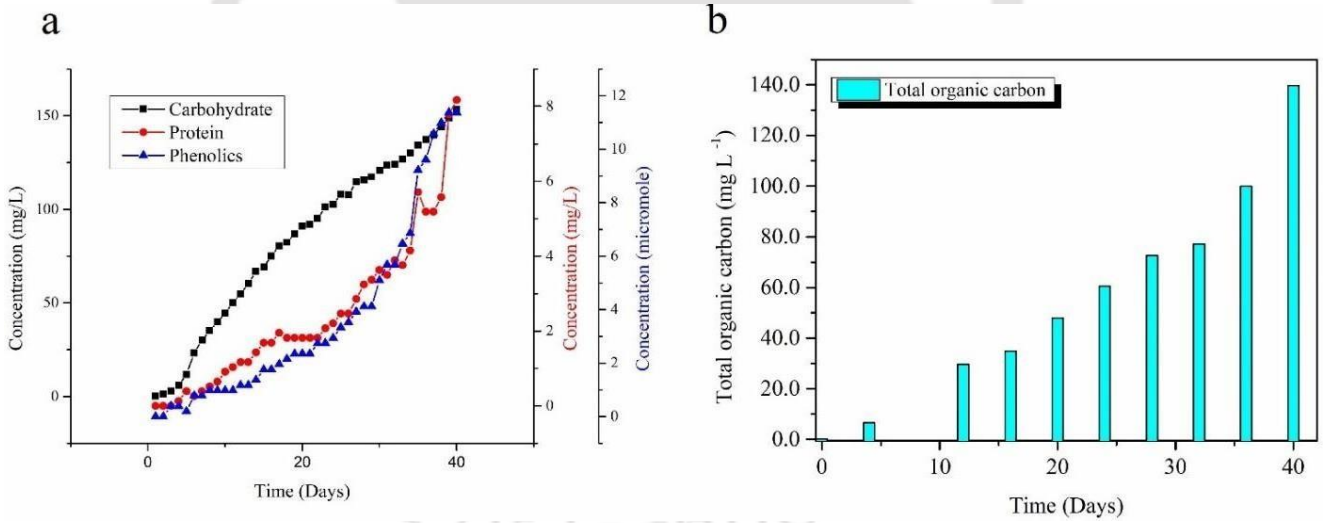

Figure 3. 3. Secretion of (a) carbohydrate, protein, and phenolic compounds and (b) total organic carbon content into the supernatant during different cultivation time of *S. subsalsa* species in a batch culture mode.

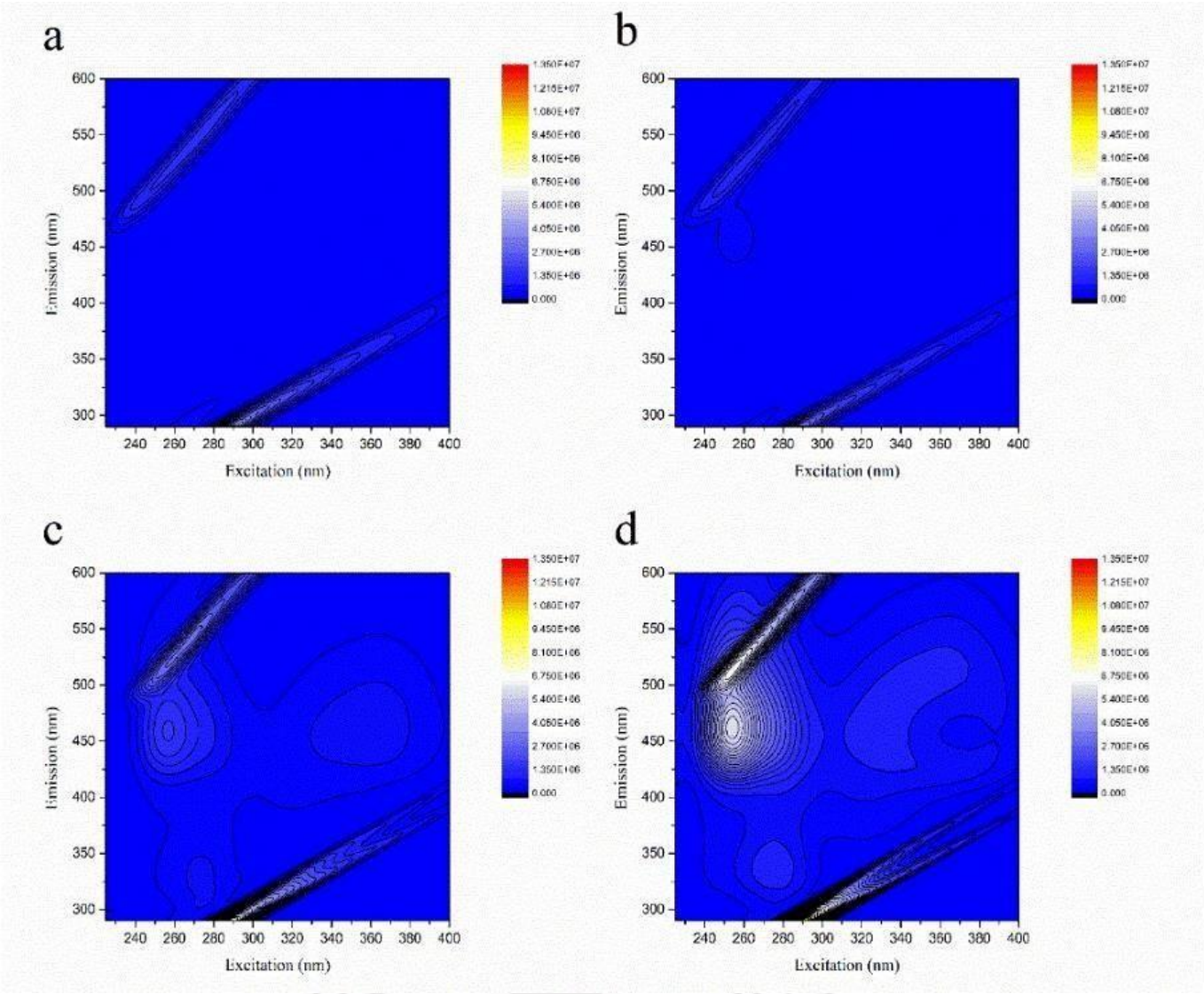

Figure 3. 4. Excitation-Emission spectra of organic matter present in the supernatant of suspension culture of *S. subsalsa* species. Spectra of (a) blank Zarrouk medium (b) early log phase, day 10 (c) late log phase, day25 (d) stationary phase, day35.

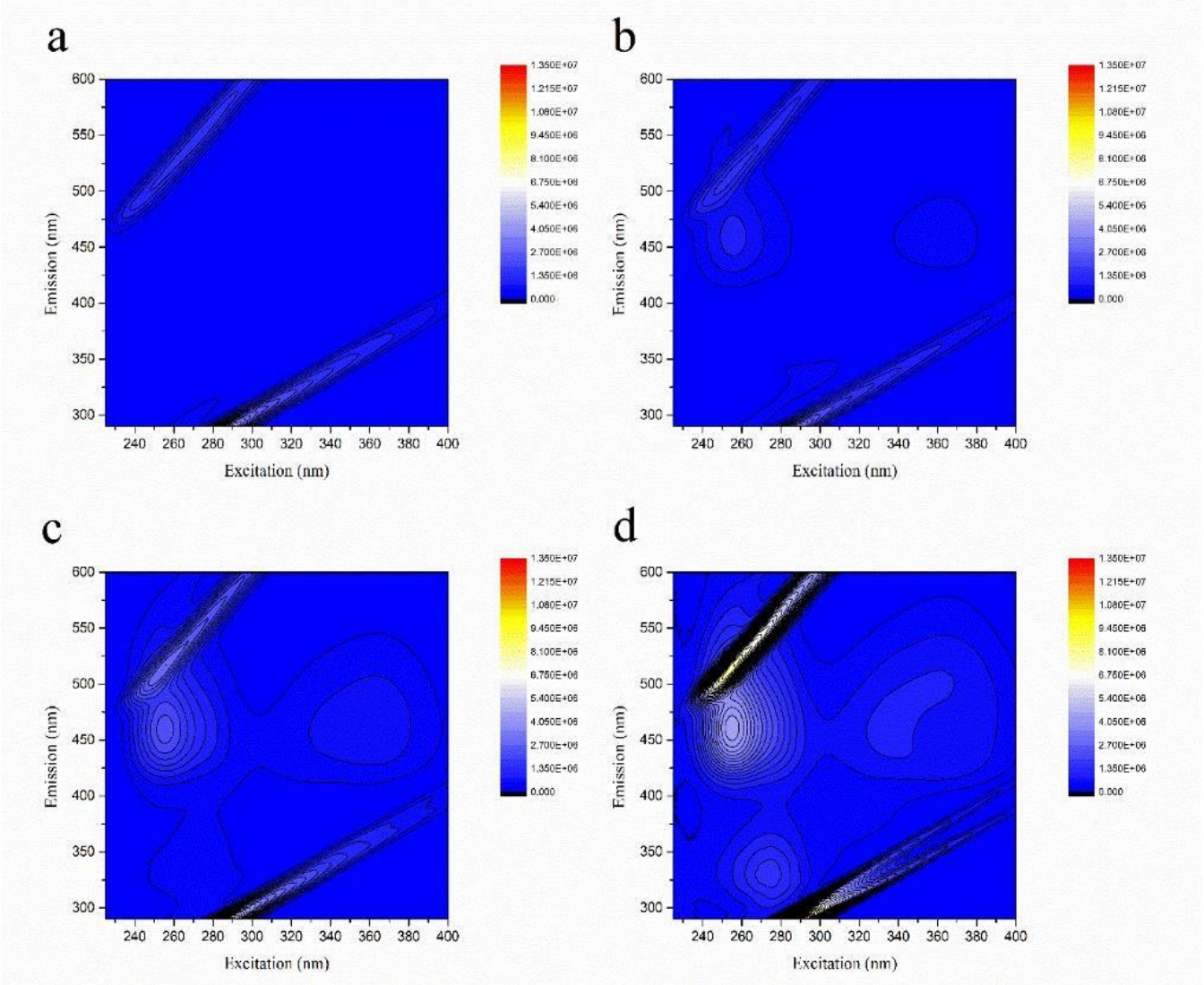

Figure 3. 5 Excitation-Emission spectra of organic matter recorded in the supernatant of *Spirulina* flocs after vortexing in fresh Zarrouk medium. Spectra of (a) blank Zarrouk medium (b) early log phase, day10 (c) late log phase, day25 (d) stationary phase, day35.

Further, four distinct heterotrophic colonies were isolated from the Zarrouk medium agar plate spread with 30 µl inoculum of late log phase culture, and the identity was determined through 16S rRNA sequencing (**Table 3.1**). Based on nucleotide homology and phylogenetic analysis, the strains showed similarity to *Halomonas saliphila, Halomonas campaniensis, Alcanivorax pacificus,* and *Pelagibacterium lentulum* (**Figure 3.6 a-d**). We inferred that these pure culture strains were the dominant members of the *Spirulina*-associated bacterial community as they could form colonies on the Zarrouk medium plate devoid of any organic carbon source, thriving on residual extracellular organic carbon and metabolites exuded by the phototrophic host (*Spirulina*). Gram staining of the strains indicated *Halomonas campaniensis* (Colony B) and *Pelagibacterium lentulum* (Colony D) were gram-negative, while *Halomonas saliphila* (Colony A) and *Alcanivorax pacificus* (Colony C) were found to be containing a mixed population of purple and pink stained bacteria (**Figure 3.7 a-d**). Earlier reports of isolation of these strains reported them to be gram-negative (Gan et al. 2018; Lai and Shao 2012). However, based on our observation we judge these two strains isolated by us to be gram-indeterminate. Colony A, identified as *Halomonas saliphila* had a mixed population of long filamentous rods around 5-6 um and short rods of 1-2um, whereas the colony B of *Halomonas campaniensis* had long filamentous rods of 4-5um. Colony C (*Alcanivorax pacificus*) and D (*Pelagibacterium luteolum*) were short rods ranging from 1.5-2 um in length (**Figure 3.8 a-d**).

Table 3. 1. Morphological and growth characteristics of the isolated pure cultures.

Characteristic	**Colony A**	**Colony B**	**Colony C**	**Colony D**
Species	*Halomonas saliphila*	*Halomonas campaniensis*	*Alcanivorax pacificus*	*Pelagibacterium lentulum*
Cell size (micrometer)	Length (3.76 ± 2) Width (0.443 ± 0.009)	Length (4.82 ± 0.436) Width (0.654 ± 0.116)	Length (1.7 ± 0.16) Width (0.396 ± 0.043)	Length (1.86 ± 0.417) Width (0.427 ± 0.051)
Gram staining	Non-determinant	Negative	Non-determinant	Negative
Cell shape	Flexuous filamentous rods	Flexuous filamentous rods	Rod shape	Rod shape
Colony color	Circular, cream	Circular, cream	Circular, transparent	Circular, translucent
Motility	Motile	Motile	Non- motile	Non- motile
NaCl (%)	0.5-10	0.5-10	0.5-5	0.5-5
pH range (optimum)	7-10 (9)	7-10 (9)	7-10 (9)	7-10 (9)
Temperature (optimum)	4-45°C (30°C)	4-45°C (30°C)	4-45°C (30°C)	15-40°C (30°C)

a

Description	Max Score	Total Score	Query Cover	E value	Per. Ident	Acc. Len	Accession
Haloмonas desiderata strain FB2 16S ribosomal RNA, partial sequence	1208	1943	100%	0	99.11 %	1495	NR_026274.1
Haloмonas kenyensis strain AIR-2 16S ribosomal RNA, partial sequence	1186	1926	100%	0	98.51 %	1371	NR_043299.1
Haloмonas saliphila strain LCB169 16S ribosomal RNA, partial sequence	1186	1907	100%	0	98.51 %	1471	NR_163654.1
Haloмonas lactosivorans strain CFH 90008 16S ribosomal RNA, partial sequence	1186	1913	100%	0	98.51 %	1495	NR_170447.1
Haloмonas campaniensis strain 5AG 16S ribosomal RNA, partial sequence	1181	1882	99%	0	98.79 %	1480	NR_042157.1
Haloмonas qiaohouensis strain YIM QH88 16S ribosomal RNA, partial sequence	1164	1839	100%	0	97.92 %	1506	NR_148256.1
Haloмonas daqingensis strain DQD2-30 16S ribosomal RNA, partial sequence	1164	1882	100%	0	97.92 %	1420	NR_044100.1
Haloмonas mongoliensis strain Z-7009 16S ribosomal RNA, partial sequence	1153	1854	100%	0	97.62 %	1372	NR_043298.1
Haloмonas aidingensis strain Ad 1 16S ribosomal RNA, partial sequence	1149	1839	99%	0	98.03 %	1468	NR_132386.1
Haloмonas campisalis strain 4A 16S ribosomal RNA, partial sequence	1146	1869	100%	0	97.32 %	1400	NR_028702.1

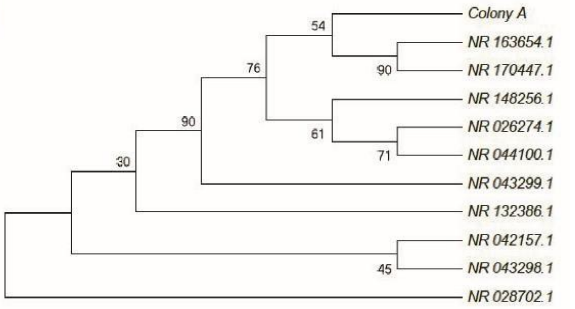

b

Description	Max Score	Total Score	Query Cover	E value	Per. Ident	Acc. Len	Accession
Haloмonas kenyensis strain AIR-2 16S ribosomal RNA, partial sequence	894	1703	100%	0	98.43%	1371	NR_043299.1
Haloмonas desiderata strain FB2 16S ribosomal RNA, partial sequence	889	1677	100%	0	98.23%	1495	NR_026274.1
Haloмonas daqingensis strain DQD2-30 16S ribosomal RNA, partial sequence	869	1717	100%	0	97.45%	1420	NR_044100.1
Haloмonas campaniensis strain 5AG 16S ribosomal RNA, partial sequence	859	1581	99%	0	97.05%	1480	NR_042157.1
Haloмonas saliphila strain LCB169 16S ribosomal RNA, partial sequence	856	1654	100%	0	97.05%	1471	NR_163654.1
Haloмonas vitrinigrifila strain N12 16S ribosomal RNA, partial sequence	852	1573	100%	0	96.86%	1502	NR_117837.1
Haloмonas mongoliensis strain Z-7009 16S ribosomal RNA, partial sequence	850	1512	100%	0	96.86%	1372	NR_043298.1
Haloмonas lactosivorans strain CFH 90008 16S ribosomal RNA, partial sequence	850	1699	100%	0	96.86%	1495	NR_170447.1
Haloмonas compisalis strain 4A 16S ribosomal RNA, partial sequence	841	1590	100%	0	96.46%	1400	NR_028702.1
Haloмonas denitrificans strain M29 16S ribosomal RNA, partial sequence	839	1549	100%	0	96.46%	1489	NR_042491.1

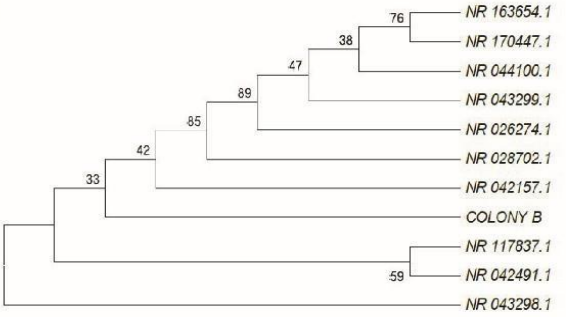

c

Description	Max Score	Total Score	Query Cover	E value	Per. Ident	Acc. Len	Accession
Alcanivorax pacificus W11-5 16S ribosomal RNA, partial sequence	953	1682	99%	0	91.01%	1506	NR_115821.1
Alcanivorax marinus strain R8-12 16S ribosomal RNA, partial sequence	856	1481	100%	0	88.33%	1504	NR_135702.1
Alcanivorax dieselolei strain B-5 16S ribosomal RNA, partial sequence	856	1438	100%	0	88.32%	1504	NR_043106.1
Alcanivorax dieselolei strain B5 16S ribosomal RNA, partial sequence	852	1437	99%	0	88.47%	1529	NR_074734.1
Alcanivorax venustensis ISO4 16S ribosomal RNA, partial sequence	852	1475	99%	0	88.47%	1532	NR_025145.1
Alcanivorax hongdengensis A-11-3 16S ribosomal RNA, partial sequence	850	1429	99%	0	88.21%	1504	NR_044499.1
Alcanivorax nanhaiticus strain 19-m-6 16S ribosomal RNA, partial sequence	845	1468	100%	0	88.06%	1504	NR_152008.1
Alcanivorax gelatiniphagus strain MEBiC08158 16S ribosomal RNA, partial sequence	835	1461	98%	0	88.32%	1152	NR_136483.1
Alcanivorax borkumensis SK2 16S ribosomal RNA, complete sequence	824	1426	98%	0	87.78%	1542	NR_074890.1
Alcanivorax borkumensis SK2 16S ribosomal RNA, partial sequence	824	1426	98%	0	87.78%	1494	NR_029340.1

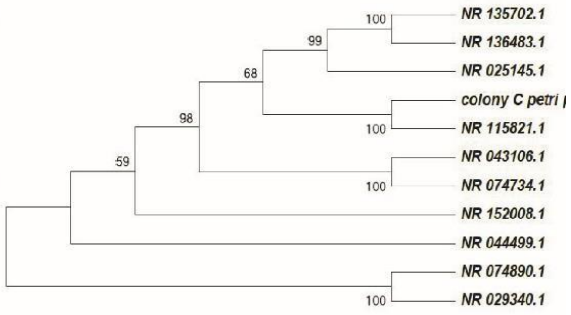

d

Description	Max Score	Total Score	Query Cover	E value	Per. Ident	Acc. Len	Accession
Pelagibacterium lentulum strain B2 16S ribosomal RNA, partial sequence	1029	2057	100%	0	100.00%	1449	NR_157986.1
Pelagibacterium lixinzhangensis strain H642 16S ribosomal RNA, partial sequence	994	1919	100%	0	98.41%	1450	NR_169382.1
Pelagibacterium halotolerans B2 16S ribosomal RNA, partial sequence	977	1935	100%	0	97.88%	1478	NR_102924.1
Youhaiella tibetensis strain fig4 16S ribosomal RNA, partial sequence	974	1832	99%	0	97.71%	1447	NR_136460.1
Pelagibacterium lacus strain XYN52 16S ribosomal RNA, partial sequence	968	1865	100%	0	97.53%	1475	NR_171532.1
Methyloterrigena soli strain M48 16S ribosomal RNA, partial sequence	957	1821	98%	0	97.67%	1420	NR_147729.1
Pelagibacterium halotolerans B2 16S ribosomal RNA, partial sequence	957	1909	99%	0	97.67%	1408	NR_116423.1
Paradevosia shaoguanensis strain J5-3 16S ribosomal RNA, partial sequence	952	1821	98%	0	97.49%	1407	NR_136441.1
Pelagibacterium nitratireducens strain JLT2005 16S ribosomal RNA, partial sequence	946	1882	99%	0	97.31%	1408	NR_132720.1
Pelagibacterium luteolum strain 1_C16_27 16S ribosomal RNA, partial sequence	946	1832	99%	0	97.31%	1408	NR_116053.1

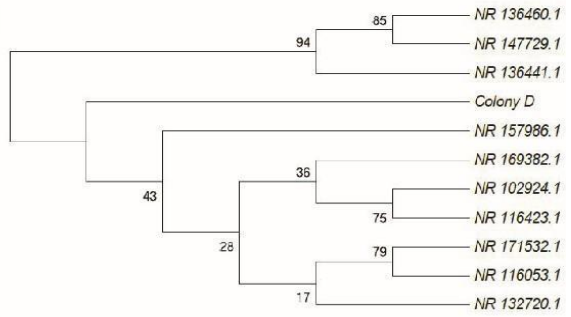

Figure 3. 6. Results of nucleotide homology and phylogenetic analysis for (a) Colony A (***Halomonas saliphila***) (b) Colony B (***Halomonas campaniensis***) (c) Colony C (***Alcanivorax pacificus***) and (d) Colony D (***Pelagibacterium lentulum***). Molecular Phylogenetic analysis was performed by the Maximum Likelihood method. (Kimura 1980)

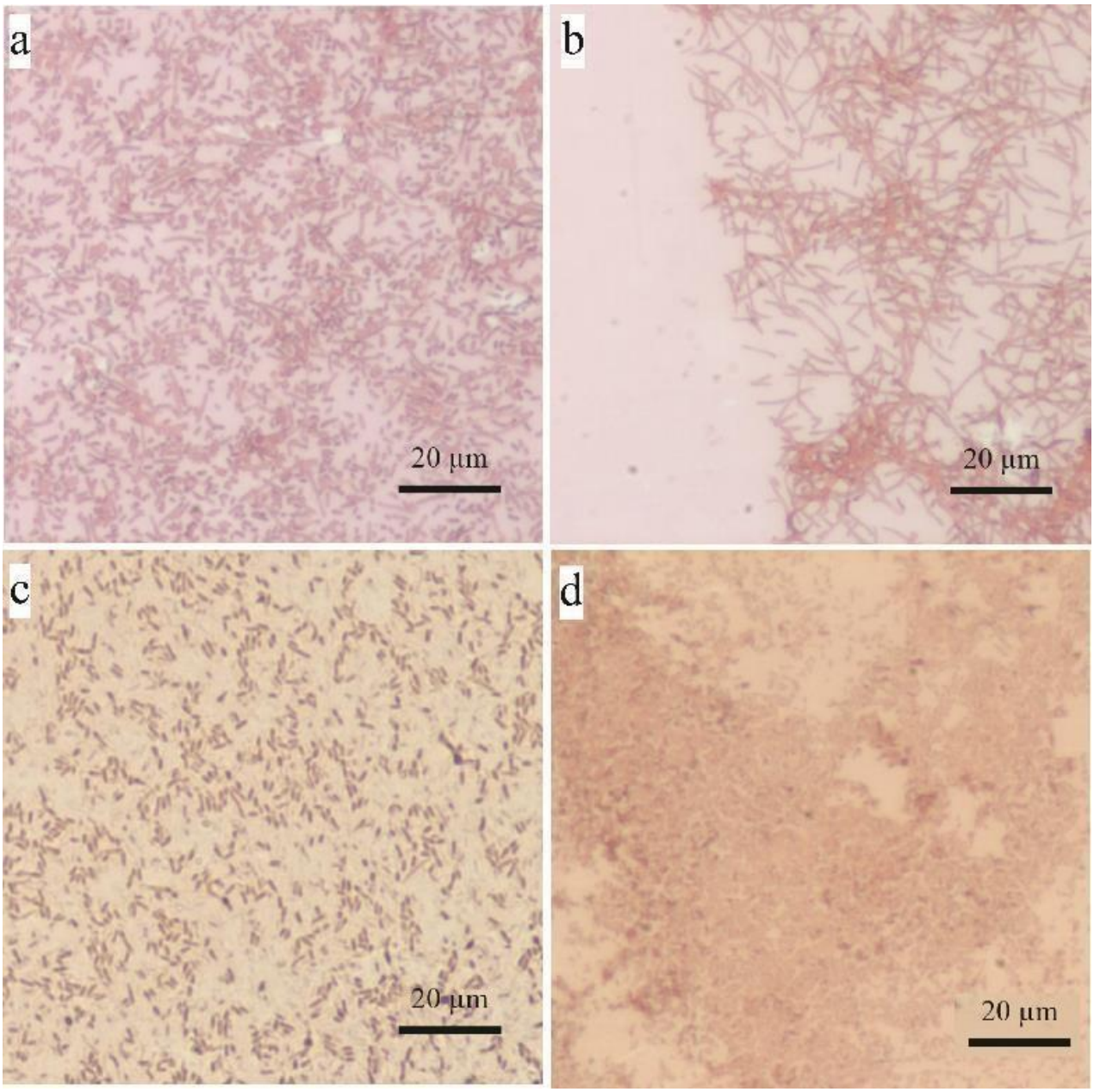

Figure 3. 7. Gram staining of isolated bacterial strains as observed under 50X magnification (a) Gram indeterminate staining of ***Halomonas saliphila***. (b) Gram-negative staining of ***Halomonas campaniensis***. (c) Gram-indeterminate staining of ***Alcanivorax pacificus***. (d) Gram negative staining of ***Pelagibacterium lentulum***.

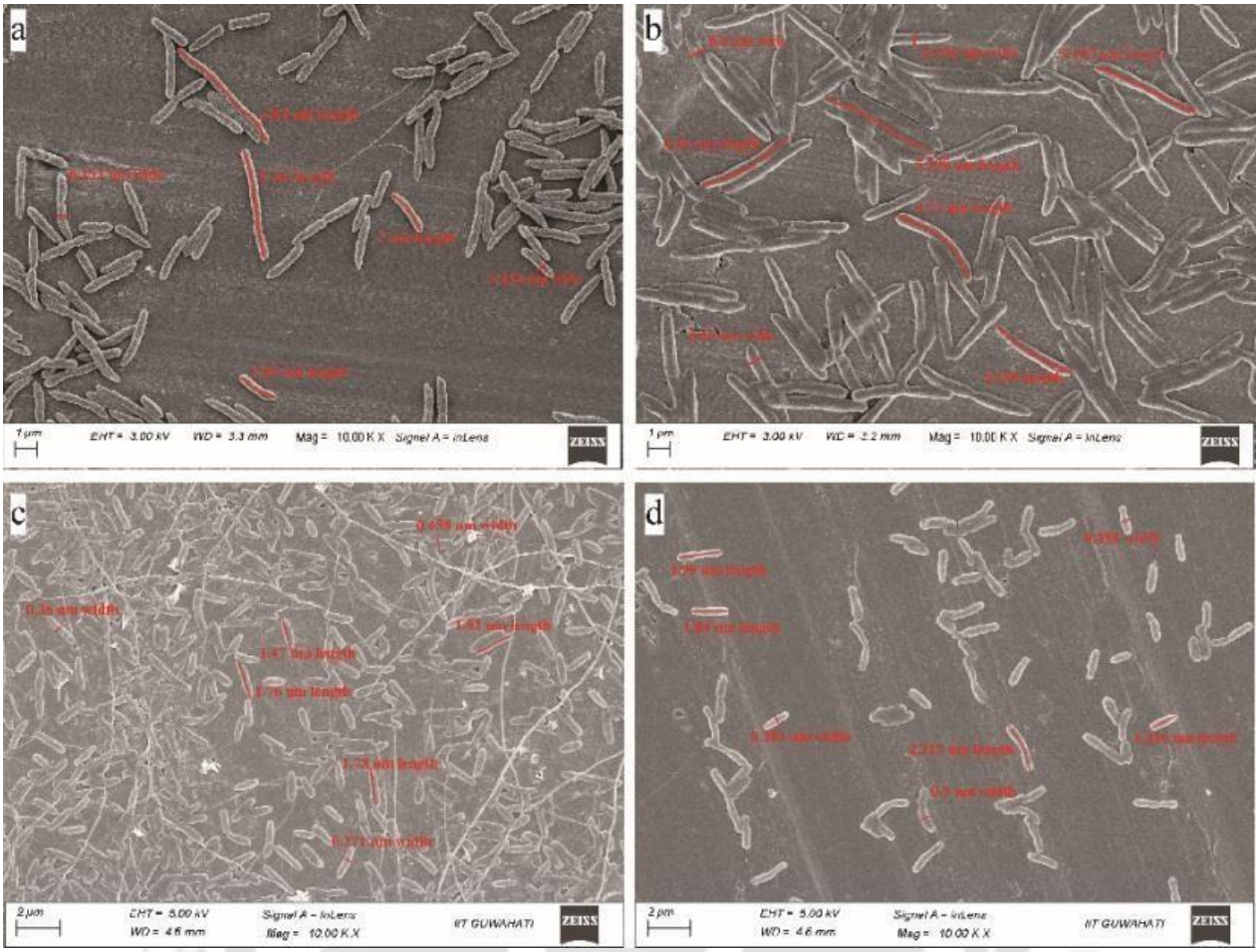

Figure 3. 8. FESEM imaging of isolated colonies. (a) ***Halomonas saliphila*** with rod shapes of variable length varying from 1.8 um to 5.8 um. (b) ***Halomonas campaniensis*** with long filamentous rods of 4-5 um. (c) ***Alcanivorax pacificus*** with short rods 1-2 um. (d) ***Pelagobacterium lentulum*** with short rods around 1-2 um.

Collectively, genera *Halomonas* and *Alcanivorax* belong to the order *Oceanospirillales*. The organisms belonging to this order derive energy by degrading organic matter. Thus, their presence indicates a copiotrophic habitat typical of a phytoplankton bloom or matured phototrophic biofilm (Zhu et al. 2016; Parveen et al. 2013). The genus *Alcanivorax* contains alkane-degrading bacteria often present in marine mats affected by oil spills (Coulon et al. 2012). Abed et al. reported the enrichment of the *Alcanivorax* genus on crude oil from a microbial consortium associated with cyanobacteria (Abed et al. 2007). The presence of this genus in our *Spirulina* culture pointed to the accrual of lipids in extracellular exudate. *Spirulina* species is known to produce a low amount of lipids which must have been released due to the cell lysis or as exudate (Jiang et al. 2019; Conde et al. 2021; Bhakar et al. 2013). The genus *Halomonas* on the other hand has been earlier reported to be growing with *Spirulina* species (Choi et al. 2008). The study by Abed et al. also reported its enrichment from the cyanobacteria-associated heterotrophic consortium on organic acids like acetate and glycolate (Abed et al. 2007). Cyanobacterial strains

produce organic acids under dark anoxic or hypoxic conditions in mat-like biofilms (Stal and Krumbein 1984; Moezelaar et al. 1996; Marquez et al. 1993). *Halomonas* have also been reported to be a predominant species present in the mucus of healthy corals positively interacting with other genera one of which included cyanobacterium, *Synechococcus* (Meyer et al. 2016). Moreover, other interesting properties of the *Halomonas* genus are their ability to undertake aerobic or anaerobic nitrate reduction (denitrification) (Argandoña et al. 2006; Wang et al. 2017), biofilm formation through extracellular polysaccharide secretion (Béjar et al. 1998) and organic matter degradation. The fourth isolated genus *Pelagibacterium*, falls under the order *Hyphomicrobiales* which is known to include nitrogen-fixing strains. The species *Pelagibacterium lentulum* has been previously reported to be isolated from a culture of marine microalga *Picochlorum* sp.122 (Wang et al. 2017). Interestingly, a similar combination of genera *Halomonas, Pelagibacterium* along with *Chelativorans* have been reported to be the core bacterial community in the rhizospheresof *Cyperus rotundus* plants exposed to mining pollution and is crucial for the recovery of plants under stressful conditions (Gao et al. 2021). We believe that this combination of predominant bacterial species isolated by us might be involved in efficient carbon and nitrogen cycling assisting the sustained growth of the host cyanobacterium (*Spirulina subsalsa*) under varied environmental conditions over months as observed in our lab culture (Ataeian et al. 2022).

The *Spirulina* suspension culture when left under static conditions arranged itself into a mat-like two-dimensional aggregated structure at air-water and substrate-water interface. The biofilms were cultured over graphite chips placed under a water column of the Zarrouk medium and in 24 well plates (**Figure 3.9 a-b**). Upon physical disturbance, the biofilm could be easily peeled off from the attachment substrate but maintained a cohesive network of closely packed filaments which was observed under light microscopy and fluorescence microscopy (**Figure 3.9 c-d**). This is a hallmark of the newly conceptualized bacterial biofilm formation process which emphasizes spontaneous cell aggregation rather than surface attachment (Sauer et al. 2022). *Spirulina* and other cyanobacterium are known to produce an excess of extracellular polysaccharide material under abundant light and nutrient conditions as carbon storage reserves (Rossi and De Philippis 2015; Mouhim et al. 1993). Moreover, stress-inducing conditions like nutrient scarcity or overabundance may also lead to the production of excessive polysaccharide secretion into the extracellular matrix (Deschoenmaeker et al. 2016; Deschoenmaeker et al. 2014; Chakraborty et al. 2015). The extracellular organic matter exuded in suspension culture ends up as an extracellular biofilm matrix in static conditions. This biofilm matrix may also contain an extracellular matrix exuded out by the associated heterotrophic consortium. The associated heterotrophic community may also be involved in the constant degradation and rebuilding of the biofilm matrix, recycling and assimilating the cell lysate, exudate, and inorganic minerals through enzymatic reactions (Flemming et al. 2022). This biofilm matrix also contains signaling molecules involved in quorum sensing and cross-talk between community

members and specialized exoproteomes secreted by both the host and heterotrophic bacteria. Many of these have been identified in recent studies and have been categorized as hypothetical proteins requiring further investigations and functional characterization. Visualization of fixed desiccated biofilm at edges revealed *Spirulina* filaments and heterotrophic bacteria encrusted within the extracellular matrix (**Figure 3.9 e-f**). To reveal the exact microbial diversity of the bacterial community, 16S community analysis of the heterotrophic bacteria present inside the matrix was carried out

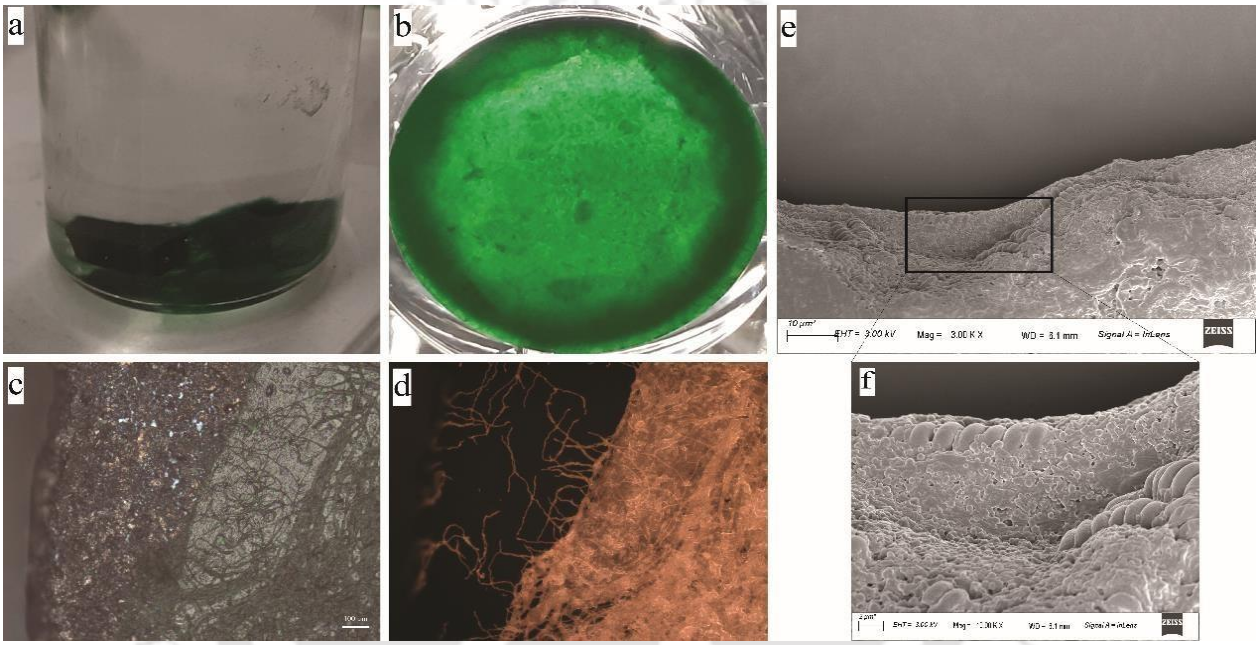

Figure 3. 9. (a) Biofilms growing at the bottom of the water column and on the graphite chip placed at the bottom. (b) Biofilms growing at the bottom of 24 well plates as visualized from below the well against a background of white light. (c) An air-dried *Spirulina* biofilm formed over the graphite chip used for culturing in figure a. The biofilm was peeled at the edge from the left side with the help of a scalpel. Image captured at 20X magnification. (d) Corresponding fluorescence image of the biofilm showing intact biofilm and *Spirulina* filament structures. (e) Electron microscopy image of the biofilm cut out at the edge. (f) Zoomed out image of figure e showing a population of heterotrophic bacteria surrounding the *Spirulina* filaments.

A 50-day-old matured biofilm (exposed to dark conditions between day 25 to 33), thriving in photosynthetic mode was used for sampling bacterial community for 16S analysis. 102 Operational taxonomical units with a low Shannon alpha diversity of 2.7 were detected (**Figure 3.10**). The predominant strains above 1% abundance were genera *Halomonas* (55.44%), *Beijerinckiaceae* family (19.55%), *Devosia* (8.9%), *Alcanivorax* (6.48%), *Streptococcus* (4.27%), *Aminobacter* (1.84%). While the *Halomonas* and *Alcanivorax* genera were the same as isolated and are the hallmark of a nutrient-rich ecological niche, the presence of 4 new genera revealed an interesting aspect of the cyanobacteria-

associated bacterial community in the context of biofilm. Three of these taxonomical units fall under the order *Hyphomicrobiales* (genera *Devosia*, *Aminobacter*, and family *Beijerinckiaceae*). Microorganisms under this taxonomical hierarchical unit are characterized by their ability to nitrogen fixation (Rivas et al. 2003; Weldmichael et al. 2021). This property of the second most abundant family *Beijerinckiaceae* is well documented (Marin and Arahal 2014). The simultaneous presence of nitrogen-fixing and denitrifying bacteria in the consortia along with cyanobacteria is the characteristic of a microbial community that has achieved a state of symbiosis amongst them. Such bacterial communities are robust where a heterotrophic population supports long-term growth and revival of cyanobacteria after stressful periods of nutrient scarcity through efficient carbon and nitrogen cycling of extracellular organic matter and nitrogen fixation (Nair et al. 2022; Zhang et al. 2021). In the context of cyanobacterial biofilm, this species' abundance profile becomes more significant as nitrogen-fixing bacteria require anoxic conditions to perform nitrogen fixation (Wang et al. 2017; Stief et al. 2016). Earlier studies by these authors (Wang and co-authors and Stief and co-authors) have clearly shown that nitrogen-fixing bacteria thrive within extracellular polysaccharide matrices where anaerobic conditions are maintained easily. The biofilm matrix of spontaneously formed *Spirulina subslasa* in our case may act similarly by harboring these nitrogen-fixing strains. Additionally, the genus *Devosia* has the capacity to utilize a wide range of substrates owing to its genomic plasticity giving it the ability to adapt to stressful conditions by catabolizing a wide range of nutrients (Talwar et al. 2020). Members of the genus *Aminobacter* have also been reported to be *methylotrophs* (Artuso et al. 2021). *Streptococcus* genus belonging to the order *lactobacillales* has the capacity to perform fermentation. An earlier study by Parada and coworkers reported enhanced growth of *Streptococcus* on *Spirulina* supernatant extracts (Parada et al. 1998). These strains present inside the biofilm matrix may play a significant role in the recycling, mineralization, and assimilation of organic carbon and nitrogen.

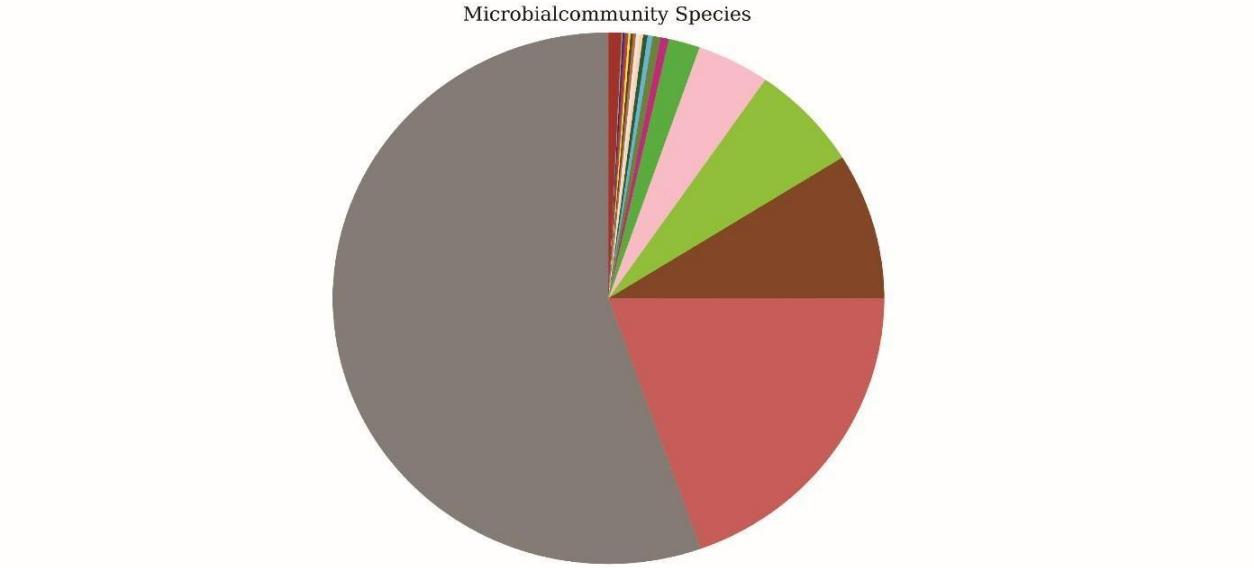

Microbialcommunity Species legend

Legends	Taxonomy	Abundance
	k__Bacteria;p__Proteobacteria;c__Gammaproteobacteria;o__Oceanospirillales;f__Halomonadaceae;g__Halomonas;s__Unclassified	55.44%
	k__Bacteria;p__Proteobacteria;c__Alphaproteobacteria;o__Rhizobiales;f__Beijerinckiaceae;g__Unclassified;s__Unclassified	19.55%
	k__Bacteria;p__Proteobacteria;c__Alphaproteobacteria;o__Rhizobiales;f__Hyphomicrobiaceae;g__Devosia;s__Unclassified	8.9%
	k__Bacteria;p__Proteobacteria;c__Gammaproteobacteria;o__Oceanospirillales;f__Alcanivoracaceae;g__Alcanivorax;s__Unclassified	6.48%
	k__Bacteria;p__Firmicutes;c__Bacilli;o__Lactobacillales;f__Streptococcaceae;g__Streptococcus;s__Unclassified	4.27%
	k__Bacteria;p__Proteobacteria;c__Alphaproteobacteria;o__Rhizobiales;f__Phyllobacteriaceae;g__Aminobacter;s__Unclassified	1.84%
	k__Bacteria;p__Proteobacteria;c__Alphaproteobacteria;o__Sphingomonadales;f__Erythrobacteraceae;g__Unclassified;s__Unclassified	0.48%
	k__Bacteria;p__Firmicutes;c__Bacilli;o__Bacillales;f__Staphylococcaceae;g__Staphylococcus;s__Unclassified	0.47%
	k__Bacteria;p__Actinobacteria;c__Nitriliruptoria;o__Nitriliruptorales;f__Nitriliruptoraceae;g__Unclassified;s__Unclassified	0.3%
	k__Bacteria;p__Actinobacteria;c__Actinobacteria;o__Actinomycetales;f__Corynebacteriaceae;g__Corynebacterium;s__Unclassified	0.26%
	k__Bacteria;p__Proteobacteria;c__Alphaproteobacteria;o__Rhodobacterales;f__Hyphomonadaceae;g__Oceanicaulis;s__Unclassified	0.23%
	k__Bacteria;p__Actinobacteria;c__Actinobacteria;o__Actinomycetales;f__Pseudonocardiaceae;g__Pseudonocardia;s__Unclassified	0.18%
	k__Bacteria;p__Firmicutes;c__Bacilli;o__Lactobacillales;f__Enterococcaceae;g__Enterococcus;s__Unclassified	0.17%
	k__Bacteria;p__Actinobacteria;c__Actinobacteria;o__Actinomycetales;f__Micrococcaceae;g__Rothia;s__mucilaginosa	0.15%
	k__Bacteria;p__Bacteroidetes;c__Bacteroidia;o__Bacteroidales;f__Prevotellaceae;g__Prevotella;s__copri	0.13%
	k__Bacteria;p__Proteobacteria;c__Gammaproteobacteria;o__Pseudomonadales;f__Pseudomonadaceae;g__Pseudomonas;s__Unclassified	0.12%
	k__Bacteria;p__Actinobacteria;c__Actinobacteria;o__Actinomycetales;f__Propionibacteriaceae;g__Propionibacterium;s__acnes	0.11%
	k__Bacteria;p__Proteobacteria;c__Alphaproteobacteria;o__Rhizobiales;f__Phyllobacteriaceae;g__Unclassified;s__Unclassified	0.1%
	k__Bacteria;p__Proteobacteria;c__Gammaproteobacteria;o__Enterobacteriales;f__Enterobacteriaceae;g__Unclassified;s__Unclassified	0.06%
	Others	0.76%

Figure 3. 10. List of most abundant taxonomical units in order from highest to lowest percentage.

3.2 Studies of different electrodes and their set-up in BPV for biofilm formation and electrochemical performance

The non-axenic nature of the biocatalyst and the inherent tendency of spontaneous aggregation over solid substrates and in suspension presented us with difficulty and opportunity at the same time. Conventionally,the mechanistic investigation of electron transfer across cyanobacteria-electrode interface has treated photosynthetic organisms as a functional photocatalytic material that drops cast on an electrode or

allowed to settle through gravity (Tanaka et al. 2021) (Saper et al. 2018). Further, after a brief period of acclimation, the biofilm electrode system is interrogated electrochemically in presence of transient illumination regimes that vary from a few seconds to hours. Thereafter, the voltage/power magnitude is normalized to the chlorophyll content or cell number to estimate electrochemical performance per unit biocatalyst. Adopting this strategy was difficult for us due to the gliding motility of *Spirulina subsalsa* which exhibited phototaxis and buoyancy. Heavy biomass flocs would settle briefly through gravity and rise due to the buoyancy of trapped oxygen afterward. The cells in the culture then move outward from the bulk volume of medium/electrolyte and aggregate into biofilms at air-water and substrate-water interfaces adopting the shape of the culture vessel. Microscopic observations of hydrated biofilms showed a major fraction of biofilm volume is occupied by the extracellular matrix that harbors a mixed population of symbionts. These conditions made it difficult to adopt a conventional approach for experiments. On the other hand, gradual biofilm formation, maturation, non-axenic nature, and simultaneous microbial community progression of the biocatalyst gave us the opportunity to analyze the biophotovoltaic system from a real-world perspective. Any practical application of Biophotovoltaics (BPVs) in open-air conditions would make it nearly impossible to maintain an axenic condition. Additionally, the biofilm matrix and dynamic biochemical reactions within it would be the major point of contact at the electrode interface rather than the cyanobacterial population itself. Recent practical demonstrations of the BPV system have revealed this crucial aspect (**Bombelli 2022**). Thus, we adopted a simple strategy to maximize cell-electrode interactions in accordance with the property of the biocatalyst. H-type MFC setups were assembled from T-25 cell culture flasks with potassium ferricyanide as catholyte. Rectangular strips of Toray and ITO-PET electrodes were stuck to the walls of the setup. A fixed quantity of physiologically healthy wet biomass harvested at the early log phase (days 10-11) was introduced into the anodic chamber (**Figure 3.11 c-d**). This approach ensured maximum biocatalyst electrode interaction as biofilms gradually assembled over the electrode surface and flask walls. The MFC setups were then operated and monitored without an electrical load in open circuit potential (OCP) mode. The MFC electromotive force (E_{emf}) represented by OCP in voltage units in both setups showed a brief period of random variations which was till 100 hours for Toray setups and 35 hours for ITO-PET setups (**Figure 3.11 a-b**). This difference in the period of random variations between the two setups represents the time required for a stable biofilm-electrode interaction to be established. Different electrode structures might be the primary reason for these variations (**Figure 3.13 a-f**). Thereafter, a pattern of sharp increase and decrease in OCP magnitude with the onset of each 8-hour dark phase and 16 hours light phase respectively was observed (**Figure 3.11 a-b**). Upon checking the contribution of individual anodes and cathodes with respect to an Ag/AgCl reference electrode, it was confirmed that these diurnal variations entrained to the illumination regime were due to anodic contribution (E_{anode}) to E_{emf}. The catholyte potential ($E_{cathode}$) was stable at

270 mV throughout the operation. This observation in our experiment indicates that more electrons were accumulating over the electrodes during the dark phase making the E_{anode} negative. This observation stands in direct contradiction to earlier reports on cyanobacterial electrode steady-state potential (E_{anode}) (Pisciotta et al. 2010; Sekar et al. 2014; Zhang et al. 2018; Jeon et al. 2013). All these previous studies have reported electron accumulation on the electrode upon illumination was reflected by a decrease in the magnitude of the E_{anode}. There are a few exceptions that were studied with *S. platensis* biomass smeared artificially on Pt anode that corroborate our finding of decreased E_{anode} during the dark phase (Fu et al. 2009, 2010). However, the reason for this decrease with the Pt electrode smeared with cells is not clear. Notably, Pt is known to possess catalytic activity for both oxygen reduction and organic matter oxidation. It is opined that the Pt electrode itself may contribute a variable magnitude of mixed potentials and internal currents across the electrode surface (McCormick et al. 2015). Herein, we confirmed the increased E_{emf} (due to decreased E_{anode}) of the MFC in the dark phase was due to the interaction of the *S. sub salsa* biofilm with the non-catalytic electrodes, TCP and ITO-PET sheets as discussed above.

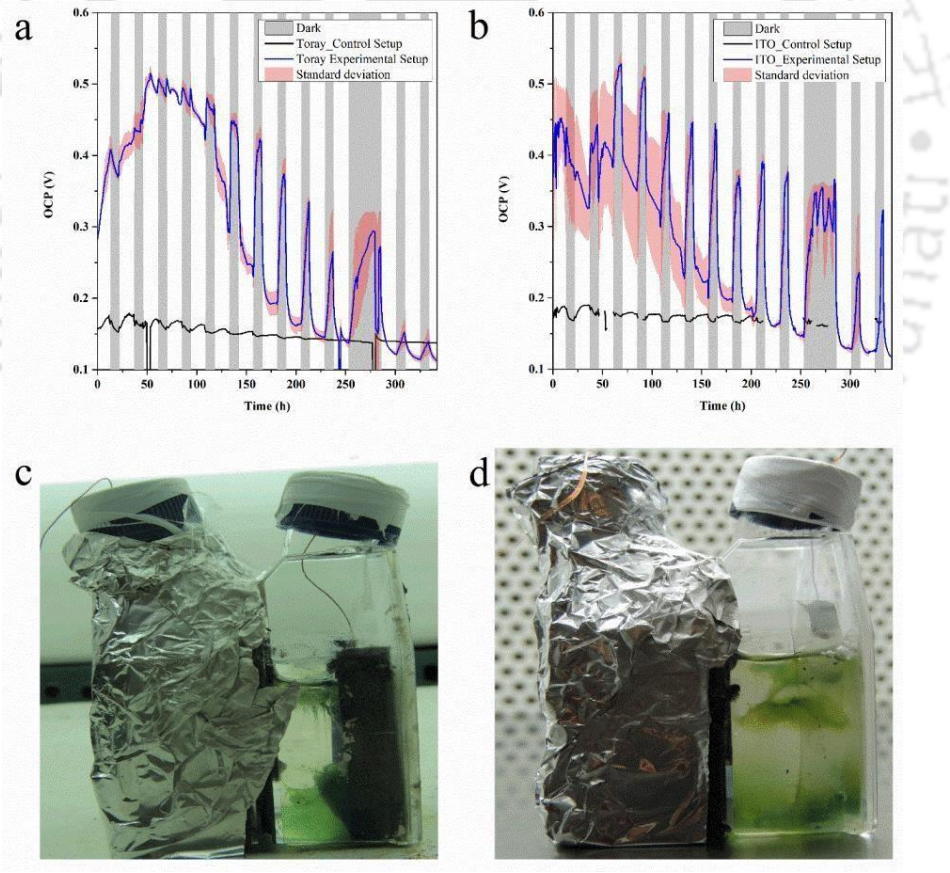

Figure 3. 11. Open circuit operation of MFC setups (a) with Toray carbon paper and (b) ITO-PET sheets as electrodes under a light-dark regime. The voltage profiles are the average of duplicate readings. Readings of MFC setups devoid of biomass are represented by control setups. H-type MFCs assembled from T-25 cell culture flask (c) containing Toray carbon paper and (d) ITO- PET sheets as electrodes.

The E_{emf} response of both the MFC setups could not be sustained beyond 350 hours (14.6 days) due to catholyte crossover or electrode fouling. Thus, these experiments were repeated in a half-cell format for evaluating the reproducibility of the observed phenomena. T25 cell culture flasks were placed horizontally and adapted as half-cell setups (**Figure 3.12a**). Another factor that we aimed to evaluate was the sustainability and renewability of a bioelectrochemical energy harvesting system driven by a photosynthetic biocatalyst. Cyanobacteria, due to their limitless biochemical reducing power, have been envisaged as promising biocatalysts for photocatalytic redox chemistry-based technologies (Jodlbauer et al. 2021). Thus, an ideal BPV system must be operational for a long time if not an eternity.

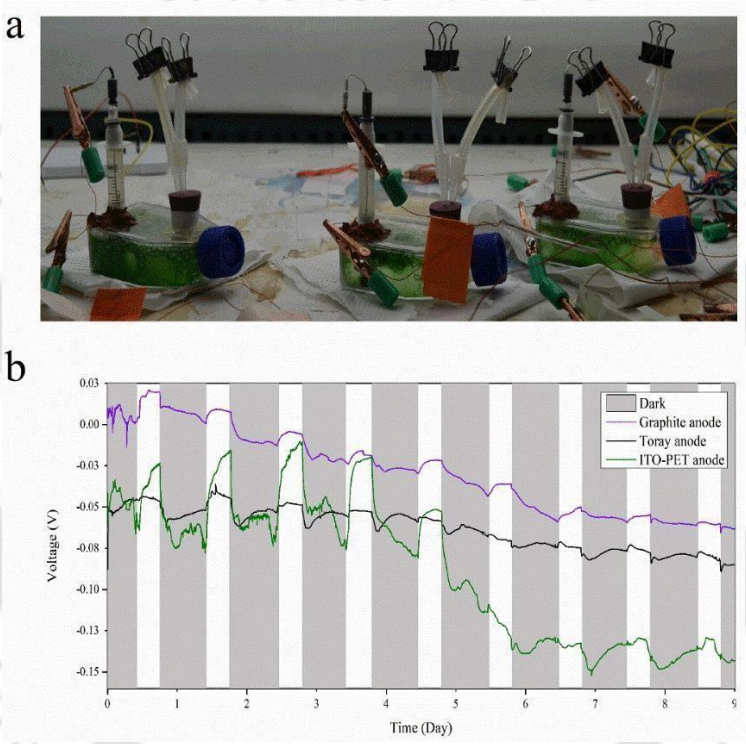

Figure 3. 12. (a) Horizontally placed T25 cell culture flasks equipped with salt bridge enclosed reference electrode, working electrodes (not visible), and a port for adding/withdrawing medium as half-cell setup. (b) Steady-state voltage profile of graphite, Toray, and ITO with respect to an Ag/AgCl reference electrode in the half-cell setup.

Voltage modulations between light-dark cycles were evident in all three setups. The E_{anode} drifted to negative in each dark phase and became positive in each light phase. The modulations were steepest with the ITO-PET setup. ITO has been the most favored material for BPV research due to its minimal surface potential difference resulting in the best electrochemical readout as demonstrated by Ng et al through the Kelvin probe method (Ng et al. 2020). The initial anode potential for both ITO-PET and Toray on day 0 started from a negative magnitude of around -50 mV. On the other hand, the magnitude of anode potential for

graphite electrode started from a positive magnitude of around 10 mV (**Figure 3.12b**). This could be due to differences in the biofilm formation process on three electrode types having different morphology and surface properties (Bombelli et al. 2012). While the ITO electrode has a flat surface (**Figure 3.13c**), the Toray electrode is a bundle of carbon fiber mesh (**Figure 3.13e**). The seemingly flat surface of the graphite electrode on the other hand was found to have a rough irregular surface (**Figure 3.13a**). The nature of the biofilm formed over these setups was different as observed under fluorescence microscopy. The biofilm formed over graphite and Toray paper electrode were visualized in reflected mode microscopy due to opacity. A thick mat of fluorescent *Spirulina* filaments entirely covered the graphite surface (**Figure 3.13b**), whereas, in the Toray fiber electrode, patches of *Spirulina* filament mats only superficially covered the electrode surface in an uneven fashion. The network of long *Spirulina* filaments could not enter the hollow space within the mesh of carbon fibers uniformly (**Figure 3.13f**). However, it can be assumed that biofilm matrix components and associated symbionts might have gained access to the inner structures of the Toray paper electrode. The transparent nature of the ITO-PET sheet allowed us to see through the bulk of the biofilm. It was observed that the bulk of biofilm was occupied by a transparent (non-fluorescent) extracellular matrix. A small subpopulation of *Spirulina* filaments was embedded within this matrix and only the ones closest to the electrode surface were in direct contact with the electrode. The biofilms attached to the ITO-PET sheet however were easiest to be detached with minimal physical force. This was probably due to the smooth flat surface of the ITO electrode.

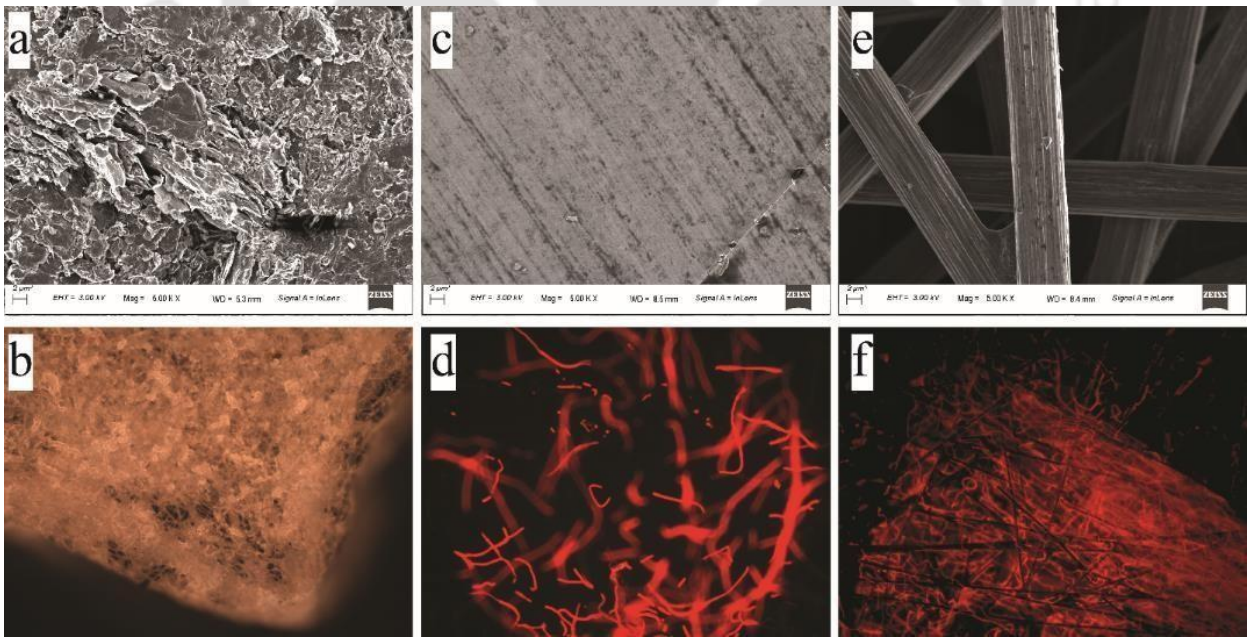

Figure 3. 13. (a) The rough surface of isomolded graphite electrode and (b) the corresponding fluorescent image of biofilm formed over an edge of the graphite electrode. (c) The smooth finished surface of ITO-PET electrode with a visible crack in the lower right corner and (d) corresponding fluorescent image seen through the bulk of *Spirulina* biofilm showing a subpopulation of fluorescent cells within the biofilm structure. (e) Carbon fiber mesh structure of Toray carbon paper electrode. (f) A patch of *Spirulina* mat formed over the Toray fiber mesh. Images b,d,f were captured at 20x.

Further attempts were made to carry out *in-situ* voltammetry investigations with the half-cell setups that indicated the non-suitability of Toray and ITO electrodes and the superiority of the graphite electrode for a long-term electrochemical study of biofilms. It was observed that an ITO electrode kept immersed within the Zarrouk medium furnished smooth voltammograms on day 1 (time-point 1) but poor voltammograms with abrupt changes in current magnitude were observed on the 7^{th} day (time-point 2) (**Figure 3.14a**). This indicates that the ITO film formed over polyethylene terephthalate was corroding in the alkaline mineral-rich composition of the Zarrouk medium over time. Moreover, in presence of biofilms at time points 1 and 2, there was an abrupt increase in both oxidation and reduction current. This pattern of voltammetry had poor reproducibility and could be a result of a combination of electrode corrosion and organic matter oxidation. Even though ITO electrodes have been the most preferred electrodes employed in BPV studies, it was judged to be incompatible with our goal of long-term voltammetric investigation during the course of biofilm formation. A similar investigation on a half-cell setup employing the Toray paper electrode revealed redox species in the Zarrouk medium that interacted electrochemically with the Toray paper. However, at time point 2 these redox peak intensities were decreased with poor resolution (**Figure 3.14b**). We attribute this observation to the gradual loosening of the Toray carbon fiber mesh bundle due to wetting from prolonged exposure to an aqueous medium. Moreover, upon the introduction of biomass and biofilm formation over the electrode, the redox features entirely vanished at time point1, indicating fouling of the electrode surface. At time point 2, this current magnitude was also decreased further (**Figure 3.14b**). Toray carbon paper and other similar carbon fiber-based electrodes have been preferred in experiments where photosynthetic cells were immobilized on the electrodes directly or through some fabrication techniques (Thirumurthy et al. 2020; Sekar et al. 2018; Kusama et al. 2021b). However, the duration of study in such experiments was only a few hours. Toray carbon paper was thus judged to be unsuitable for our goal of long-term electrochemical investigation. Finally, the half-cell setup employing graphite electrodes was evaluated through *in-situ* electrochemistry. It was clearly observed that the blank electrode immersed in the Zarrouk medium after 7 days did not have any redox feature (**Figure 3.14c**). The voltammetry of matured biofilms formed over graphite electrodes showed a consistent irreversible oxidative peak with an onset of around 0.6 V. Moreover, voltammetry between light and dark phases showed a difference in the reduction peak with an onset of around -0.25 V (**Figure 3.14c**). This variation between light and dark phase voltammograms was consistent over many days and represented a change in dissolved oxygen concentration due to the photosynthetic production during the day and its respiratory consumption at night (Zhang et al. 2018; Wenzel et al. 2018a). Graphite electrodes have also been employed in a number of BPV studies and seemed to be a good choice for our objective of long-term electrochemical investigation (Saper et al. 2018; Darus et al. 2015).

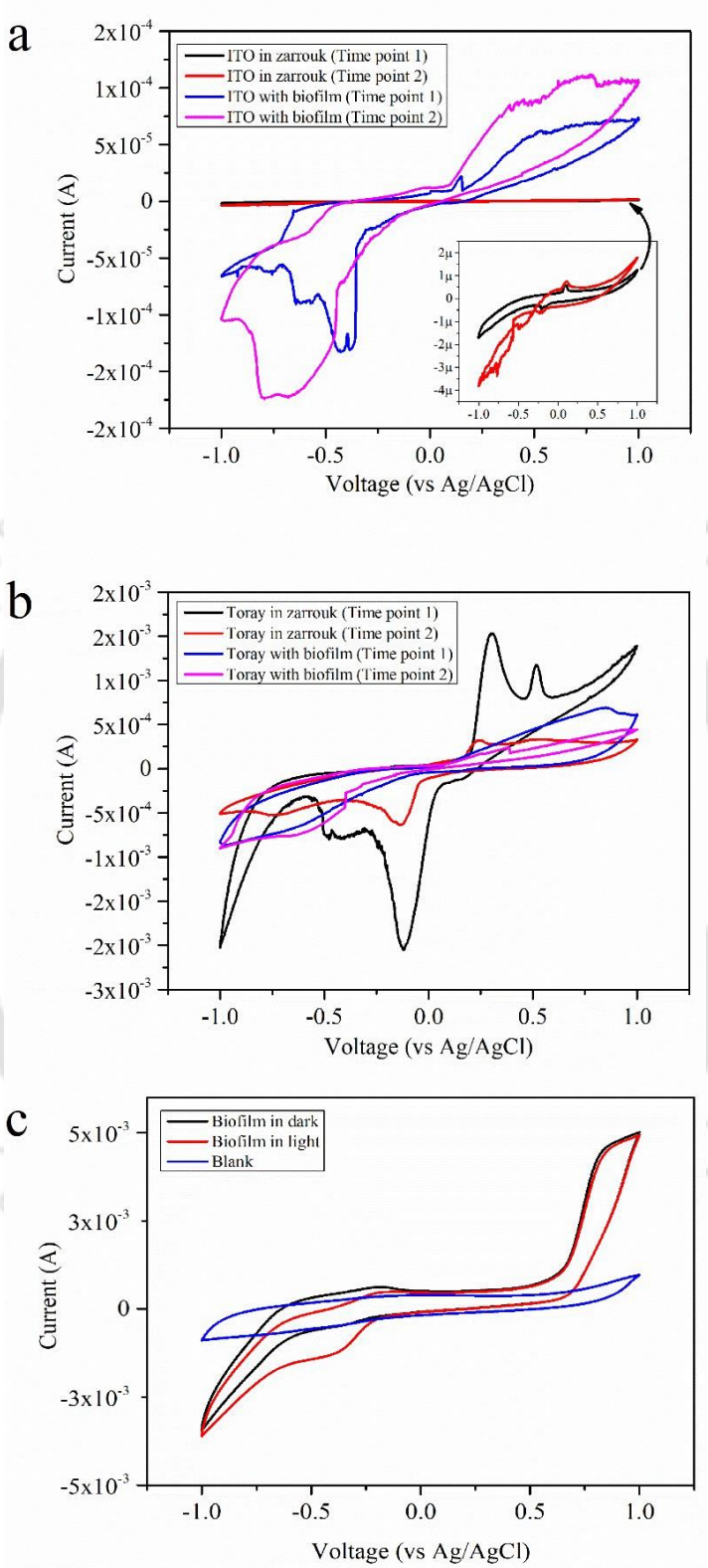

Figure 3. 14. (a) Voltammetric investigations of ITO electrodes within half-cell setups at day 1 (time-point 1) and day 7 (time-point 2). (b) Voltammetric investigations of Toray paper electrodes within half-cell setups at day 1 (time-point 1) and day 7 (time-point 2). (c) Voltammetric investigation of graphite electrode in Zarrouk medium after 7 days (Blank) and 7-day-old biofilm during light (red) and dark (black).

The alkaline nature of the Zarrouk medium and the proximity of the observed redox peak with onset at 0.6 V to the water-splitting region raised doubt regarding the true chemical/biochemical nature of the peak and the associated dissolved oxygen peak. Notably, the biological bicarbonate assimilation process causes the pH drift of the culture towards alkalinity and the alkaline pH favors the water-splitting reaction. Thus, a separate set of *ex-situ* voltammetric investigations of washed *Spirulina* biomass and the supernatant from the cyanobacterial growth curve corresponding to Figure 1b was carried out (**Figure 3.15 a,b**). The voltammetry of the isolated buffer-washed biomass pellet obtained from the suspension culture, acclimated under light for 24 hours, over a 4 mm glassy carbon electrode was carried out at a rate of 1 mV/s. The CV of the biomass indicated the occurrence of two redox reactions: The oxygen reduction peak at -0.250 V (-530 V vs SHE) and an unknown reversible peak with a formal potential of 0.260 V (0.457 V vs SHE) (**Fig. 3.15a**). The peak at 0.260 V was not prominent at higher scan rates indicating the concentration of the linked redox species accumulated in the extracellular exudate was low. This redox species was absent in the voltammograms of the culture supernatant indicating its physical presence in the spaces closely associated with the cell wall (**Figure 3.15b**). Wey et al and coworkers demonstrated the role ofperiplasmic space and associated gated ion channels in imparting characteristic inflection patterns to chronoamperograms of *Synechococcus* and *Synechocystis* (Wey et al. 2021). Moreover, Saper et al and coworkers reported surface-associated redox species that diffused out upon partial fluidization of the cell wall. The redox species were attributed to putative quinones, flavonoids, or temperature-sensitive redox peptides. It is likely that these phenomena occurred in the *Spirulina* cell, releasing redox entities out of periplasmic ion channels following the incubation of cells under non-native conditions, leading to its accrual in extracellular space. The results of cyanobacterial cell voltammetry in the literature are, inconsistent, albeit, most of which have been reported in a positive potential range (**Table 3.2**). Moreover, attributions in most cases are without any molecular validation and largely based on theoretical assumptions.

Table 3. 2. List of redox peaks reported for phototrophs in literature and attributions made therein.

References	Electrode used	Redox peak	Attribution/Observation	Hypothesis
(J. Z. Zhang et al. 2018)	Inverse Opal-ITO electrode	0.34 V vs SHE (0.143 V vs Ag/AgCl)	Benzoquinone or Flavin	(1) Cellular function and osmotic pressure (2) Protection against over reduction of electron transport system (3) Means of

				multicellular communicatio n
(Ng et al. 2020)	ITO and Carbon cloth	-0.45 vs SCE reduction current	Unidentified	To show the presence of reducible species.
(Gonzalez-Aravena et al. 2018)	ITO-PET sheet	0.397 to 0.447 V vs SHE (0.2 to 0.25 V vs Ag/AgCl)	Sigmoidal Cyclic Voltammogram under iron limitation	Redox physiological response to iron limitation.
(Saper et al. 2018)	Pyrolytic Graphite electrode	0.147 to 0.397 vs SHE (-0.05 to 0.2 V vs Ag/AgCl)	Soluble quinone, a flavonoid or a small peptide that is temperature sensitive.	Release of redox entity upon partial membrane fluidization.
(X. Li et al. 2015)	ITO sheet	0.347 vs SHE (0.15 V vs Ag/AgCl) & 0.647 vs SHE (0.45 V vs Ag/AgCl)	Two unidentified redox entities or one compound with two redox active moeities	Probable redox active functional groups like quinone, phenol, phenazine in Humic and Fulvic acid like substance.
(Wu et al. 2013)	Glassy Carbon electrode	297 mV to 397 mV vs SHE (100 mV to 200 mV vs Ag/AgCl)	Cytochrome like protein	Not discussed
(P. Bombelli et al. 2022)	Aluminium filaments	Many unidentified peaks	Not discussed	Not discussed
(Gacitua et al. 2020)	Pyrolytic Graphite electrode with immobilized osmium polymer	0.6 V vs Ag/AgCl	Hypothetical protein	Hypothetical protein
(Tanaka et al. 2021)	ITO sheet	Many unidentified peaks	Peaks similar to Zhang et al,2017 and Saper et al, 2018.	Not discussed
(Kusama et al. 2021a)	ITO electrodes	Centered around 0.1 V vs Ag/AgCl	Peaks similar to earlier studies attributed to quinones and flavins	Low molecular weight compounds (< 3000 Da) secreted in supernatant
Current study	Glassy carbon electrode and Graphite electrode	260 mV vs Ag/AgCl (457 mV vs SHE) and 0.6 V vs Ag/AgCl	Unidentified	Not discussed

The magnitude of the irreversible oxidation peak current at ~0.6 V obtained from the cell-free supernatant increased with the culture age, from 2 µA on day 4 to 42 µA on day 26. This potential was distinct from the oxidative water-splitting reaction identified at ~ 1.15V. Unlike at ~ 0.6 V, the peak current at 1.2 V was accompanied by oxygen reduction at ~ -0.25V (**Fig. 3.15c**). The alkaline pH of the native supernatant (pH 10.66) of a 26-day culture when neutralized down to pH 7, the corresponding peak intensity both at 1.15 V and -0.25 V decreased. The change in pH, however, did not significantly alter the peak intensity at 0.6 V, which proves that this peak is biotic in nature and distinct from the water-splitting reaction (**Fig. 3.15 d-f**). Similarly, peak potentials at 0.6 V from *Gloeocapsopsis* (Gacitua et al. 2020) and 0.5 V from *Synechocystis* (Bombelli et al. 2022) were reported, without, however, attributing any concrete chemical identity to the linked redox potentials. We noticed that the increase in peak current at 0.6V coincided with the upsurge of total organic carbon content including proteins, carbohydrates, and phenolic compounds in the supernatant described above (**Fig. 3.3-3.5**). Thus, we attribute this peak to the irreversible oxidation of biofilm matrix components in direct contact with the electrode surface asobserved in Figure 3.14 c with a graphite electrode.

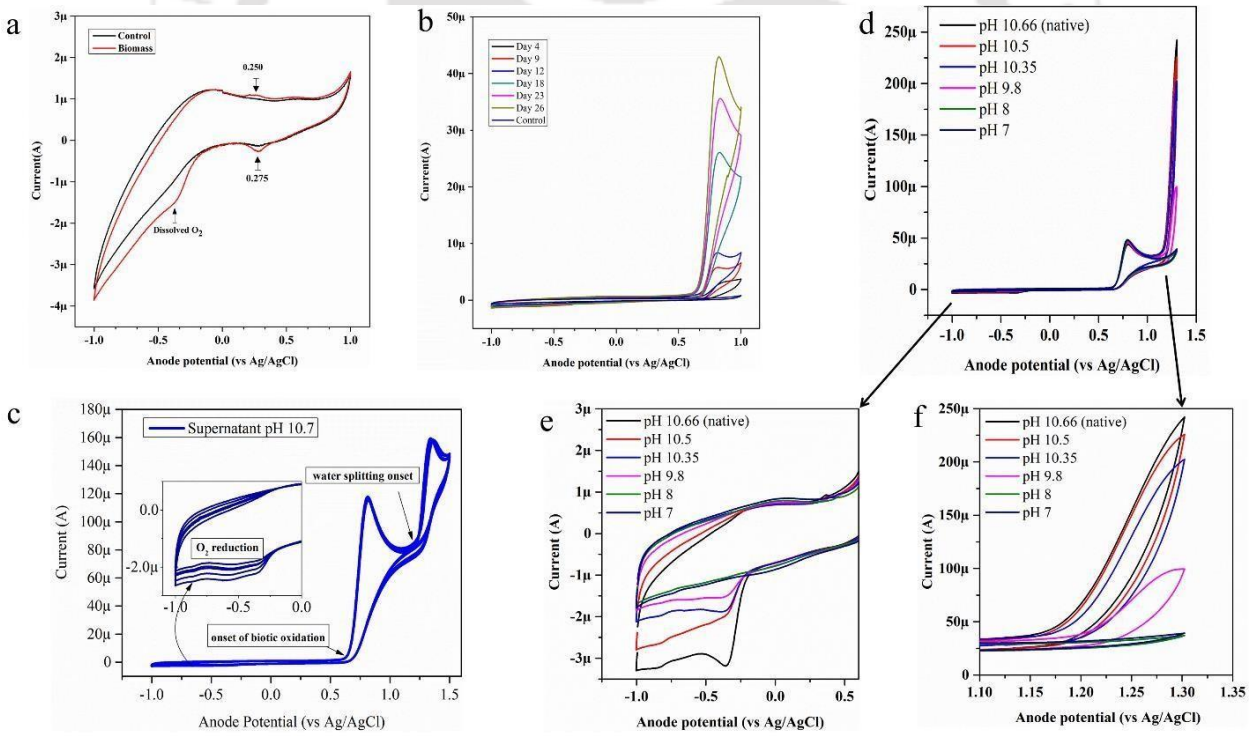

Figure 3. 15. (a) CV of the wet biomass pellet cultured for 48 hours immobilized over GCE (10 mg/12.5 mm^2). For stable immobilization, the biomass immersed in a drop of phosphate buffer (pH 7) over the electrode was incubated for 48 hours under light (2500 lux) prior to analysis. (b) CV of the supernatant (5000 rpm) of the culture harvested on different days. (d) Voltammogram of 26-day-old supernatant showing distinct biotic oxidative peaks and water splitting reactions. (e) CV of supernatant harvested on Day 26. Voltammograms were obtained by lowering the pH to 10.5, 10.35, 9.8, 8, and 7 from 10.66. (e) Zoomed inset of voltammograms in the range of -1 to 0.5 V. (f) Zoomed inset of voltammograms in the range of 1.1 to 1.3 V.

Based on our results from macromolecular estimation, biofilm microscopy, and electrochemistry we propose a hypothetical model. Firstly, any electron flux emanating out of cells (both cyanobacteria and symbionts) because of the primary metabolic activity like photosynthesis, respiration, or fermentation will first end up with the supramolecular assembly of biofilm matrix containing redox moieties and metabolites interspersed in it. These redox moieties may be diverse and dynamic as these are formed because of microbial metabolic activities, macromolecular degradation, cell lysate recycling, and assimilation and are akin to autochthonous humic and fulvic-like substances in the composition (**Figures 3.4 and 3.5**). Further, many unknown exoproteome may also be present in this extracellular compartment with putative redox activity as described in recent literature (Stuart et al. 2016, 2014; Liyan et al. 2014; Vilhauer et al. 2014; Christie-Oleza et al. 2015; Oliveira et al. 2015; Giner-Lamia et al. 2016). While these diverse molecules may act as redox buffers storing electrical charges, their interactions with oxygen under oxic conditions may lead to partial electron quenching leading to peculiar voltage modulation patterns observed in our experiment (**Figures 3.11 and 3.12**). The phenomenon of redox interactions of humic substances with oxygen under recurring oxic-anoxic conditions has been described earlier (Aeschbacher, Sander, and Schwarzenbach 2010; Klüpfel et al. 2014). Further, the voltage output may also be influenced by the presence of artificially introduced redox mediator molecules and their chemical and physical interaction with the biofilm matrix components. A conclusive chemical identity of the endogenously produced redox molecule is often missing in BPV literature because much of it is inaccessible to the electrode surface being enclosed in the tertiary structure of natural organic matter within the extracellular matrix (Pavitt and Tratnyek 2019). As a result of this, voltammograms often show a broad continuum of redox moieties without a distinctive peak as observed at 0.6 V in our study (Helburn and MacCarthy 1994; Wu et al. 2013). A study with *C. raphidophyte* indicates that extracellular humic-like organic matter may contain some redox moieties still accessible to the electrode surface (Li et al. 2015). Further, it was also shown that cyanobacterial exudates of *M. aeruginosa* contain redox moieties capable of reducing iron or dissolved oxygen (Wang et al 2017). The collective electrochemical output of these numerous possible redox reactions within the extracellular matrix and their interaction with oxygen may be responsible for the peculiar decrease of the E_{anode} during the dark period observed in our experiment. Secondly, alternate metabolic modes of *Spirulina* and associated symbionts in direct contact with the electrode surface may be directly interacting with the electrodes through an exoelectrogenic process.

In continuation to the work described above, we examined the electrochemical performance of Toray carbon paper, carbon cloth, and graphite electrodes separately (active geometrical surface area of 1 cm^2 foreach) in the Zarrouk medium using ferri-ferrocyanide as redox indicator at a variable scan rate ranging from 1 to 100 mV s^{-1} in potassium chloride electrolyte (**Figure 3.16 a-c**). This experiment was performed

to see if the electrodes we use show consistent voltammetric behavior for the well-behaved ideal one-electron redox molecules after prolonged exposure to the inorganic growth medium used for growing *Spirulina*. Fitting the obtained voltammograms according to the Randles-Sevcik equation through NOVA 1.11 software furnished values of anodic and cathodic peak currents and anodic and cathodic peak potentials. It was clearly observed that the correlation between the square root of the scan rate and peak current was linear for graphite and carbon cloth. However, for Toray carbon paper, the correlation was not perfectly linear and also showed abrupt variations. Secondly, the highest peak current was observed for graphite electrodes rather than carbon cloth and Toray carbon paper electrodes (**Figure 3.16d**). This indicates that the graphite electrodes had a higher electrochemical surface area in comparison to the other two carbon-based electrodes because of their rough irregular surface. The ratio of the anodic peak current and the cathodic peak current was close to 1 at 1 mV/second and was in the range of 0.9 to 0.87 throughout graphite electrodes. For carbon cloth, the ratio was in the range of 0.79 to 0.84 throughout. For Toray, the value of this ratio showed abrupt variations indicating an unstable electrode structure (**Figure 3.16e**). For an ideal reversible system like a ferri-ferro couple, the difference between anodic and cathodic potential (ΔE) should be 59/n mV where 'n' represents the number of electrons. Thus, ΔE was consistently a minimum for graphite electrodes. These results combined with results of half-cell setup *in-situ* voltammetry indicated the suitability of graphite electrodes for long-term investigation of cyanobacterial biofilm.

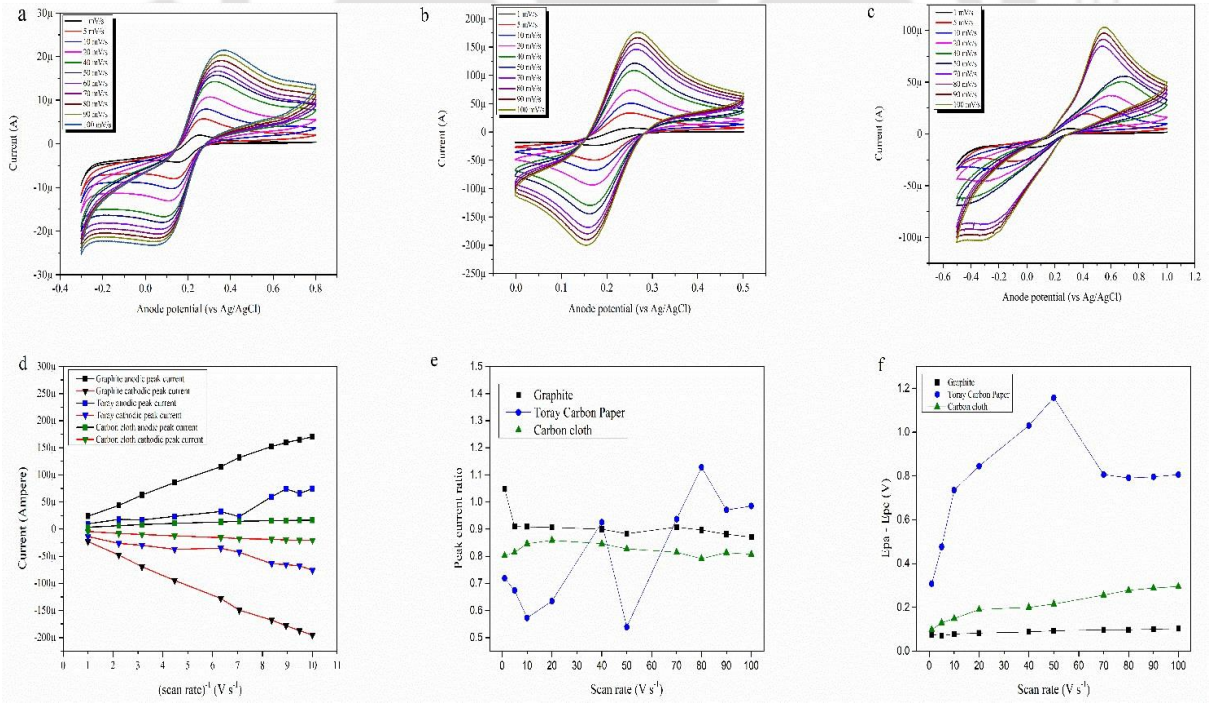

Figure 3. 16. Voltammetry of 1mM potassium ferricyanide at variable scan rates ranging from 1 mVs^{-1} to 100 mVs^{-1} for (a) carbon cloth, (b) graphite electrode, and (c) Toray carbon paper electrode. (d) Correlation between scan rate and peak current. (e)Correlation of peak current ratio and scan rate. (f) Correlation between scan rate and ($E_p - E_p = \Delta E$).

We chose a 2 x 5 cm rectangular piece of graphite material to maximize the interaction between biofilm and electrodes. The voltammetric investigation of this electrode was carried out in Zarrouk medium at different pH to determine the extremities of the potential range at which water-splitting reactions will start. This helped us in distinguishing the irreversible biotic oxidative reactions of the extracellular matrix described above (**Fig 3.15e**) from water-splitting reactions. The results indicated that the water-splitting reaction until pH 10 within 1 V (vs Ag/AgCl) was negligible (**Fig 3.17**).

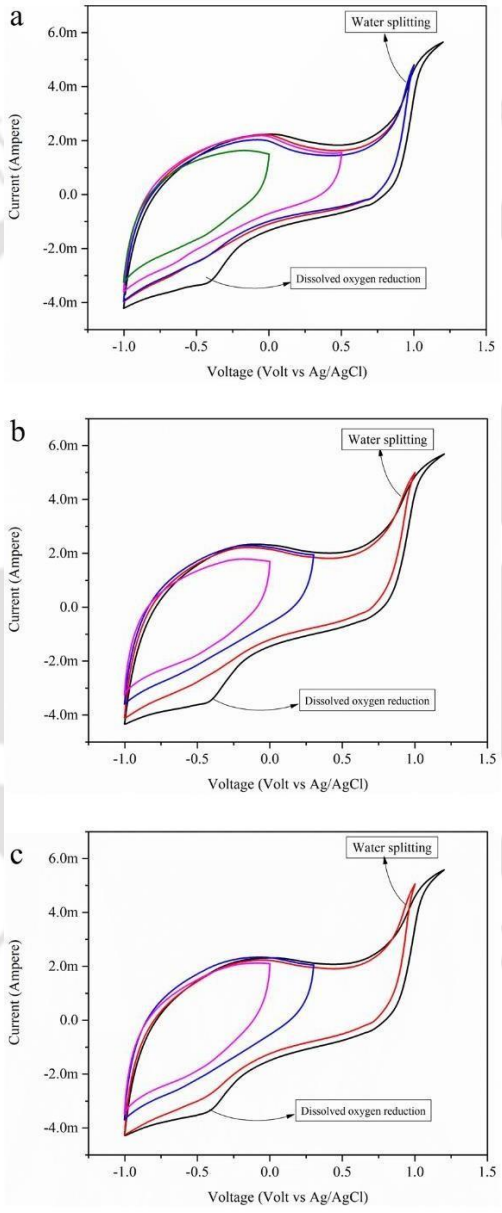

Figure 3. 17. Voltammetry of a 2 x 5 cm graphite bar in Zarrouk medium at variable potential ranges of -1 V to 1.2 V versus Ag/AgCl at pH (a) 9.92 (b) 10 and (c) 10.6.

Finally, a group of five biofuel cell reactors made of glass, plexiglass, and shapes ranging from cube, cuboid, and round bottle were equipped with ITO-PET electrode strips and operated at open circuit potential for 20 to 25 days (**Figure 3.18)**. Two setups made out of T75 cell culture flasks were also operated. Oneof these setups was equipped with a Toray paper electrode. Setups in **Figure 3.18 a,b** were cube and cuboidal in shape and were made out of plexiglass. This material though transparent turned translucent gradually upon repeated usage. Thus, the voltage response in these setups was not entrained in the illumination regime. Moreover, cross-over was quick across the Nafion membrane apposed between the anodic and cathodic half making these setups unsuitable for the long-term study of biofilms. The setup in **Figure 3.18 c** was round and had transparent glass material. The light easily passed through it and photoresponse was visible. However, this setup having activated Nafion apposed between two half also succumbed to a cross-over of toxic catholyte over time. Finally, the transparent walls of the new cell culture flask were highly permeable to light and consistent light-dependent variations in voltage response were observed for 25 days. Moreover, the cross-over across the membrane was slow enough such that the biocatalyst did not die and oxygen could still be detected in the setups after day 25 (**Figure 3.18d**). This slow rate of cross-over across setups could be due to the usage of epoxy resin glue used to seal the leakage between the anodic and cathodic half making the system leakproof. Further, it was also observed that the internal resistance of the t75 flask-based setups was much lower than other setups probably due to reduced electrode distance (data not shown).

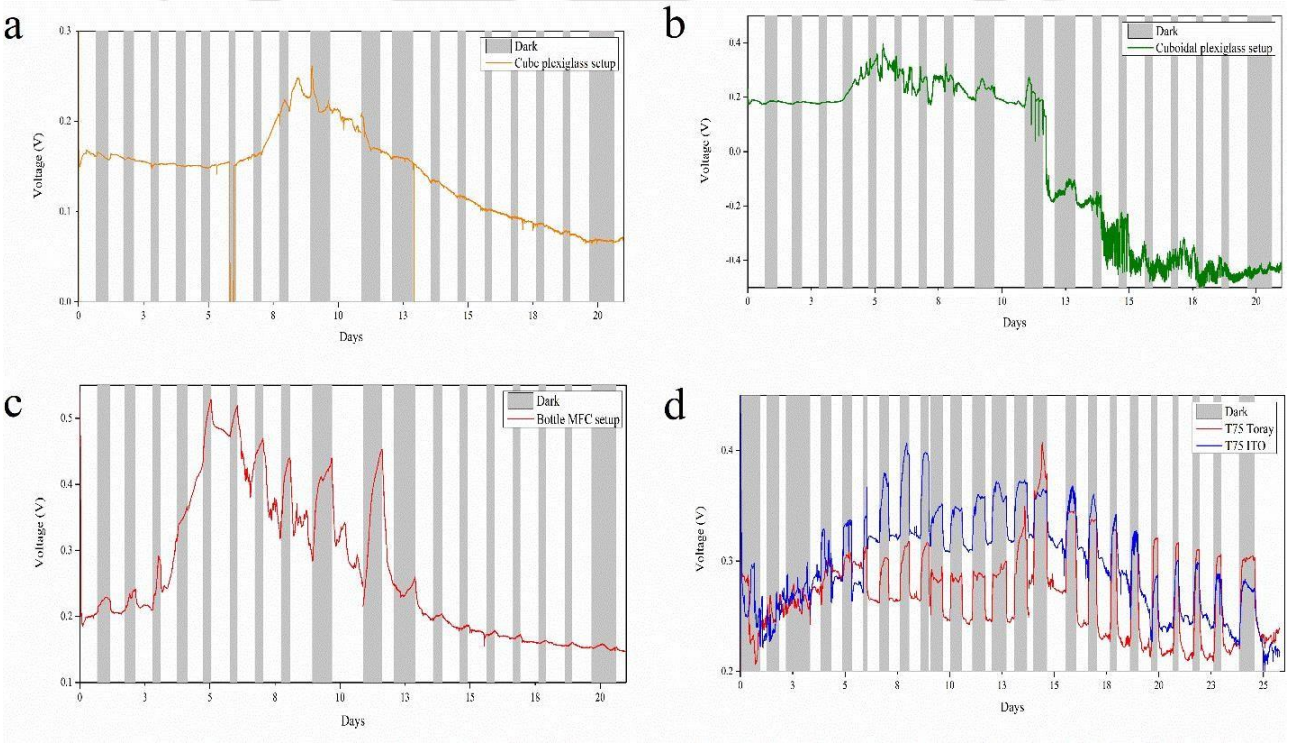

Figure 3. 18. Long-term open circuit operation of biofuel cell setups. (a) A cube-shaped MFC setup made up of plexiglass. (b) A cuboidal shaped MFC setup made up of plexiglass. (c) A round bottle-shaped MFC setup made up of glass. (d) MFC setups assembled from T75-based flasks.

A novel phenomenon of dark-dependent electron accumulation of electrodes was identified. Relevant electrochemical peaks pertaining to *Spirulina* multispecies biofilm were identified. Graphite as a suitable electrode and an MFC setup was confirmed. These setups were used for a thorough electrochemical investigation of the BFCs as described in the following sections.

3.3 The photosynthetic biofilm: Formation, Dark metabolism induction, and Photosynthetic recovery

As visualized in the previous section, the *Spirulina* species had a microbial community associated with it. The cyanobacterium was the primary producer and played the role of host in the multispecies community. Based on the community composition and available scientific literature, it could be inferred that a symbiotic relationship involving an exchange of fixed nitrogen, organic carbon, and its mineralized products was sustaining this mixed community. Further, a multispecies biofilm could be visualized through FESEM imaging of biofilm cross-section (**Fig 3.9 e, f**). Development of such host-dependent multispecies biofilm is inevitable when an energy harvesting system based on the biophotovoltaic principle is taken to the onsite field for real-world applications in an open-air condition (P. Bombelli et al. 2022). Under such conditions, the biological catalyst will have to survive in the face of variable illumination regimes and environmental conditions over time. Accidental exposure to prolonged dark periods is one such scenario, which may cause complete failure of a BPV device driven by photosynthetic organisms that sustain primarily on light accessibility. Cyanobacteria, including *Spirulina* species, during prolonged dark periods, do not grow and divide. Rather, they switch to a maintenance mode thriving on respiratory and fermentative metabolism at the cost of intracellular and extracellular carbon reserves. This maintenance mode however will sustain only until carbon reserves last. Thus, unlike photosynthetic metabolism, dark metabolism is not a sustainable mode for energy harvesting from pure cyanobacterial cultures. On the other hand, the associated bacterial community may play the role of current production during dark periods. A dark metabolism period (around 12 h) of the diel cycle is important for overall health and sustained current generation from cyanobacteria (Hatano et al. 2022; Welkie et al. 2019). From a device point of view, electric performance and viability during prolonged dark phases are crucial for enhancing the shelf-life of the device and minimizing the probability of its failure in absence of light for long periods. Thus, it is imperative to evaluate a multispecies biofilm driven by a cyanobacterial host for its electrochemical performance in the context of versatile metabolic conditions.

Taking this aspect into consideration, a series of biofilm culture experiments were designed with an aim of evaluating the biofilm under versatile metabolic modes i.e. photosynthesis, dark respiration, anaerobic fermentation, and photosynthetic revival. The experiments included the following:

(i) Effect of illumination orientation on biofilm structure.

(ii) Biofilm formation process monitoring through the (light) microscopy in photosynthetic conditions till maturation (12 days) followed by a 9-day period of dark phase to induce respiration and auto fermentation sequentially as reported for *Spirulina* cultures in literature. This followed a brief period of photosynthetic recovery.

(iii) Quantification of the change in extracellular macromolecular composition of biofilms normalized to wet biomass and intracellular glycogen concentrations.

(iv) Field emission scanning electron microscopy (FESEM) of cyanobacteria-dominated multispecies biofilms at the photosynthetic stage, dark metabolism stage, and photosynthetic recovery stage.

(v) Monitoring the change in dissolved oxygen concentration and pH profile of high-volume (250ml) biofilm cultures.

(vi) Studies of the change in redox status of NAD(P)(H) cofactors, and metabolite composition during the dark induction period.

(vii) Effect of ferricyanide exposure on matured biofilm as judged by dissolved oxygen concentration and motility observation through microscopy.

Biofilms initiated in 24 well plates from a fixed wet biomass (~12 mg) of photosynthetically active culture were illuminated from two orientations i.e. bottom and top of wells (**Figure 3.19a, c**). Thereafter the process of biofilm formation was monitored at the same spot through light microscopy at 20X magnification in a time-dependent manner. This approach was adopted to verify the intuition drawn from the observation of static cultures that motile *Spirulina* filaments driven by phototaxis were adopting a flat two-dimensional biofilm configuration on the air-water interface and solid-liquid interface. It was clearly observed that in the well illuminated from below, the filaments were arranged themselves as a neat tightly packed mat-like monolayer within 24 hours of incubation. The filaments in the mat were not motile and this configuration never changed further (**Figure 3.19b**). Whereas, in the well illuminated from the top, highly motile filaments were observed which constantly changed position under microscopic view (**Figure 3.19d**). After a period of 7 days, a gradual thickening of the *Spirulina* biofilm was observed. A group of *Spirulina* filaments was observed to be gliding slowly due to being surrounded by a settled viscous slimy matrix. In the background, a second layer of similar *Spirulina* filaments was visible that showed relatively higher motility (**Figure 3.19e**). Further, on day 12, it was observed that the biofilm became thick enough such that it had to be observed across its thickness by gradually rotating the course adjustment of the microscope. The filaments at the bottom glided at a low speed due to being enclosed in a biofilm matrix. Cells at the middle layer too moved and wiggled at a relatively higher speed due to being close to the top of the biofilm. However, the movement was slow enough to be snapped in an image (**Figure 3.19f-g**). Filaments in the topmost layer, however, moved so rapidly that it was difficult to capture the cell

structure in the image (**Figure 3.19h**). This happened because cells in the topmost layer were not physically bound in the matrix and moved upwards towards light exuding extracellular material that settled down trapping a subpopulation of filamentous cells and other associated symbionts (not visible in light microscopy). Thus, the influence of illumination direction on biofilm structure and the stepwise sequential process of its formation and maturation was revealed and recorded (video available with authors).

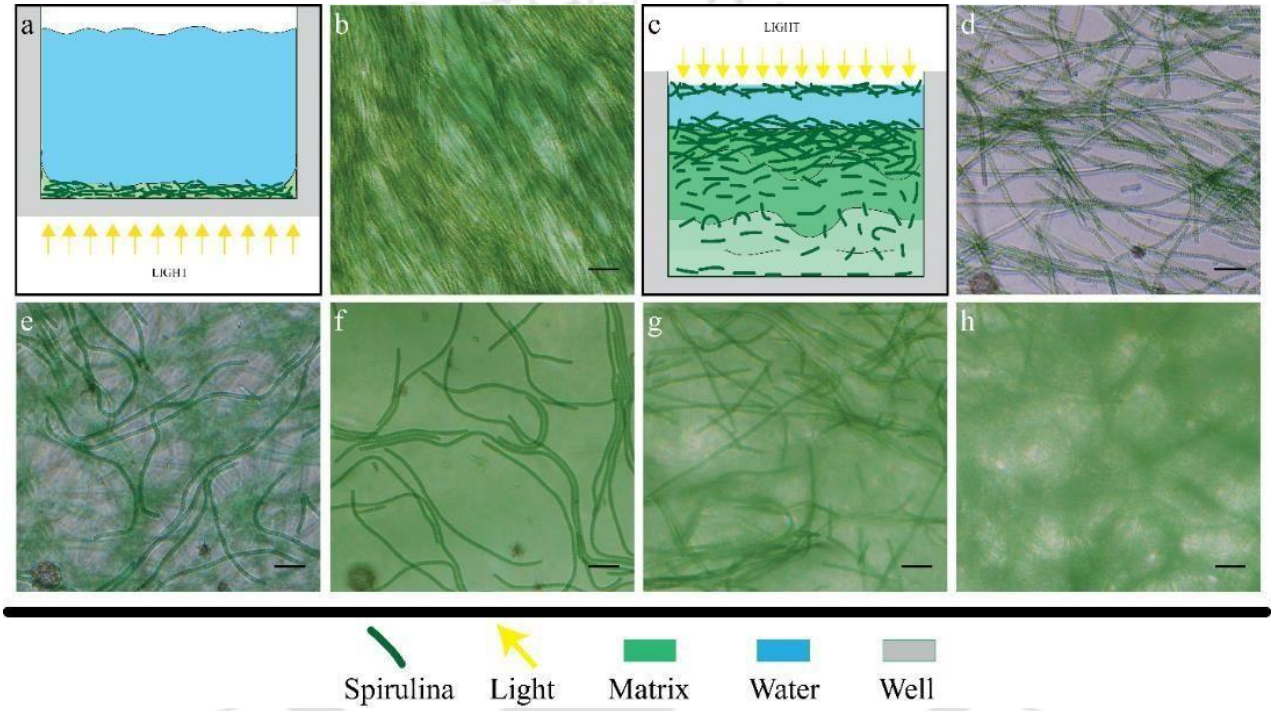

Figure 3. 19. (a) Representation of a well illuminated from below and the thin biofilm monolayer formed at the bottom as a result of it. (b) Inverted light microscopy image of monolayer biofilm. (c) Representation of a well illuminated from above and its effect on biofilm structure. (d) Motile filaments observed in the well on day 0. (e) Spirulina filaments trapped in the bottom layer with a layer of filaments above it seen in background. (f) Bottom layer of Spirulina biofilms with a subpopulation of cells gliding within it. (g) Spirulina filaments in the bulk structure of biofilms. (h) Motile Spirulina filaments in the topmost layer. Scale bars represent 100 µm (20X).

On the 15th day when the biofilm was matured, the culture well plates were sealed and placed in a dark condition for a period of 9 days. Thereafter, the microscopic images were captured before and after dark exposure at two spots i.e. spot 1 (**Figure 3.20 a-c**) and spot 2 (**Figure 3.20 d-f**). Simultaneously, the flat biofilms formed from downward illumination were also observed after 9 days of dark exposure (**Figure 3.20 g-h**). Cells in the flat biofilms illuminated from the bottom showed signs of cell structure disintegration

(red arrows in **Figure 3.20 h**). Upon resuming the illumination, these cells did not recover and no motility was observed in them afterward. A heterotrophic microbial population dominated the flat biofilm after the cell death. The possible competitive interaction causing inhibition of cyanobacterial growth likely led to this stage, as cyanobacteria-heterotroph interaction is dynamic in nature that changes from mutualism to antagonism and vice-versa (Ramanan et al. 2016). On the other hand, motile *Spirulina* cells could still be observed in the thick biofilm cultures developed by illuminating from the top (video captured). However, the color of the extracellular biofilm matrix turned murky green. Upon resumed illumination, the color of the biofilm matrix again gradually changed to a lighter shade of green color. The pigment composition of the biofilms extracted with 90% methanol did not show statistically significant change due to dark exposure. Moreover, the pigment profile of the biofilms was unchanged before and after the dark period (**Figure 3.21 a**). This observation is akin to the earlier observation of Tanaka et al, where no change in chlorophyll concentration of *Synechocystis* under anaerobic dark conditions during ferrihydrite reduction in presence of glucose was observed (Tanaka et al. 2021). The authors inferred that the cellular structures were intact during this period. However, the murky green color of the biofilm matrix background in our experiment could be due to the physiologically stressed cyanobacterial cells (undergoing starvation in dark) with the increase in abundance of the heterotrophic bacterial population relative to cyanobacteria. Nair and coworkers reported this color-changing phenomenon in cyanobacteria- heterotrophic bacteria co-cultures that became older than day 45. The authors attributed this to the physiological stress on cyanobacterial cells and a concomitant increase in the population of heterotrophs (Nair et al. 2022). *Spirulina* and other related species are reported to produce organic acids and hydrogen during dark anaerobic conditions (Ananyev et al. 2008; Carrieri et al. 2010; Marquez et al. 1993). In a mixed-species biofilm microenvironment, organic acids produced by fermentation might have supported the increase in bacterial population as reported by Stuart and coworkers (Stuart et al. 2016; Rabaey and Verstraete 2005). Further, the same group also reported a change in the macromolecular composition of the biofilm matrix due to extracellular organic matter assimilation by cyanobacteria and associated symbionts through enzymatic degradation during both light and dark periods (**Figure 3.20 i**).

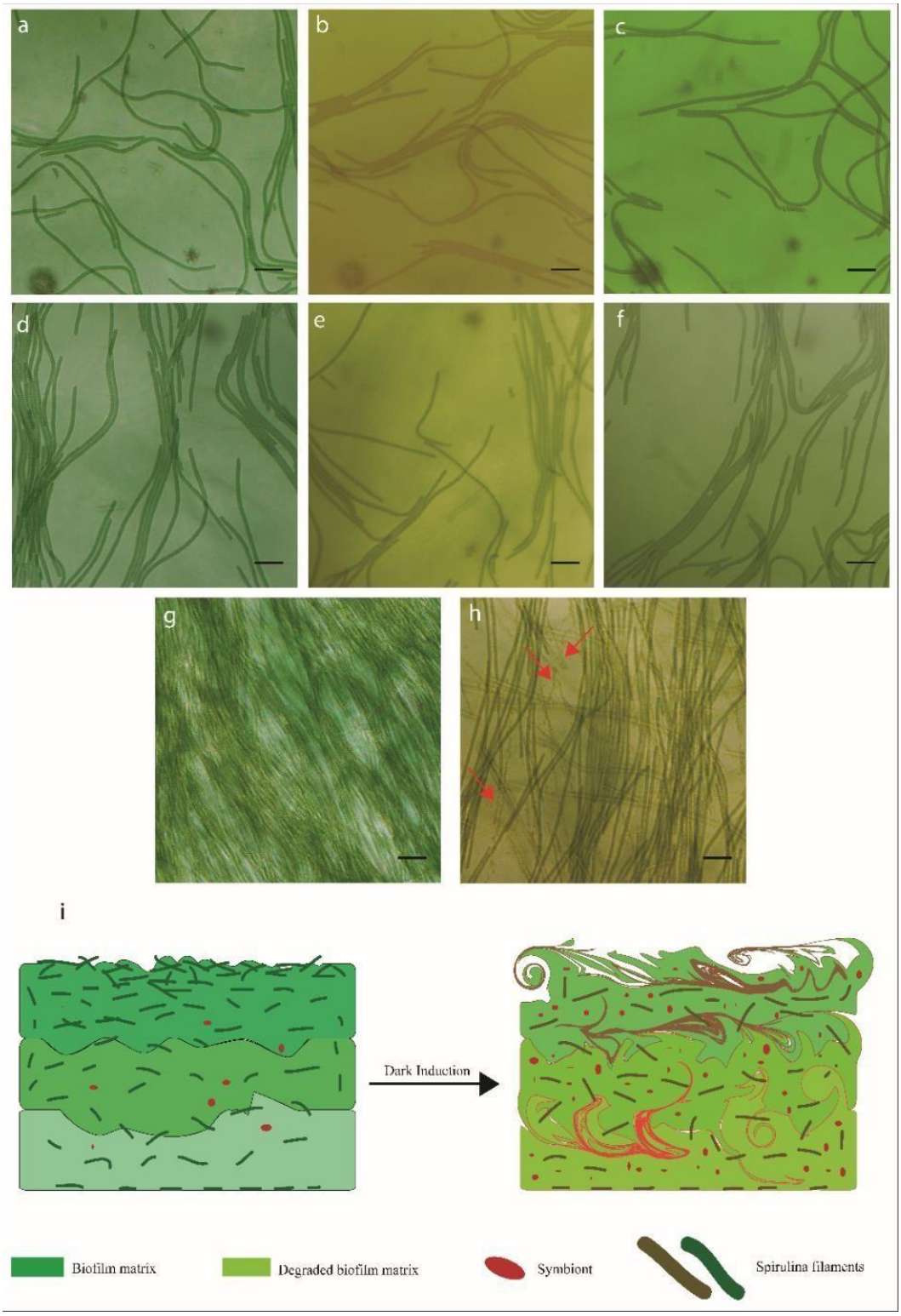

Figure 3. 20. Photosynthetic Spirulina biofilm observed from the bottom layer at two different spots corresponding to (a) and (d). Spirulina biofilm was exposed to dark conditions for 9 days at two different spots corresponding to (b) and (e). Spirulina biofilm after one week period of photosynthetic recovery at two different spots corresponding to (c) and (f). (g) Photosynthetic Spirulina flat biofilms formed from bottom illumination. (h) The flat biofilm after 9 days of dark induction. (i) A cartoon representation of changes in the Spirulina biofilm structure. Scale bars represent 100 µm (20X magnification).

Thus, we analyzed the change in extracellular carbohydrate and protein concentrations during the biofilm initiation, maturation, dark induction, and photosynthetic recovery. Biofilms were cultured in 24 well plates and allowed to mature until 20 days. This is followed by 9 days period of dark induction (days 20 to 29). On the 29th day, the illumination was resumed and photosynthetic mode in the biofilm cultures was revived (**Fig. 3.21b**). It was clearly observed that there was a steep increase in the wet biomass of biofilm from the day of inoculation until day 10 at the rate of ~6 mg day^{-1} prior to reaching the matured growth phase. This period corresponds to the microscopic images shown in Figure 3.19. Within days 10 to 20 of biofilm maturation, the rate of increase in wet biomass was relatively slow (~0.599 mg day^{-1}). During days 20 to 29 of dark metabolism induction, the wet weight of the biofilms marginally changed from 65.35 ± 0.061 mg to 63.62 ± 0.259 mg. Upon resuming the illumination regime, the wet biomass gradually increased to 70.32 mg until day 40. The overall concentration of total carbohydrates was much higher than that of proteins throughout the growth phases (**Fig. 3.21c**). Concentrations of total carbohydrates and proteins started to increase steeply from the early phase of biofilm formation, while at the later phase when the biofilm maturation started (~15th day), the concentration of carbohydrate and protein stabilized to around 17240 ± 53 µg/gm wet weights and 183 ± 7.17 µg/gm wet weights of biofilms, respectively. After 9 days period of dark exposure (~29th day), the extracellular carbohydrate concentration decreasedto 15508 ± 71 µg/gm wet weight and extracellular protein concentration increased to 194 ± 4 µg/gm wet weight. Further, on resumed illumination carbohydrate concentration increased to 16556 ± 85 µg/gm wet weights and protein concentration decreased to 180 ± 5 µg/gm wet weights till day 38. The increase in protein concentration may be due to the secretion of degradative enzymes by heterotrophs and cyanobacteria as reported in studies on cyanobacterial mats and psychosphere (Stuart et al. 2016; Moezelaar et al 1996).

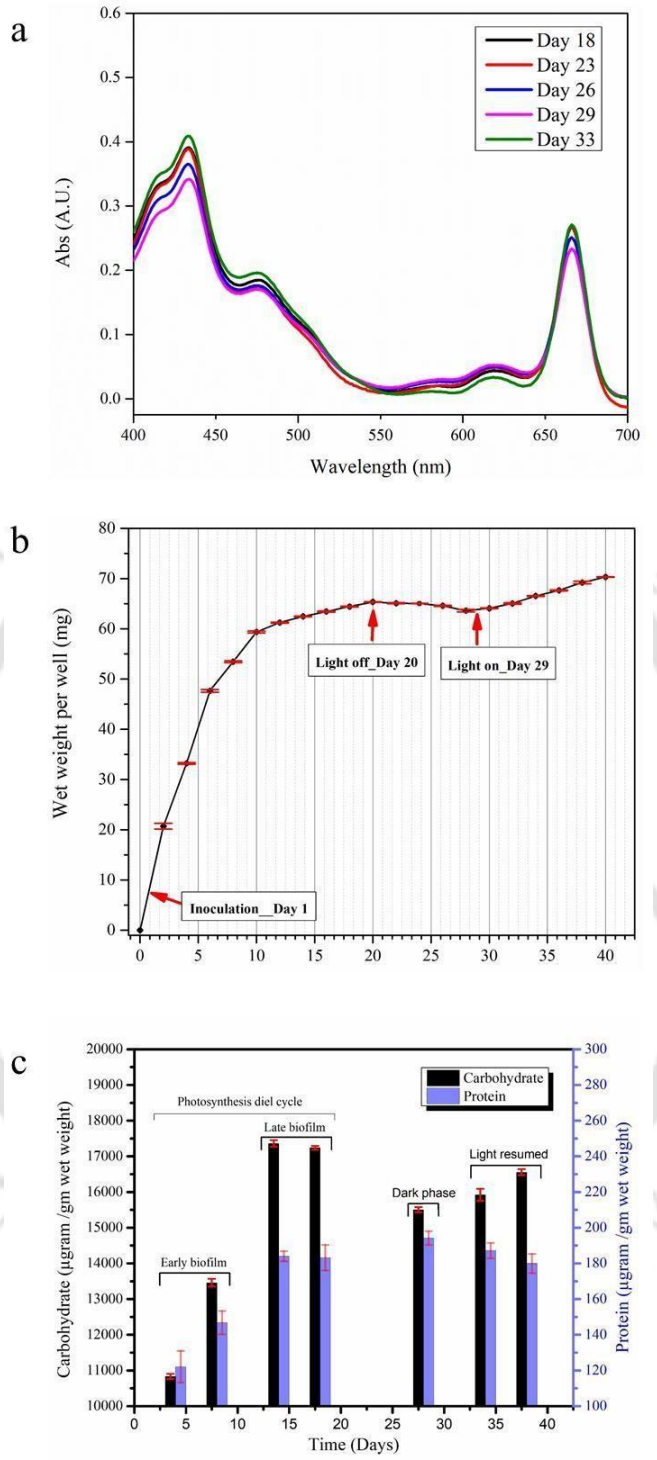

Figure 3. 21. (a) Photosynthetic pigment profile of cyanobacterial biofilms as observed before, during, and after dark exposures. (b) Change in wet biomass from the day of inoculation throughout the process of biofilm maturation, dark induction, and photosynthetic revival. (c) Change in macromolecular composition of biofilm at various stages.

To verify the reproducibility of this observed change in macromolecular composition during a prolonged dark period, three independent experiments (each n = 3) were carried out for extracellular carbohydrates, proteins, and intracellular glycogen (**Fig. 3.22**). Approximately 12.7% decrease in extracellular carbohydrate concentration (p-value < 0.0001) and a 23.58% decrease in intracellular glycogen concentration (p-value < 0.0001) were observed after dark induction of 9 days. The increase in protein concentration on the other hand was ~ 2.24 % which had no statistical significance. Based on these results and the literature survey we make the following inferences: (i) Cyanobacteria fermented intracellular carbon reserves (glycogen) and possibly utilized extracellular carbon reserves as well. In presence of oxygen, energy generation through respiration occurred; further due to the formation of anaerobic zones within the biofilm, anoxic fermentative mode might have been adopted by cyanobacteria. This led to the accumulation of organic acids in the microenvironment. (ii) The organic acid and labile extracellular organic carbon were consumed by the heterotrophic community that included nitrogen-fixing bacteria of primarily family *Beijerinckiaceae* and *gammaproteobacteria* members like *Halomonas* and *Alcanivorax*. This led to a significant increase in the heterotrophic bacterial population with a concomitant decrease in both extracellular and intracellular carbon reserves.

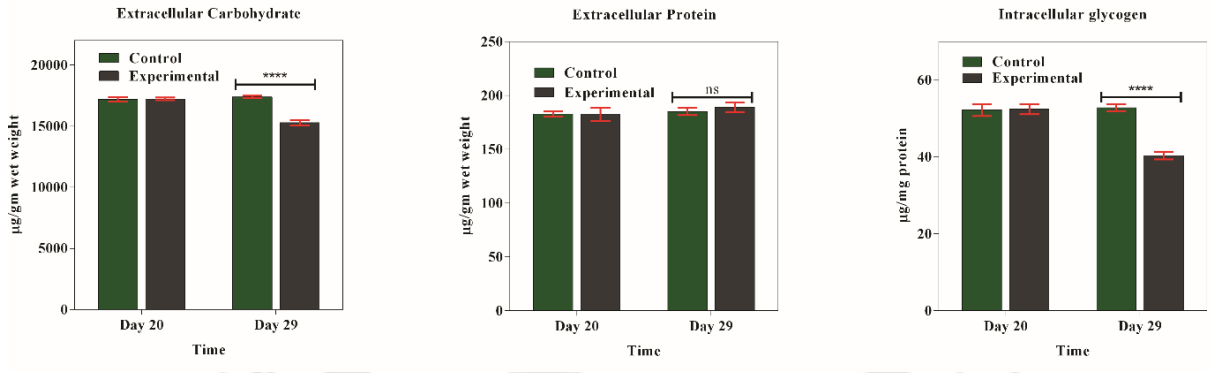

Figure 3. 22. Change in macromolecular composition of photosynthetic biofilms before and after 9 days dark exposure. Extracellular carbohydrate decreased by ~ 12.17 % with a p-value < 0.0001; Extracellular glycogen decreased by ~ 23.58 % with a p-value < 0.0001; Extracellular protein contents increased by 2.24 % with a non-significant p-value = 0.2006.

To verify these inferences, we further carried out FESEM analysis of the biofilms before and after dark exposure and also after photosynthetic recovery. 20 days old, matured photosynthetic biofilms had a clear top view with distinctly visible *Spirulina* filaments. A negligible bacterial population was visible in the image (**Figure 3.23a**). The thick cross-section of biofilm with a width of 36.27 µm was visible within the cellular structure embedded in the matrix at the edge of biofilm at 1900x magnification due to the presence of extracellular polysaccharide (**Figure 3.23b**). After dark induction, the top view of biofilm at 10000x clearly showed a high abundance of the heterotrophic bacterial population, obscuring the distinct

Spirulina filament structures (**Figure 3.23c**). The cross-section of the biofilms was reduced to 18.51 µm due to metabolic consumption of the extracellular matrix (**Figure 3.23d**). A week after the resumed illumination of the biofilm, the bacterial load was reduced to a certain extent. However, the distinct features of the *Spirulina* filaments were not clearly visible at higher magnification (10000x) as earlier (**Figure 3.23e**). This could be due to collective exudate secretion by the cyanobacteria and microbial community concealing the filament structures. However, the width of the biofilm edge/ cross-section increased again to 41.71 µm due to resumed matrix production. In this case, the cellular structures were not visible at the edges. This could be due to enhanced photosynthetic activity after the dark conditions that furnished a lot of dissolved inorganic carbon that was utilized in resumed photosynthetic conditions. Glutaraldehyde fixation and further critical point drying steps cause considerable shrinking of the biofilm structures. Under a water column, in a hydrated state, the real biofilm volume would be much higher due to water retention. The images, however, do accurately capture the change in biofilm structure as inferred from the results of the macromolecular analysis. Moreover, the increased bacterial cell population also verifies our explanation for the color change from green to murky green.

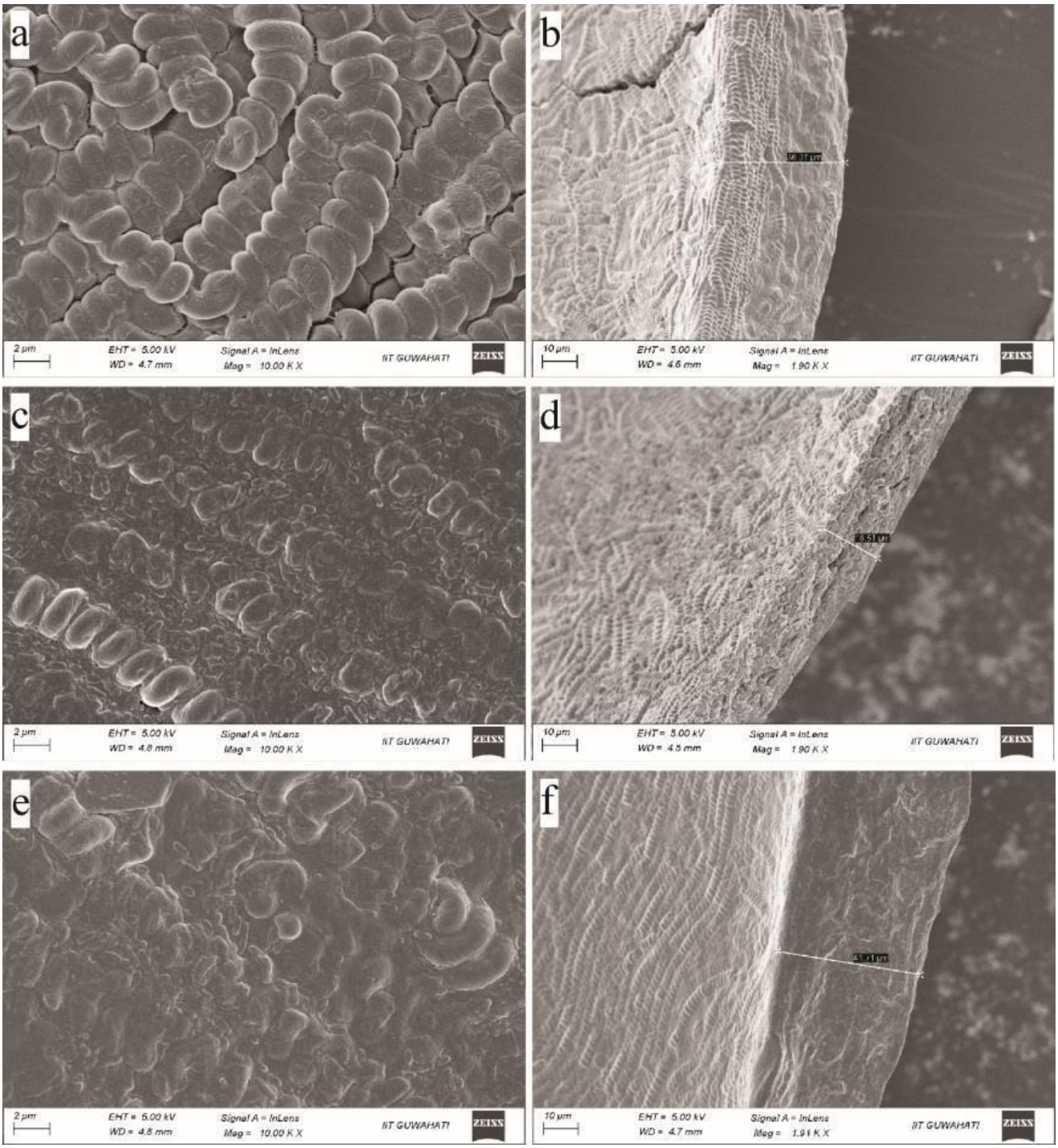

Figure 3. 23. FESEM imaging of Spirulina biofilms in photosynthetic stage (a) Top view of biofilm at 10kx magnification. (b) Side view of biofilm approximate biofilm thickness at 1.9kx; Dark metabolism stage (c) Top view of biofilm at 10kx magnification showing heavy bacterial load. (d) Side view of biofilm approximate thickness at 1.9kx; Photosynthetic recovery stage (e) Top view of biofilm at 10kx magnification showing reduced bacterial load and (f) a thick biofilm structure with an approximate measurement of 41.71 µm.

The metabolic modes adopted by photosynthetic bacteria within the biofilm matrix are influenced by multiple factors like illumination status, oxygen concentration in the microenvironment, and the availability ofcarbon resources. Whether a truly anoxic condition really thrives within the biofilm matrix was further verified by measuring variations in dissolved oxygen concentrations within a biofilm culture grown insidea 250 ml narrow neck conical flask similar to T75 flasks used for the MFC assembly. The probe was placed in the center of the flask, and the readings reflected the equilibrium state between photosynthetic oxygen production and microbial respiratory activity at each instant. Further, the net outcome of the metabolic state adopted by the biofilm can be reflected by the change in pH values. A drift to alkalinity indicates photosynthetic activity whereas a drift to less alkaline pH reflects respiratory activity. A perfect synchrony between illumination status and change in oxygen concentration could be observed for the first10 days as the upper limit of oxygen concentration increased in magnitude at the end of each 12-hour light phase and seemed to stabilize at 300% and beyond (due to upper limit of probe measurement capacity). This indicates a high rate of respiratory oxygen consumption by cells within the biofilm and gradual maturation of the phototrophic biofilm mirroring the pattern of early biomass increase as detected in Fig 3.21b (**Fig 3.24a**). The day-night variation in oxygen concentration must have still occurred between days10 to 25, which seems to be stable at 300% due to probe limitation. Upon cessation of illumination on day25, a sharp decline in the oxygen concentration started which decreased down to a level of ~12% following ~ 30h of onset (25^{th} day) of the dark phase. Intense respiratory activity of cells within the biofilm for a prolonged dark phase must have led to the formation of anaerobic zones in the biofilm. Under such conditions, cells might have adopted a fermentative mode of metabolism for survival. Once the illumination regime was resumed on day 33, dissolved oxygen concentration immediately started to upsurge. Further,it bounced back to 300% saturation within 4 days, showing a sharp increase on each 12-hour light phase. This indicates that the photosynthetic machinery of cells was activated swiftly leading to gradual re-oxygenation of the biofilm microenvironment. The pH profile of the biofilm culture recorded with a similar setup with a dark phase period set around 30-39 days further validated these inferences (**Fig 3.24b**). A gradual increase in the pH magnitude of the medium was observed starting from pH 9.2 to 9.69 until day 30. During the 9 days dark phase, a trend of a gradual decline of pH was observed due to the absence of photosynthesis and possible production of organic acids as a result of fermentative metabolism. Upon resumption of the illumination, a trend of gradual increase in pH was again observed due to revived photosynthetic metabolism that reached 9.82 on day 50. We conclude from these experiments that the metabolic state of a matured cyanobacterial biofilm can be transformed from photosynthesis, respiration to fermentation to photosynthesis again just by modulating the illumination pattern in a lab-based static biofilm culture. Under these conditions, the cellular entities within the biofilm produce and consume

macromolecules depending on their adopted metabolic state, influenced by the illumination status and oxygen concentration in the microenvironment.

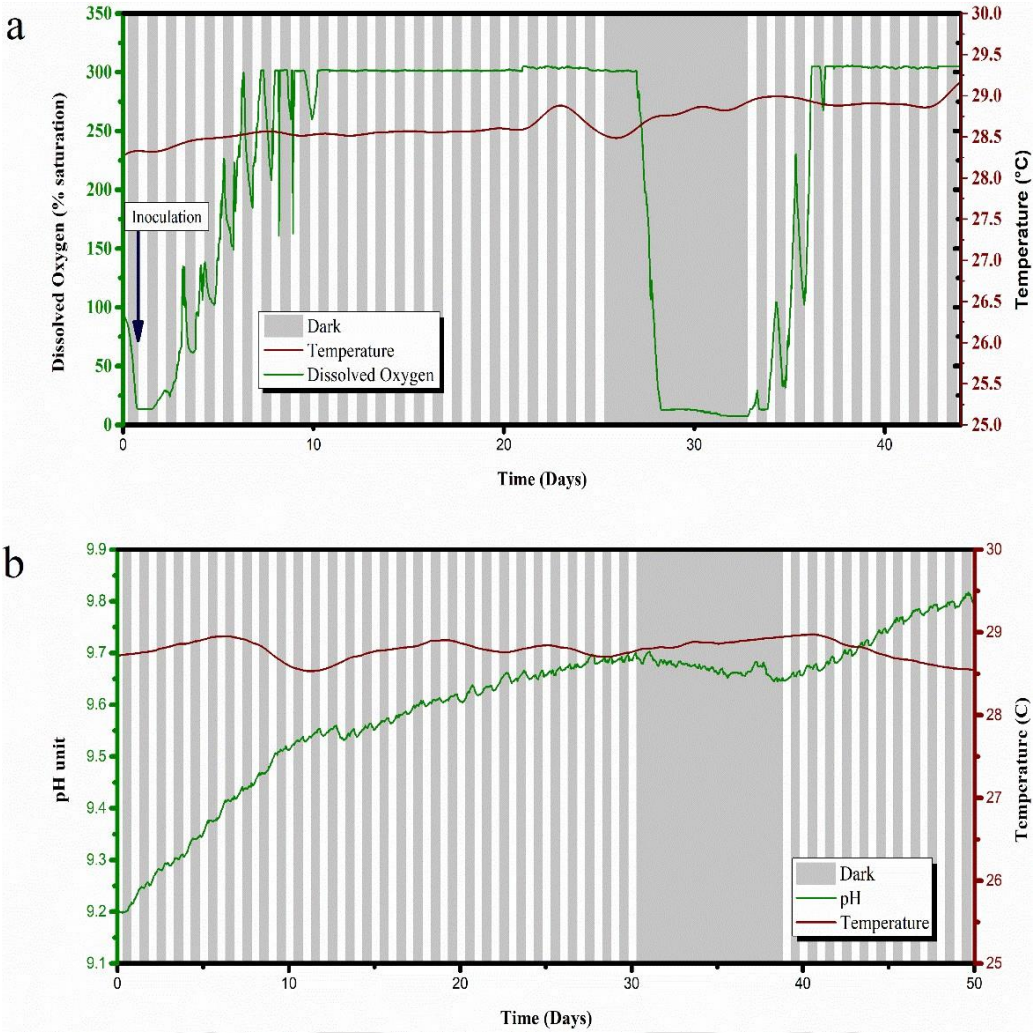

Figure 3. 24. Online monitoring of (a) dissolved oxygen profile and (b) pH profile of static biofilm cultures set up in 250 ml volumetric flasks.

Intracellular redox cofactors like NAD(H) and NADP(H) are involved in metabolic pathways. While NADP(H) is the prime redox cofactor in photosynthetic organisms and its redox state changes transiently in response to illumination status, NAD(H) is the prime redox cofactor of heterotrophic organisms (Welkie et al. 2019; De Graef et al. 1999). These redox metabolites and the relative concentrations of their reduced and oxidized states reflect the intracellular redox state and are directly related to the electrochemical activity of the microbial cells (Guzman et al. 2019; Yong et al. 2014; F. Li et al. 2018). Since our biocatalyst was basically a mixed species biofilm sustained by photosynthetic metabolic

activity of cyanobacterium, we measured the change in both (NADH: NAD) and (NADPH: NADP) ratio starting from the photosynthetic state at day 0 to early aerobic dark conditions which gradually entered into dark anaerobic conditions by day 10. It was clearly observed that the concentration of reduced cofactor for both NAD^+ and $NADP^+$ increased during anaerobic conditions with time (**Fig 3.25**). de Graef and coworkers reported an increase in reduced cofactor of NADH at semi-aerobic conditions that was enhanced significantly under anaerobic conditions. They attributed this phenomenon to fermentative metabolism (De Graef et al. 1999). Fermentative consumption of extracellular carbon compounds in the biofilm matrix by the bacterial community may have led to this observed increase in NADH concentration in our experiments. Simultaneously, Diamond and coworkers and Hatano and coworkers have demonstrated that NADPH production by oxidative pentose phosphate pathway during the dark is essential for redox homeostasis, oxidative stress management during the dark and subsequent current production upon light illumination (Hatano et al. 2022; Welkie et al. 2019; Diamond et al. 2017). Thus, this gradual increase in the reduced state of intracellular redox cofactors under anaerobic conditions is an outcome of a multiplicity of metabolic pathways adopted by diverse cells within biofilm with complex microenvironments having access to diverse nutrients and carbon sources. This state of reduced intracellular microenvironment has a direct consequence for electrochemical studies described below in the next section.

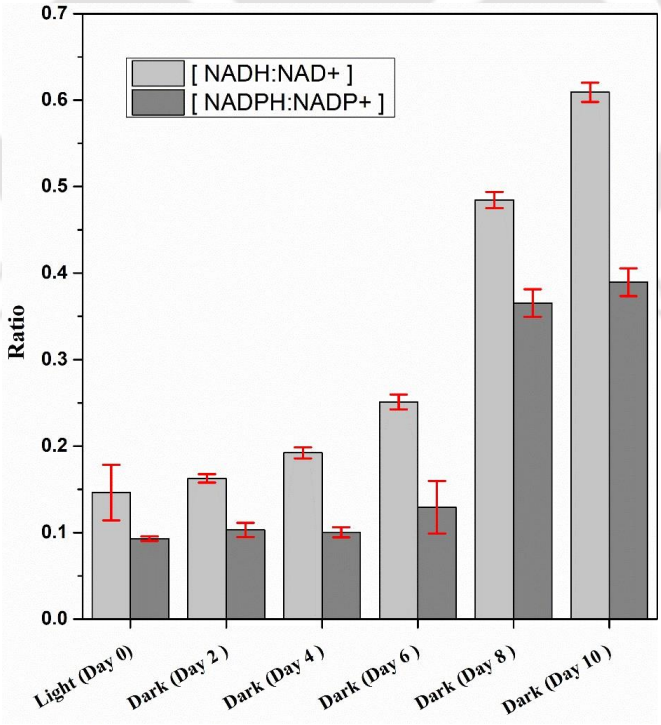

Figure 3. 25. Increase in the concentrations of reduced cofactors with onset of anaerobic conditions.

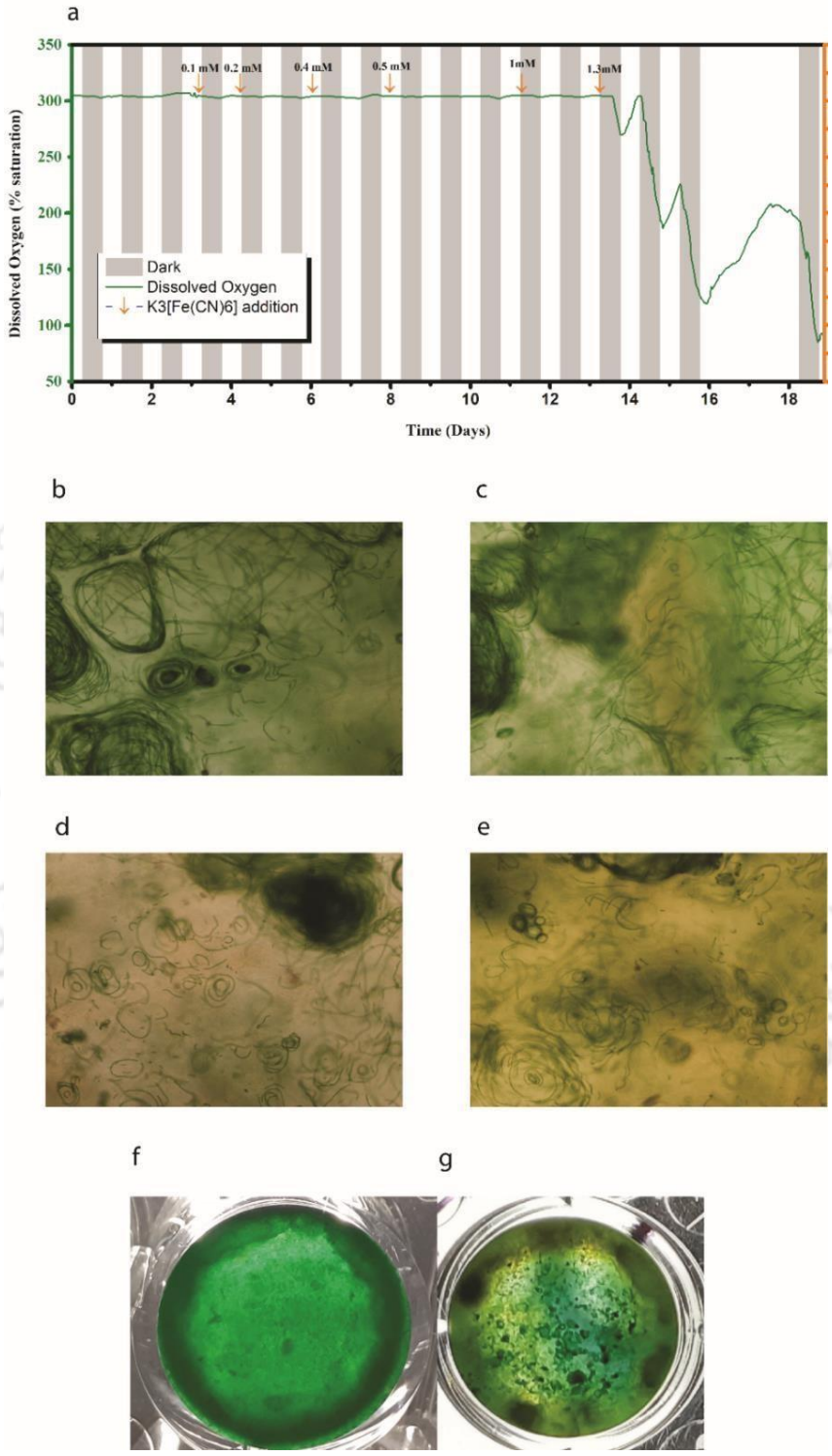

Figure 3. 26. (a) The effect of ferricyanide on the dissolved oxygen concentration of Spirulina subsala biofilm. The biofilms exposed to (b) 0 mM (c) 0.2 mM (d) 0.5 mM and (e) 1 mM ferricyanide. Images of biofilm formed at the bottom of 24 well plate (f) without ferricyanide and (g) with ferricyanide.

Potassium ferricyanide has been a molecule widely used to quantify the exoelectrogenic behaviour of cyanobacterial cells (Bombelli et al. 2011; Saar et al. 2018b; Bradley et al. 2013). However, it is also widely used as a catholyte in the conventional MFC as well due to its stable performance and high diffusioncoefficient (Logan et al. 2006). However, in the context of algal studies it has been demonstrated that upon reduction by cells, much of it gets trapped on the extracellular polysaccharide matrix of cells in suspension culture (Thorne et al. 2015). In the context of a multispecies biofilm used by us, the diffusibility of this mediator molecule will never be uniform. In subsequent sections on electrochemical studies, we have managed to study this aspect electrochemically. However, the understanding of how the presence of ferricyanide in a matured biofilm will affect the viability of the cells in it is a prerequisite. In order to determine the extent of influence a redox molecule like ferricyanide can have on the viability of the matured biofilms during the course of long-term MFC operation, we designed a simple experiment based on inverted light microscopy and online monitoring of dissolved oxygen concentration. Ferricyanide was introduced into a matured biofilm culture (30 days old), in a manner such that the final concentration inthe vessel was increased gradually. It was observed that the oxygen concentration did not dip below 300% saturation upon an incremental increase of ferricyanide upto the final concentration of 1 mM. Any change in dissolved oxygen concentration was not detectable till this stage due to probe limitation of a maximum of 300% detection. At 1.3 mM of final ferricyanide concentration, the dissolved oxygen concentration started dipping (**Fig. 3.26a**). Upon prolonged light illumination, the rate of fall in dissolved oxygen concentration was much more rapid. It may be noted that the toxic effect of ferricyanide is mediated by a light-dependent breakdown of $Fe(OH)_3$ and KCN. Matured biofilms formed in culture vessels were exposed to ferricyanide concentrations of 0, 0.2, 0.5,, and 1 mM (**Fig. 3.26b-e**). Brown patches appeared in the biofilm matrix exposed to 0.2 mM concentration of ferricyanide. At its higher concentrations from 0.5 and 1 mM, the matrix color changed from light brown to yellowish brown. However, upon observing under a microscope, the movement of the trichomes in the spatially confined regions within the biofilm was clearly observed (Video available with authors). Visualizing the biofilms from the bottom of the well clearly shows patches of filamentous cell aggregation in ferricyanide-exposed wells. Whereas healthy control biofilms have a uniform green color (**Fig. 3.26f-g**). These observations imply that the biofilm structure protects the enclosed cells against the ferricyanide in the bulk and bottom of the biofilm. The infusibility of ferricyanide molecules through the biofilm matrix is probably reduced, giving time for the cells inside the biofilm to physiologically adapt to the redox stress.

3.4 *In-situ* electrochemical investigation of biofilm- electrode interface

Electrochemical investigations including BPV studies with cyanobacteria have so far focused on using it as a biocatalytic functional material interfaced with the electrode mostly through direct contact of cell mass or mediated electron transfer from planktonic cells (Tschörtner et al 2019). Such an approach though gives insights into the electrogenic behavior of cells at a cellular level but misses the real-world scenario when the cells end up forming a biofilm on electrodes during a long-term operation (Bombelli et al. 2022). Under such natural conditions, the complexity of the redox reactions at the electrode interface increases manifold due to, complex reactions occurring within the aged extracellular compartment of the biofilm (Sauer et al. 2022; Flemming et al. 2022). Further, factors like non-uniform cellular distribution within the biofilm, heterogeneous biochemical microenvironment, uneven distribution of redox mediator molecules within a biofilm, and ecological succession of bacterial community the during biofilm formation process make such systems more complex and challenging to investigate. Therefore, it is necessary to study the electrochemical behavior of cyanobacterial mixed species biofilms. Delineating such complex systems will yield results paving the way for the rationale designing of phototrophic biofilms for bio photovoltaic applications (Mukherjee and Cao 2021). Based on the observations made from the preceding sections on OCP (E_{emf}), community composition, biofilm structure, macromolecular concentrations, and redox status of intracellular cofactors, we aimed to understand the biofilm-electrode interface through time-dependent electrochemical investigations including a dark phase period focusing primarily on voltage due to its novelty and promise of improving the overall functionality of a BPV device irrespective of illumination status. This investigation was carried out in H-type MFC setups that used ferricyanide as catholyte, taking anode as the working electrode, and cathode as the counter electrode for *in-situ* voltammetry. This study also aimed to investigate the effect of ferricyanide cross-over across the Nafion membrane on the performance of cyanobacterial anodic biocatalyst during the long timescale. While ferricyanide cross-over across the membrane is reported to be detrimental to MFC performance due to toxicity to anodic biocatalyst (Penteado et al. 2017), the same ferricyanide has also been one of the prime redox molecules used as a mediator to demonstrate electrogenic behavior of phototrophs for BPV applications (Saar et al. 2018b). Estimation of cyanobacterial electrochemical capacity based on spectroscopic and electrochemical estimation of reduced ferricyanide has been carried out on planktonic suspension cultures in most of the reports. However, Thorne and coworkers clearly demonstrated that a fraction of these redox molecules are trapped on the cell surface polysaccharide matrix leading to inaccuracies in measurement (Thorne et al. 2015). Thus, in the context of a biofilm with matured extracellular matrix, the diffusion coefficient of the redox molecule will be less due to the entrapment of these redox molecules within the matrix. As observed in our ferricyanide-biofilm interaction studies in the previous section (**Fig. 3.26**), the biofilm matrix preserved motile cells within

itself preventing acute toxicity, buying time for the cells within it to physiologically adapt to the redox stress. How and for what period the cellular systems fare in such confined redox environment and what electrochemical output they give was the question that motivated us to design following experiments as shown in the schematics (**Fig 3.27)**. A half-cell setup without catholyte chamber was included here to deduce the effect of ferricyanide diffusion on electrochemical performance and viability of the cells within a biofilm. This strategy allowed us to acquire an uninterrupted OCP and voltammetry profiles of biofilms simultaneously to gain a mechanistic insight into the interfacial electrochemical phenomena. The setups were operated by following a regimen similar to the one described in the previous section (**Fig 3.21b**) with inclusion of an initial 40 days abiotic operation prior to biomass loading. We used 2 x 5 cm rectangular piece of graphite electrode horizontally placed at bottom of MFC setups to maximize the interaction between biofilm and electrode surface. The voltammetry of these electrodes at various pH was carried out previously and described in **fig 3.17**. The results indicated that the water-splitting reaction until pH 10 within 1 V (vs Ag/AgCl) was negligible.

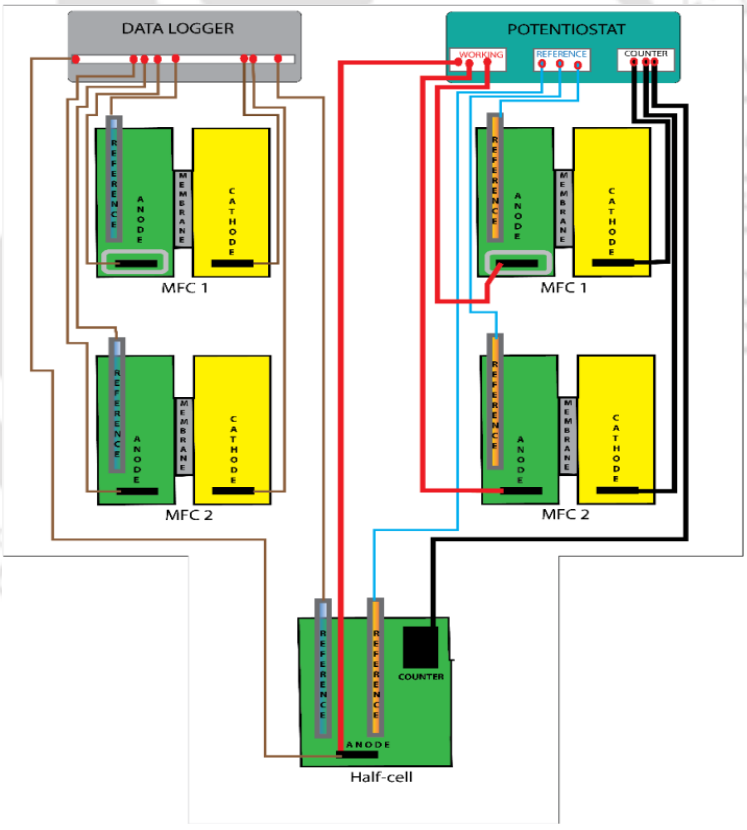

Figure 3. 27. The schematic on the plan of experiment. MFC-1: MFC setup where the anode is enclosed in dialysis bag, which is represented by the gray rectangle enclose; MFC-2: MFC setup where the anode is opened. A duplicate couple of MFC-1 and MFC-2, one connected to datalogger for continuous voltage monitoring, while the other attached to a potentiostat for electrochemical investigation was assembled. The catholyte of the MFC is ferricyanide. A half-cell setup without membrane and catholyte was used for both OCP monitoring and voltammetry.

All the MFC setups were operated in open circuit potential i.e., without a load and each individual electrode in a setup was monitored with respect to an Ag/AgCl reference electrode (**Fig 3.28)**. The cathodic potentials for both MFCs (1 and 2) were the same, oscillation free, started with ~ 0.320 V on day 0, and slowly reduced to the level of 0.270 on day 80 of operations. A negligible variation in the anodic potential of the MFCs occurred until day 10 possibly due to temperature fluctuations as there were no biotic activities during the period (un-inoculated phase). Beyond this period, the anodic voltage modulation in these two setups started that became highest on day 16 and eventually, stabilized at ~ +170 mV on day 40. We attribute this phenomenon to the gradual crossover of ferricyanide through the membrane, since no such voltage modulation occurred in the half-cell, which did not contain ferricyanide. Photodegradative reactions of ferricyanide that crossed over into the anodic chamber and underwent homogenous redox reactions with biologically unutilized inorganic ions like Fe^{2+} complexes must have been responsible for these modulations in anodic potential. After day 40, the anodic chambers were cleaned, and biomass was inoculated. In a short span of time following the inoculation, the anodic voltages of MFC-2 and half-cells started to surge towards -ve magnitude with the onset of each dark phase. This shows that *Spirulina* biomass with associated consortia interacts electrochemically, facilitating the electron accumulation on the anodes in MFC-2 and half-cell, which was not observed in the case of MFC-1 due to lack of direct interaction of the biofilm with the electrode. The magnitude of anode potential in MFC-1 was consistently maintained at 80 mV from day 40 to 60, whereas in MFC-2 it was much negative with a magnitude far higher than that of the half-cell setup (~ -40 mV in dark; half-cell setup) and reaching the value of ~ – 200 mV on day 57. On days 58 to 59, there was a slight increase in the anodic potential of MFC-2, possibly due to transient disturbance in the biofilm matrix causing oxygen perturbation on the anode surface. The anodic potential in MFC-1 did not exhibit any discernible variation pattern between the light and dark phases throughout the experiment and the overall value in this period of day 40 to 60 was high indicating a lack of significant electron accumulation at the electrode.

In the prolonged dark phase (day 60-69), the anode potentials started dipping towards negative magnitude inall the setups with the highest dipping observed in the range of -300 to -410 V (**Fig 3.28**), indicating the overwhelming influence of the dark metabolism on all the anodic redox potentials. As an immediate inference, the depletion of oxygen (an electron scavenger) due to the cessation of photosynthesis during this phase could be ascribed to the above facts. Now, the next inference is to be made on the potentiometric pattern variations among the MFC-1, 2, and half-cells, even though all these configurations have delivered closer anodic potentials at the end of the dark phase.

In the case of MFC-1, the redox potential from day 60 swung to the negative magnitude at a slow rate at the beginning, following which the potential steeply reached ~ -375 mV in the middle of the dark phase. This trend is due to slow electrochemical communication between the biomass and the electrode partitioned by the membrane, as cells are not in physical contact with the anode. This phenomenon implies that the mediating electron transfer also plays a critical role in generating the potential, where ferricyanide (accruing through cross-over) or other biological redox molecules are involved in the electron shuttling process.

MFC-2, on the other hand, showed a sharp dip in the anodic potential that occurred prior to the effect started in the half-cell and MFC-1 on the day between 61 and 62. This could be due to the rapid depletion of oxygen levels in the vicinity of the biofilm-anode caused by the switching of metabolic mode from photosynthetic to aerobic respiration. However, the potential during the phase was perturbed due to unknown reasons, though at the end of the phase, it was regained.

The half-cell exhibited closer potential patterns to the MFC-1 during the dark phase. However, unlike MFC-1, it showed light-dark modulation of potential, which started dipping from the onset of the dark phase. Its slow potential dip may be attributed to the high concentration of oxygen in the vicinity of the anode of the membrane-less setup that reduced electrode kinetics due to the diversion of metabolic electrons to the biofilm respiration process, which eventually entered the anaerobic fermentation process with the depletion of oxygen level (**Fig. 3.24 a**). Worth mentioning that the cells in the biofilm switch to alternate metabolic modes in sequential order, from aerobic respiration to anaerobic fermentation once the dark phase starts following the photorespiration event.

Beyond day 69, when the diel cycle illumination resumed, anodic potentials drifted toward the positive direction due to the generation of oxygen from the resumed photosynthetic process. The rate of reduction, however was initially slow for MFC-1 and MFC-2 as compared to the Half-cell. The reason may be ascribed primarily to the effect of oxygen, and likely the positive influence of the redox mediator, ferricyanide in the MFCs. The amount of oxygen generated from the photosynthetic recovery in both the MFCs was less than the total oxygen produced by the half-cell anode biofilm from the combined effect of photosynthesis and its membrane-less set-up.

In this third phase of operation, very sharp modulations in anodic potentials for the Half-cell system, with minor modulation in MFC-2 synchronizing with the light-dark cycle were observed. The modulations in these set-ups are an indication of some unidentified redox process occurring in the interface of the biofilm-electrode interactions in addition to the effect of the photosynthetically generated oxygen. An abrupt increase in redox potentials for the MFC-1 and 2 was observed following days 75-76 indicating

drastic reduction of electron density on the anode even though the oxygen concentration did not adequately recover following the anaerobiosis phase. It is likely that the rapid depletion of carbon reserves with gradual ferricyanide accumulation has stressed up the intracellular metabolic machinery to thepoint of death (effect of ferricyanide on biofilm: **Fig. 3.26**).

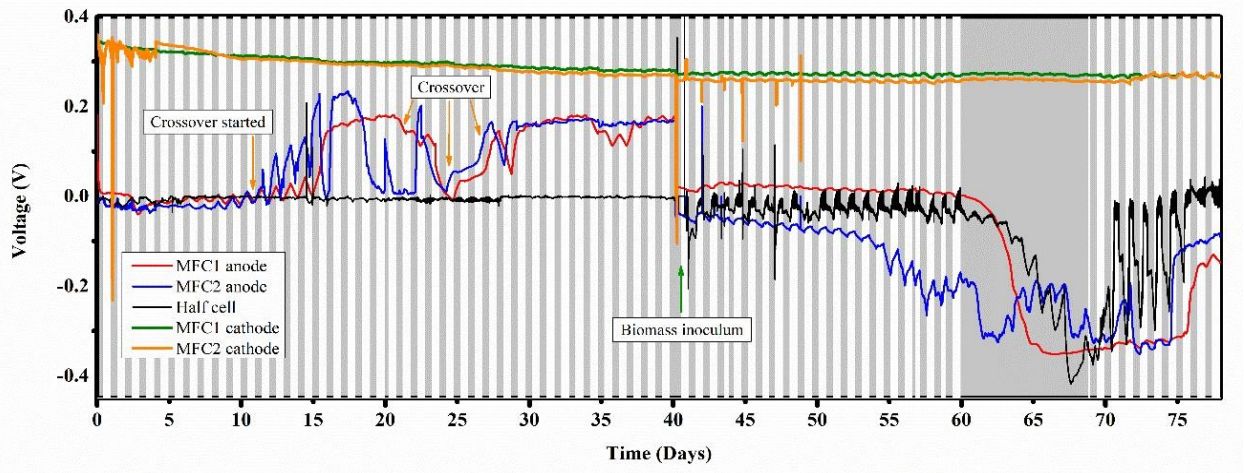

Figure 3. 28. Independent steady state potential of anodes, cathodes in MFC setups, and the anode in single half-cell set up in a 12- 12 hour light-dark cycle (white for light and shadow for dark phases) and a prolonged dark period between days 60 to 69 were recorded. The biofilm was initiated in 250 ml MFC anodic chambers. Culture equivalent to wet biomass of 1.1 gm harvested on day 10 at pH ~ 9.27.

The half-cell setup that showed revived photosynthetic activity was again monitored after a few days. The pattern of dark-dependent decrease in anodic potential still persisted with significant variations in the pattern of complexities (**Fig. 3.29**). Changes were also observed in the pattern of corresponding voltammograms on these days which will be discussed below (**Figure 3.37**).

Based on this observation, we make the following conclusions. (i) Ferricyanide quenches cellular electrons at the biofilm-electrode interface, reducing the anodic redox potential. At its high concentration level, the potentiometric response was though enhanced, simultaneously, a toxic effect of this redox mediator on the cells was also confirmed. Thus, the selection of an optimum concentration of the mediator is critical to realize a desired potential benefit (Clifford et al. 2021). (ii) A periodic oscillation in the redox potential values were observed in MFC-2 and half-cell setup possibly due to the change in oxygen concentration in the vicinity of the biofilm microenvironment. Additionally, some unidentified redox processes in thebiofilm matrix unique to the *Spirulina subsalsa*, or bacterial community members may also be involved inthis phenomenon. Which is, however not yet reported for BPVs. (iii) Direct contact of cells with the electrode is essential for generating the oscillation between diel cycles as revealed from the lack of this potential trend in MFC-1 where the biofilm was secluded from the electrode by a separating membrane.

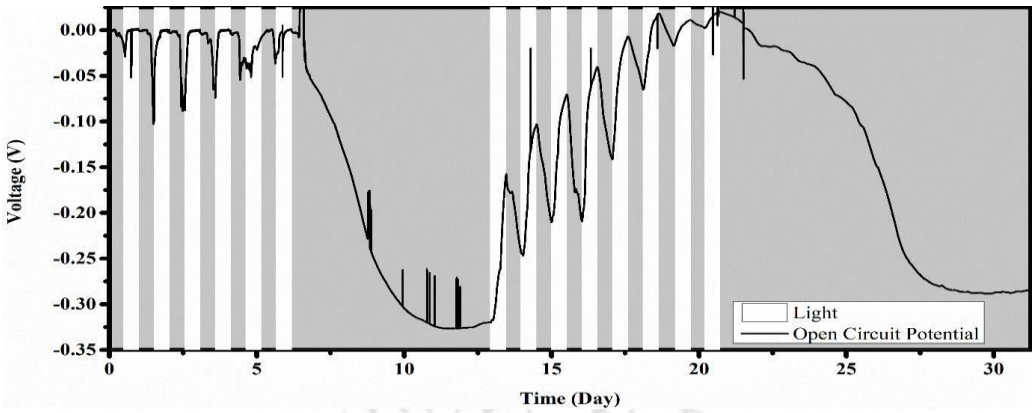

Figure 3. 29. Half-cell setup anodic potential profile after a few weeks following experiments in fig.3.28.

Voltammograms (CV and Pulse Voltammetry) and Impedance analysis of the duplicate MFC-1, MFC-2 setups, and the half-cell setup revealed crucial insights regarding the biofilm microenvironment at electrode-biofilm interface (**Fig. 3.30a-c, 3.31a-c, 3.32a-c)**. Tafel plots were derived from anodic sweeps of cyclic voltammograms and fitted through NOVA 1.11 metrohm software to yield interpretable values like anodic/cathodic slopes, polarization resistance, corrosion current, and corrosion potential which allowed further interpretations (**3.33a-c**). The coordinates used for fitting are mentioned in **Table 3.3.** A first look at the overall electrochemical data allowed us to infer a few critical pieces of information. (i) Firstly, the presence of ferricyanide in the anodic chambers in MFC-1 and 2 due to gradual catholyte diffusion across the membrane (peaks in voltammetry and semi-circle in impedance spectra. **Fig. 3.30, 3.31, 3.32**); (ii) Second, broadening of cyclic voltammograms for MFC-1 and 2 in comparison to the half-cell pattern indicating increased capacitive charge in these two setups due to accumulation of ferricyanide in the biofilm matrix and (iii) emergence of a new oxidation peak at ~ -0.25 V in MFC-1 and 2 setup implies that the interaction of ferricyanide with the biofilm matrix induces secretion of an oxidizable entity into the matrix (**Fig. 3.30**).

Table 3.3. Coordinates used for fitting the slopes of a Tafel plot.

Category	Time point	Cathodic slope, point 1	Cathodic slope, point 2	E_{ocp} obs	E_{ocp} cal	Anodic slope, point 1	Anodic slope, point 2
Half-cell setup	Dark_Day 40	-964.36 mV	-908.20 mV	-834.56 mV	-836.16 mV	-769.04 mV	-720.21 mV
	Light_Day 41	-556.64 mV	-495.61 mV	-428.420 mV	-431 mV	-366.21 mV	-290.53 mV
	Dark_Day 43	-622.56 mV	-566.41 mV	-492.8 mV	-489.28 mV	-434.57 mV	-368.65 mV
	Light_Day 44	-510.25 mV	-454.1 mV	-375.86 mV	-374.280 mV	-312.5 mV	-241.7 mV
	Dark_Day 46	-646.97 mV	-585.94 mV	-513.19 mV	-514.86 mV	-437.01 mV	-380.86 mV
	Light_Day 48	Not available	Not available	Not available	Not available	Not available	Not available

	Dark anaerobic_Day 69	-979 mV	-937.5 mV	-873.28 mV	-884.720 mV	-798.34 mV	-749.51 mV
	Resumed illumination_Day 70	-922.85 mV	-859.38 mV	-791.560 mV	-789 mV	-722.66 mV	-681.15 mV
	Light recovered_Day 78	-434.57 mV	-378.42 mV	-307.820 mV	-307.360 mV	-239.26 mV	-178.22 mV
	Light recovered_Day 100	-520 mV	-451.66 mV	-379.170 mV	-379.890 mV	-305.18 mV	-251.46 mV
MFC1 (Dialysis bag setup)	Dark_Day 40	-778.81 mV	-725.1 mV	-646 mV	-642.690 mV	-576.17 mV	-517.58 mV
	Light_Day 41	-859.38 mV	-798.34 mV	-728.15 mV	-726.390 mV	-664.06 mV	-600.59 mV
	Dark_Day 43	-708 mV	-651.86 mV	-580.180 mV	-579.160 mV	-510.25 mV	-451.66 mV
	Light_Day 44	-678.71 mV	-629.88 mV	-559 mV	-559.810 mV	-485.84 mV	-429.69 mV
	Dark_Day 46	-883.79 mV	-837.4 mV	-765.440 mV	-765.380 mV	-703.13 mV	-637.21 mV
	Light_Day 48	-871.58 mV	-810.55 mV	-741.5 mV	-743.220 mV	-671.39 mV	-610.35 mV
	Dark anaerobic_Day 69	-959.47 mV	-898.44 mV	-831.81 mV	-833.650 mV	-764.16 mV	-700.68 mV
	Death_Day 79	-925.29 mV	-861.82 mV	-793.390 mV	-793.480 mV	-725.1 mV	-659.18 mV
MFC2 (Non-dialysis bag setup)	Dark_Day 40	-932.62 mV	-871.58 mV	-797.730 mV	-797.670 mV	-729.98 mV	-659.18 mV
	Light_Day 41	-771.48 mV	-695.8 mV	-638.560 mV	-638.570 mV	-576.17 mV	-512.7 mV
	Dark_Day 43	-854.49 mV	-783.69 mV	-723.350 mV	-723.740 mV	-661.62 mV	-595.7 mV
	Light_Day 44	-710.45 mV	-651.86 mV	-578.760 mV	-576.350 mV	-510.25 mV	-449.22 mV
	Dark_Day 46	-830 mV	-773.93 mV	-701.770 mV	-700.150 mV	-634.77 mV	-571.29 mV
	Light_Day 48	-639.65 mV	-605.47 mV	-528.650 mV	-528.910 mV	-461.43 mV	-400.39 mV
	Dark anaerobic_Day 69	-930.18 mV	-861.82 mV	-798 mV	-798.370 mV	-729.98 mV	-671.39 mV
	Death_Day 79	-881.35 mV	-830 mV	-755.960 mV	-754.950 mV	-688.48 mV	-622.56 mV

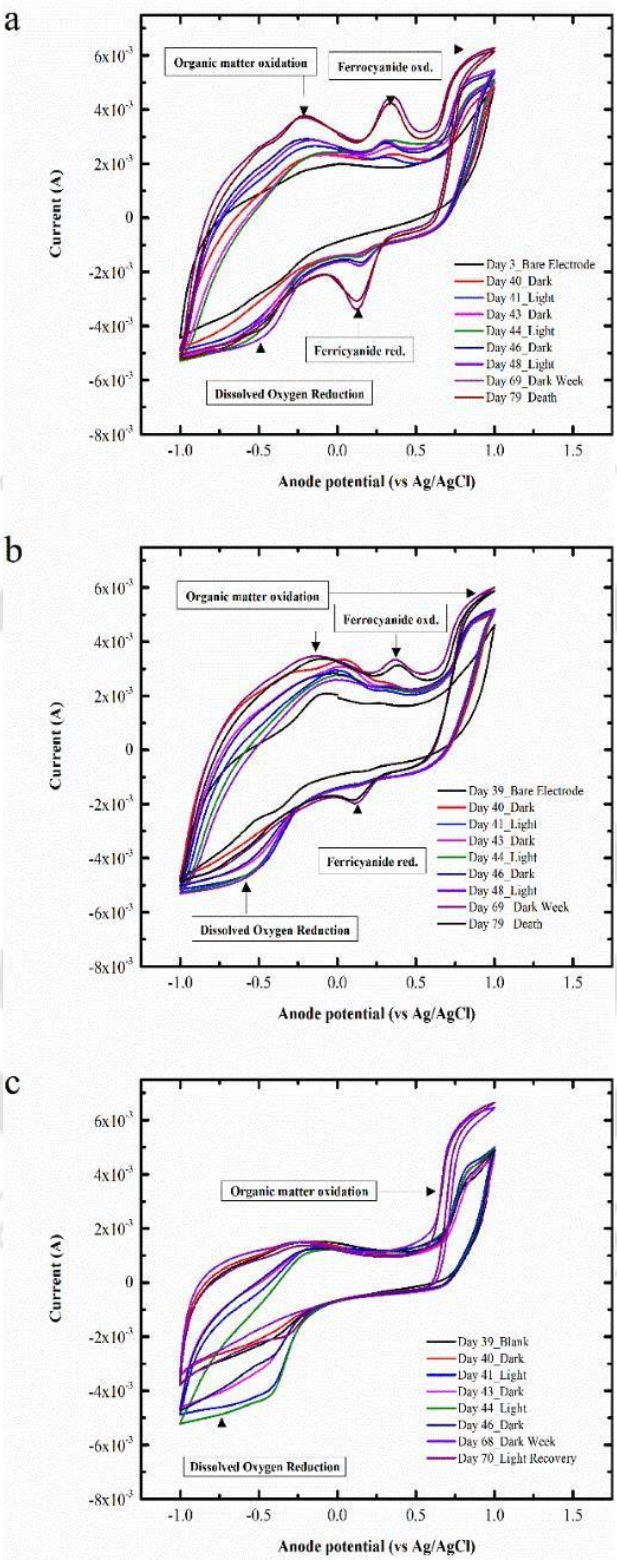

Figure 3. 30. Time-dependent CV of (a) MFC1, (b) MFC2, (c) Half-cell on days corresponding to graphs in figure 3.28.

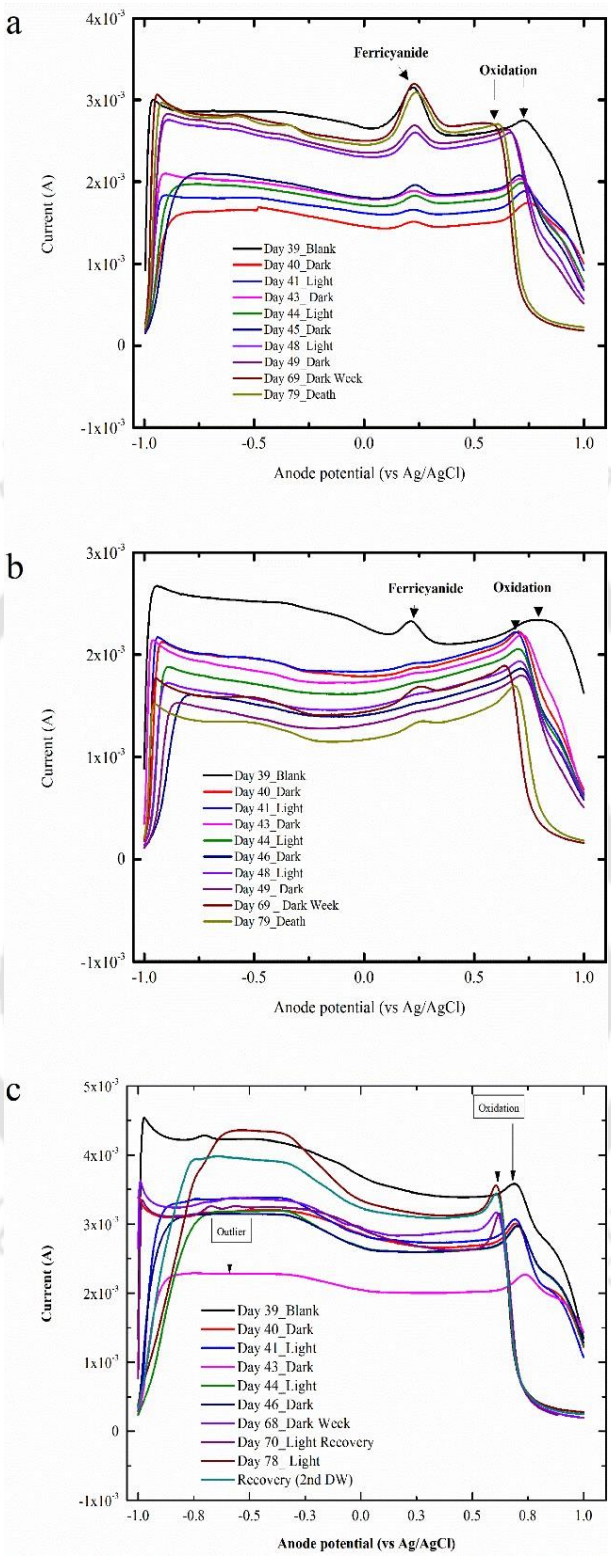

Figure 3. 31. Time-dependent DPVs of (a) MFC1, (b) MFC2, (c) Half-cell on days corresponding to graphs in figure 3.28.

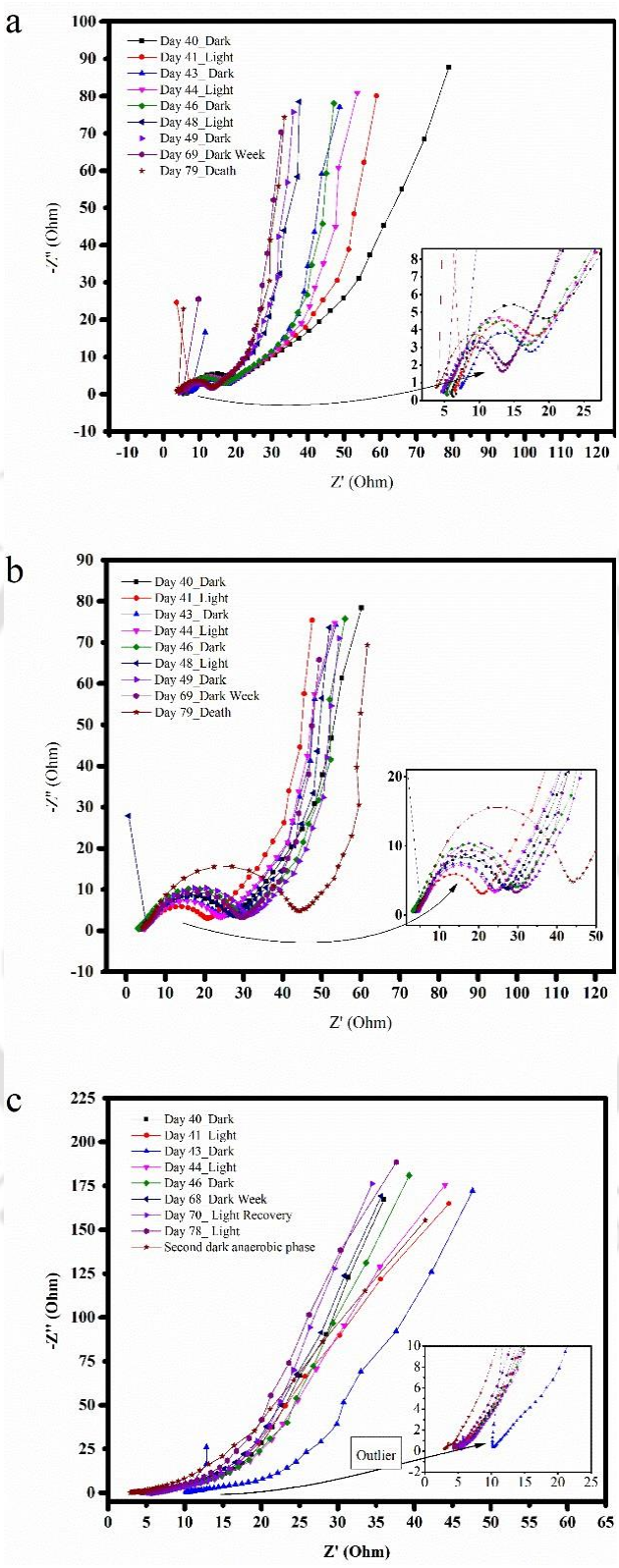

Figure 3. 32. Time-dependent Impedance spectra of (a) MFC-1, (b) MFC-2, (c) Half-cell on days corresponding to graphs in figure 3.28.

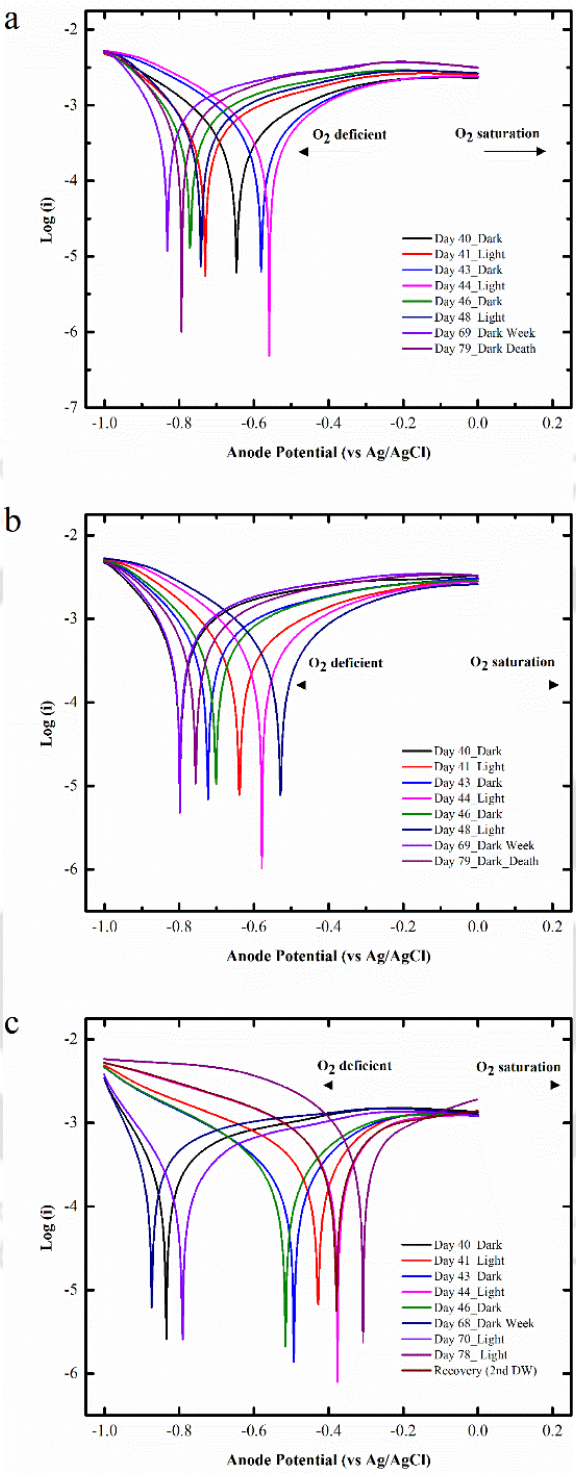

Figure 3. 33. Tafel plots derived from the linear sweep of CV in figures 3.31 of (a) MFC-1, (b) MFC-2, and (c) Half-cell on dayscorresponding to graphs in figure 3.28.

The above propositions were verified by analyzing Tafel plots **(Fig. 3.33 a-c**), derived from the anodic sweep of cyclic voltammograms (**Fig. 3.30 a-c**). A high reductive current (low cathodic current slope) in MFC-1 and 2 throughout the period of operation was detected **(Fig.3.34. b-c)**. Under such conditions, majority of the extracellular electron flux on an unpolarized electrode would be quenched by the biofilm matrix, either with ferricyanide or with the matrix components. In spite of the high reductive reaction, the anodic potential in MFC-1 was positive (**Fig. 3.28**) during the initial diel biotic period (day 40 – 60), indicating that direct contact of the biofilm with the electrode is necessary for a potential generation as endorsed by the –ve of anode potential in MFC-2 (**Fig. 3.28**). Further, the ferricyanide-led redox mediation is possible only over a short distance (**Thorne et al. 2014**), which did not comply well in the case of MFC-1 due to the partitioning dialysis membrane. Thus, in the extended dark phase, the enhanced anodic potential in MFC-1 was due to a combination of ferricyanide that crossed over and other intrinsic molecules released due to biofilm matrix degradation. Contrary to the two MFC set-ups, the reductive and oxidative reactions in the half-cell setup gradually converged in the initial days (**Fig. 3.34a**), indicating that the extracellular matrix in the biofilm had a higher tendency of losing electrons to photosynthetically produced oxygen, saturating the biofilm microenvironment on early days. In all setups, at the end of the anaerobiosis period on day 69, the reductive reaction reached the highest levels as expected, due to declining oxygen levels. Subsequently, since the day of illumination resumed (day 70), the reductive reactions were still dominant in half-cells till day 78 (**Fig. 3.34a**). The electron flux emanating from the cellular structure quickly saturated the extracellular redox components in the half-cell between days 70-78 as judged by sharp variations in half-cell OCP on these days. This indicates the presence of some unidentified reductive process in the biofilm matrix due to cellular activity or some uncharacterized exoproteome that was highly sensitive to light or local oxygen concentration. As to why the magnitude of reductive decrease in anodic potential decreased with time can be explained by observation in **figure 3.24**, where it was clearly observed that oxygen concentration rose up gradually while being entrained to illumination status. The oxidative and reductive reactions converged graduallyby day 100 following the complete photosynthetic recovery. This day 100 falls on the 6^{th} day of **Fig.3.30**. On these days, the biofilm microenvironment must have been again saturated by photosynthetic oxygen. This along with the physiological activities of microorganisms in biofilm must have significantly altered the chemistry of the extracellular organic matter (aging) which is also reflected by changes in the voltage profiles of the biofilms in **Fig. 3.30** over time as described in the literature (Zhang et al. 2018). In Tafel plots, the drifting towards higher reductive potential in oxygen-deficient conditions and towards higher oxidative potential in oxygen-saturated conditions is clearly visible from the pattern of change in the magnitude of E_{ocp} (**Fig. 3.35a**). This shows local oxygen concentration produced by photosynthesis and consumed by respiration also had a significant influence over steady-state potentiometric profiles of

biofilms. The half-cell consistently showed higher polarization resistance and lower corrosion current density (except on day 44 for possible temporary biofilm detachment). We make this inference on the basis of abrupt change in solution resistance and pulse voltammetry baseline on this day in both impedance spectra and pulse voltammetry that went back to original conditions on subsequent readings (**Fig. 3.31c and 3.32c**). Between MFC-1, 2, and half-cell, on the other hand, a consistent difference in corrosion current and polarization resistance indicates that the presence of ferricyanide significantly increased the electron density in the biofilm anode by capturing electrons from cells and matrix components thus altering the microenvironment significantly (**Fig. 3.35b, c**).

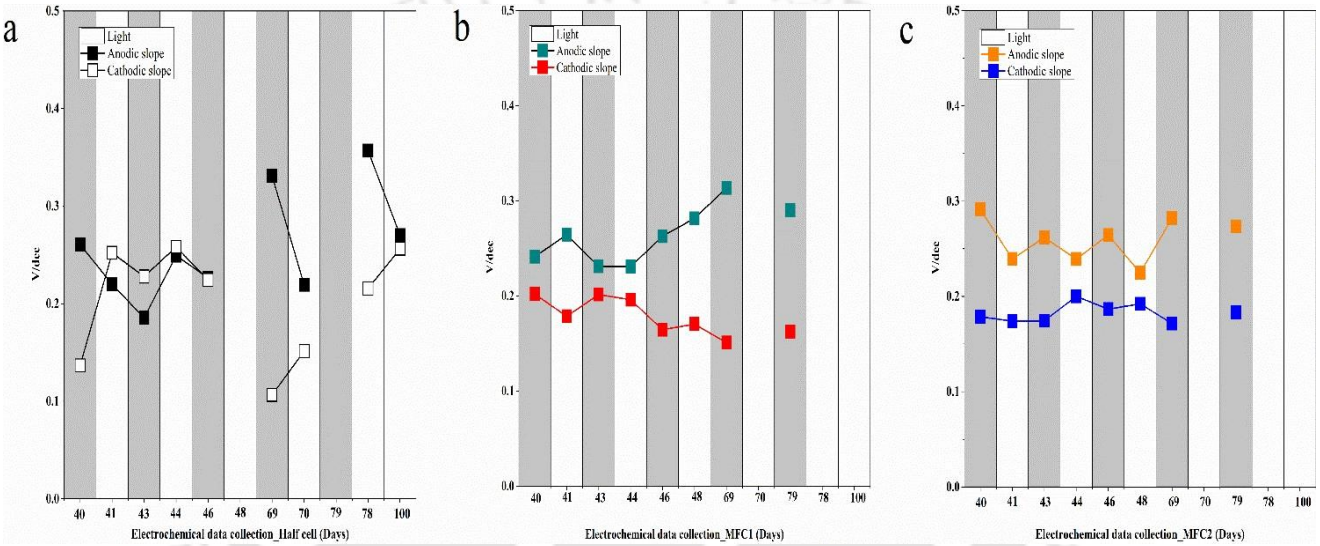

Figure 3. 34. Anodic and cathodic slopes derived from Tafel slopes of (a) MFC-1, (b) MFC-2, (c) Half-cell setups.

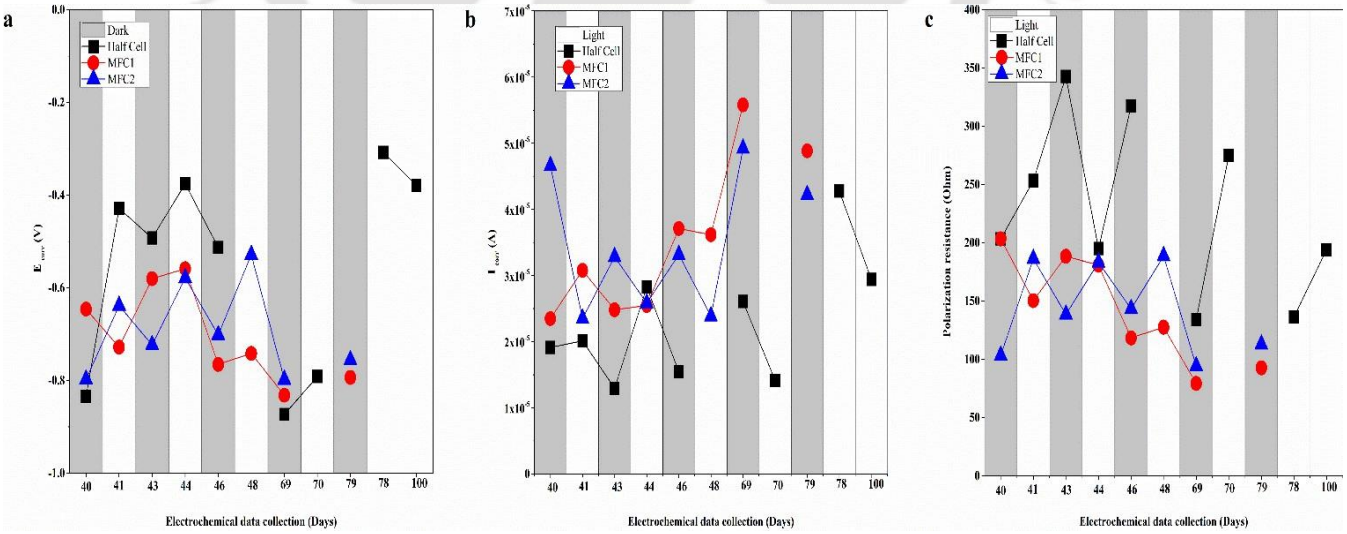

Figure 3. 35. Change in (a) corrosion potential, (b) corrosion curent, and polarization resistance of the three electrochemical setups.

The other two distinguishing features among the 3 setups were irreversible oxidation and reduction current with onset at 0.6 V and -0.25 V, respectively. The oxidation current corresponds to the oxidation of extracellular organic matter produced by cells in the biofilm as demonstrated through *ex-situ* voltammetry of supernatant. Whereas the reductive current is a summation of dissolved oxygen (on set) and organic matter reductions. The data are expressed in a quantitative manner by integrating the area below the curve normalized to the corresponding value obtained from the blank electrode (**Fig. 3.36a, b**) that nullifies the possible contributions from the water-splitting reaction at the extreme ends. The values on day 39 are blank when biomass was not introduced. The pattern of residual oxidation charge changes shows that the MFC-2 oxidation current was higher than the half-cell until day 48, whereas in MFC-1 the value of the oxidation current increased in a gradual and linear fashion during this period. This indicates that exposure to ferricyanide caused higher production of extracellular matter as a biological response to redox stress. Contrary to this, the linear pattern of increase in oxidation current in MFC-1 indicates gradual fractionation of low molecular weight EPS components across the dialysis membrane. These fractionated matrix components accumulating in the dialysis bag or the ferricyanide present there did not cause any decrease in the magnitude of anode potential. This again verifies the inference that most of the reduced ferricyanide remained confined inside the biofilm matrix and could not be detected over the electrode due to being physically separated across the dialysis membrane. Further, all setups showed a significant increase in the magnitude of oxidation current after dark induction on days 68-69. This pattern correlates well with the phenomenon of extracellular matrix degradation by the combined activity of photosynthetic cells and associated symbionts that releases EPS fractions oxidizable at high anodic potential (**Fig. 3.23**). While the current in MFC setups did not recover subsequently in the photosynthetic stage due to ferricyanide toxicity, the oxidation current in the half-cell setup continued to be higher after recovery. This was the case even after two rounds of dark induction. Notably, a broad oxidation current between 0 V to 0.6 V also appeared in the voltammograms of the half-cell after recovery on the 78th day (**Fig. 3.37**). The magnitude of oxidation and reduction currents again varied upon voltammetry of a subsequent day. Such oxidation current can be attributed to the presence of oxidizable molecules with a continuum of redox potential entrapped in the tertiary structure of natural organic matter (Pavitt and Tratnyek 2019; Li et al. 2015). The minute, complex features of the potentiometric profile of the half-cell anode also changed during this time (**Fig. 3.29**). Based on these observations we infer that the redox milieu of the extracellular matrix of a biofilm alters with time in response to various environmental stimuli and metabolic states of the cells init.

Similarly, the magnitude of reductive charge varied between the day-night phase and the photosynthetic-dark metabolism phase (**Fig. 3.36b**). It increased in the light phase and decreased in the dark phase. The most drastic change was observed in half-cells after anaerobiosis. We attribute this pattern of variation to changing dissolved oxygen concentration. This pattern of variation is in complete agreement with the pattern of change in E_{ocp}, which is also influenced by oxygen saturation and depletion (**Fig. 3.35a**). Notably, even though the magnitude of reductive current varied between light-dark conditions in MFC setups, its magnitude was not as high as half-cell. This was probably because of the toxic effect of ferricyanide on cells that compromised photosynthesis. As determined through dissolved oxygen study, photosynthesis of all the cells in the biofilm did not stop immediately; a significant subpopulation was sustained inside the biofilm matrix (**Fig. 3.26**). Secondly, after anaerobiosis on day 69, the reductive current was entirely diminishedin the half-cell setup, while this was not the case in the two MFC setups. This indicates that some reducible moieties were present in the extracellular matrixes that were produced as a response to ferricyanide exposure.

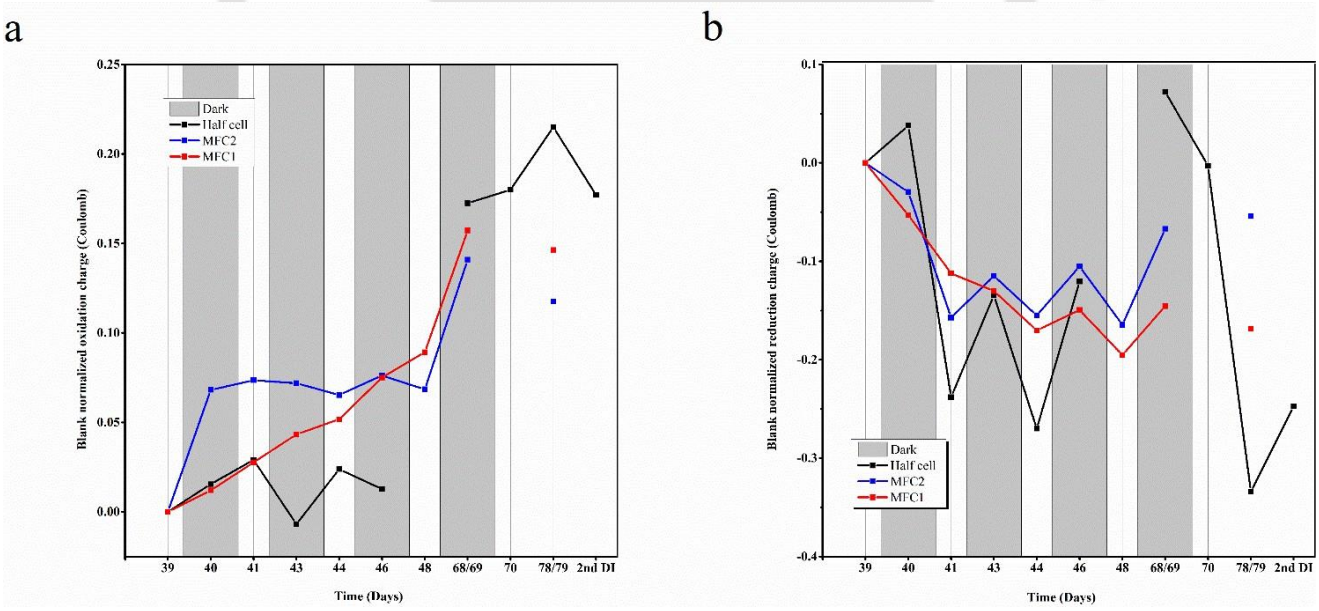

Figure 3. 36. (a) Reductive charges were obtained by integrating the area below the cathodic sweep (-0.2 to -1 V) and (b) Oxidative charges were obtained by integrating the area below the anodic sweep (0.6 to 1 V). The values were normalized to the charges obtained by integrating the corresponding cathodic and anodic sweep of voltammograms obtained from the blank operation.

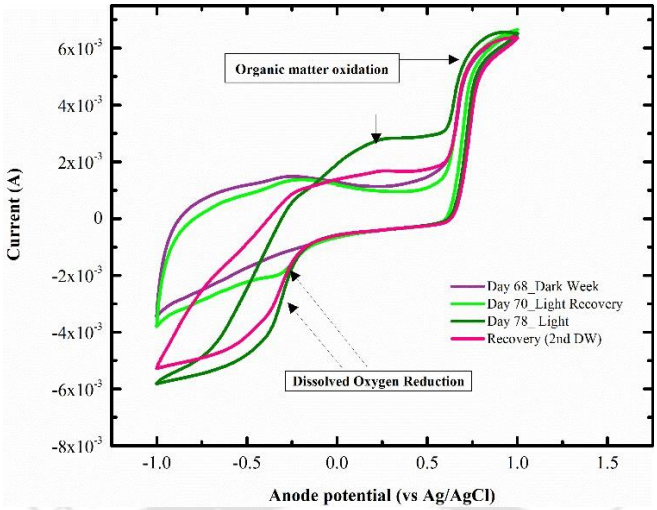

Figure 3. 37. Voltammograms of the half-cell setups after dark exposure, subsequent recovery, and after aging of the biofilm matrix.

Further, pulse voltammograms allowed us to measure the precise potentials and peak currents (concentration detected on the electrode surface) of the ferricyanide on the electrode. Though ferricyanide acts as a redox mediator and can be toxic beyond a certain concentration, from an analytical perspective it can also act as a redox probe. It allowed us to quantitate the redox probe concentration accessible to the electrode following its diffusion through the biofilm matrix. The overpotential required to drive the redox reaction is due to the electrode surface covered by the partially permeable biotic material retaining the redox molecule affecting the mass transfer diffusion (Wang et al 2006; Goyal et al. 2006). On day 39 after the catholyte crossover, prior to the addition of biomass, the peak potential was 218 mV. As judged by the calibration curve obtained by pulse voltammetry (**Fig. 3.38**), the peak current was 547 µA (equivalent to 182 µmole) in MFC-1 and 201 µA (equivalent to 66.6 µmole) in MFC-2 on day 39.

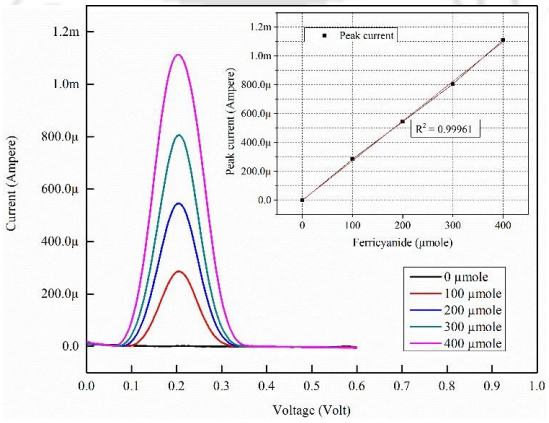

Figure 3. 38. Peak currents of ferricyanide on 10 cm^2 graphite electrode at various redox probe concentrations.

After the introduction of biomass into it, two distinct patterns of variations were observed in the two MFC setups (**Fig. 3.39 a-b**). In MFC1, a peak current of 73.6 µA was observed that reduced on the subsequent day 41. This happened because some amount of residual ferricyanide remained even after the washing step. Subsequently, the culture supernatant gradually refilled and equilibrated the content inside the bag causing a reduction in peak current. Further, as the catholyte cross-over trickled in, increasing concentrationwas detected on the anode. During this period, the overpotential did not change significantly except on day 44 and after the cell death on days 78/79. This indicates that the low molecular weight fraction of EPS that could pass through the dialysis bag membrane only affected the overpotential gradually. However, after the cell death on day 78/79, a certain fraction of the cell debris must have entered the dialysis causing an increase in overpotential. On this day a minor decrease in peak current from 606.69 µA to 558.21 µA was observed. This may be due to surface blockage by fallen cell debris. Contrary to this, the magnitude of the peak current did not change significantly from day 40 to day 49 in MFC-2. The cross-over might have increased the concentration in a linear fashion but it is due to the thick biofilm matrix that it was not detected on the electrode. The overpotential varied from 218 mV to 228 mV during this period. As the *Spirulina* biofilm and the biotic component has a dynamic structure owing to motile cells, the overpotential kept on varying during this period with no increase in peak current observed. After the period of dark induction, a sudden jump in peak current and peak potential was observed which were 106.57 µA and 243.6 mV, respectively. This indicates that EPS degradation triggered the opening of passage for more ferricyanide to diffuse through biofilm and reach the electrode because of enhanced access and increased crossover. After the cell death on day 78, a decrease in peak current coupled with an increase in overpotential was observed. We attribute this to the falling of cell debris on the electrode that blocked the surface.

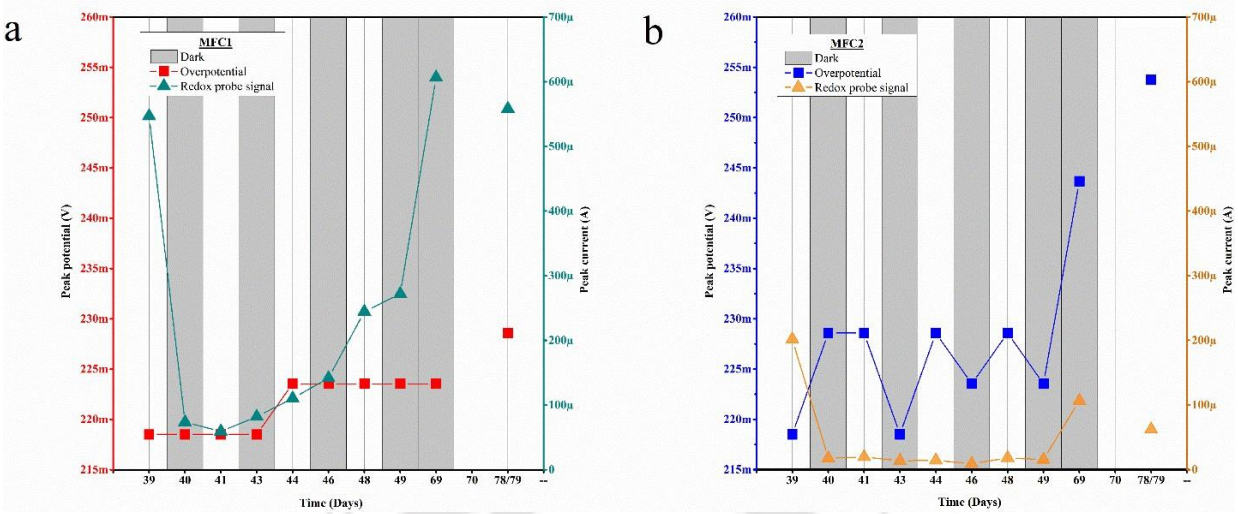

Figure 3. 39. Variations in the magnitude of ferricyanide peak currents (redox probe signals) and peak potentials (overpotential) over time in (a) MFC-1 setups and (b) MFC-2 setups.

This trend was also verified by the R_{ct} values derived by electrochemical circuit fitting of impedance spectra for MFC-1 and 2 (**Fig. 3.32 and 3.40**). The R_{ct} value in MFC-1 increased only twice on days 44 and79, whereas in MFC-2, the value varied throughout with a sudden jump after death. The variations in R_{ct} value in MFC-2 can be attributed to the combined effect of motile cells and multiple biochemical reactions, delineating which is beyond the scope of this study.

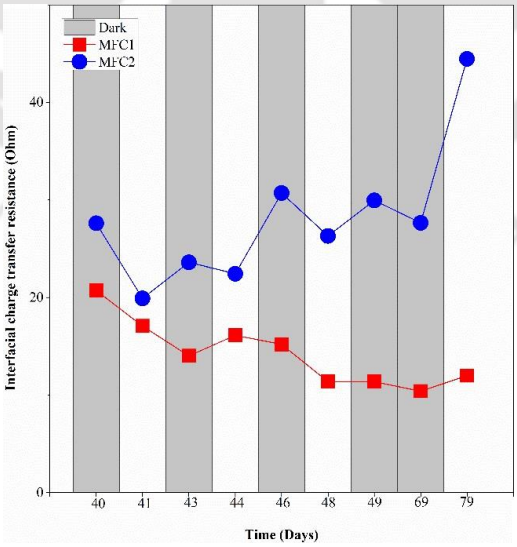

Figure 3. 40. Variations in charge transfer resistance of MFC-1 and 2 setups

Based on these results we could clearly visualize that any redox molecule exposed to a cyanobacterial biofilm matrix would heavily modify the redox milieu and would be mostly trapped inside the biofilm structure. The interactions between redox mediator molecules and biofilm-embedded living entities have two components. One is toxicity after a certain concentration or time. Second is the physiological response of the cells to a highly oxidizable redox microenvironment.

3.5 Insights from closed circuit operations

The capacity of the biofilm to deliver current through the MFC was probed by the fixed resistance method after the OCP attained stability following the prolonged dark phase (**Fig. 3.41**). Notably, the variable resistance method encounters two technical glitches. Firstly, the variation in time spent with each resistor in a closed circuit due to operator bias leads to an overestimation of power density. Due to this sustainable power density is often achieved at a resistor of higher magnitude than determined (Chandra et al. 2009). Secondly, even if enough time (upto 30 minutes) is given for adaptation to each resistor, the phenomenon of power overshoot is observed. These problems could be resolved by employing a fixed resistor for a complete fed-batch cycle of substrate depletion in MFC as demonstrated with a heterotrophic community-based biofilm (Watson et al. 2011). This approach revealed that if a longer time is given to the biofilm to adapt to a particular resistor, the MFC may exhibit higher sustainable power generation at lower resistances. Since earlier reports on cyanobacteria current profiles have shown transient complex features, especially during light-to-dark transitions, we judged the variable resistor method of power estimation unsuitable for our objective (Zhang et al. 2018; Wey et al. 2021). Whereas, in the BPV format of operation no external carbon sources are added, hence, making it difficult to decide the time span of a single fed-batch cycle. Therefore, we decided to operate multiple MFC-2 setups (n = 6), each with an external resistance of fixed magnitude.

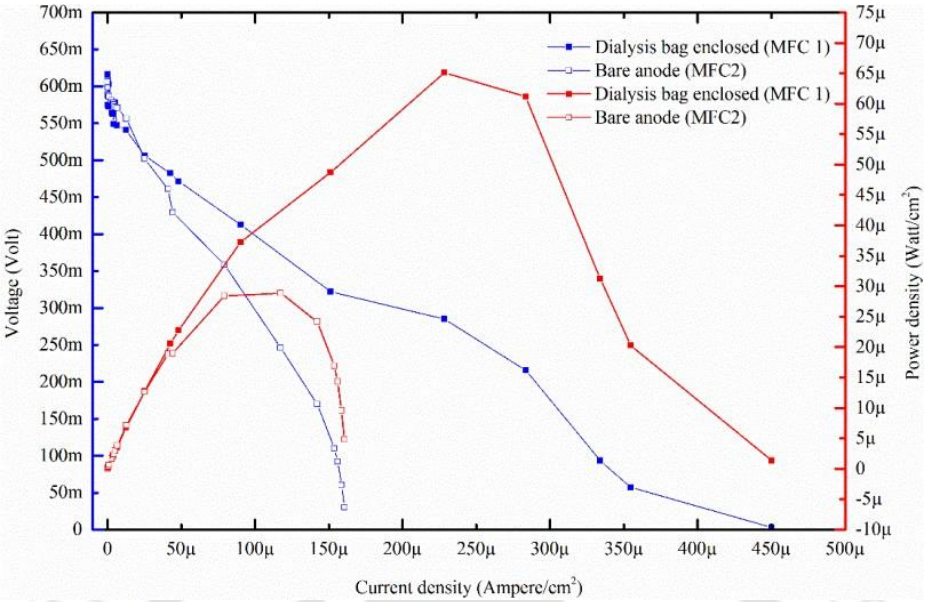

Figure 3. 41. Polarization and power density curve obtained by variable resistance method in MFC-1 (n = 2) and MFC-2 (n=2).

First, six MFC setups (MFC-2), anodes of which were filled with photosynthetically active culture (1.1 gm wet weight) were incubated for 15 days to generate matured biofilms in illuminated conditions. The catholyte was introduced into the cathodic chamber on the 16th day and setups were then operated in a closed circuit for 8 days in dark period. These setups were again monitored for 3 days in light-dark cycle after a 4 day period of photosynthetic recovery. This approach helped us to study the biofilm before the ferricyanide catholyte crossed into the anode in a mediator-less condition in both dark metabolism and photosynthetic conditions. The magnitude of fixed external resistances used were 330 kilo-ohms, 10 kilo-ohms, 1 kilo-ohms, 327-ohms, 220 ohms and 1.2 ohms. A brief one-day period of marginal decline in power density was observed in all setups from until day 1 except 330 kilo-ohms and 220 ohms (**Fig. 3.42**). This period corresponds to the time period required by the matured biofilms to equilibrate in response to electrode polarization. The reason this phenomenon was not observed in the 330 kilo-ohm setup was that at a higher resistance, the biofilm redox milieu was already primed for delivering enough electron flux in response to polarization, whereas at lower resistances, it required a certain time for the biochemical redox reactions at the electrode to equilibrate with respect to current demand. The setup 220 ohm was an exception as voltammetric investigation after day 8 revealed that a low concentration of ferricyanide equivalent to 24 µM was detected on the anode surface (**Fig. 3.43**).

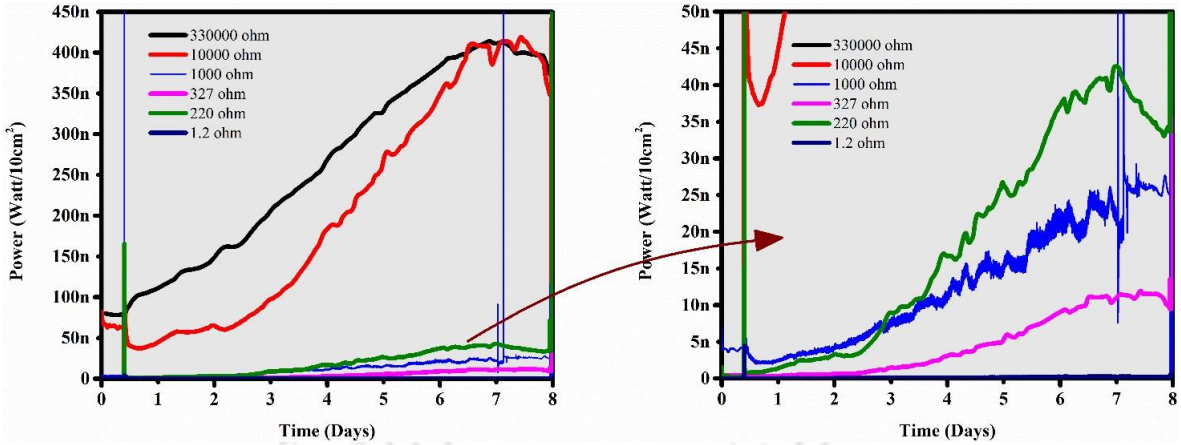

Figure 3. 42. Power generation of cyanobacterial biofilms upon deliberate dark induction for 8 days.

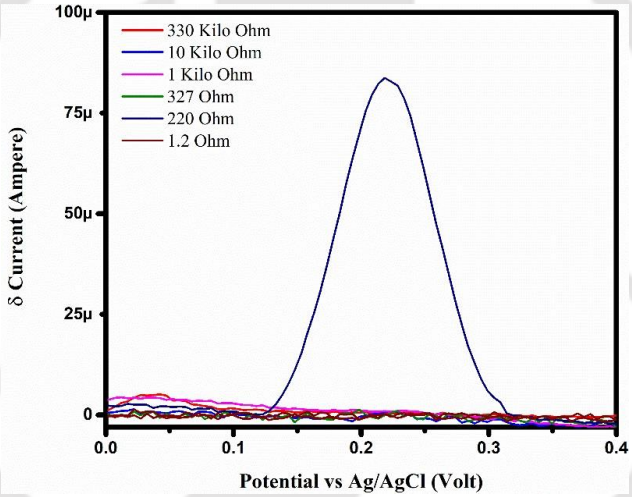

Figure 3. 43. Pulse voltammograms of MFC setups at the end of 8 days of MFC operation.

This caused an immediate rise in current owing to mediated mode of electron transfer. Further, the power density gradually increased in all the setups till day 7. This indicates that the high-magnitude resistor did not limit the power density. On the contrary, the rate of redox reactions slowly and gradually increased with time. This pattern is reminiscent of the gradual change in anode potential during dark metabolism in OCP mode operation in (**Fig. 3.28-3.29**). On day 8th, there was a general pattern of decline in power density in all setups. We assume that the slow release of extracellular polysaccharides from the biofilm matrix due to enzymatic degradation by the cyanobacteria-associated microbial community during this time must have led to its utilization in respiratory metabolism or auto fermentation. This is reflected by the slow increase in the magnitude of current that may have been mediated by humic-like substances

present in the matrix as shown in excitation–emission spectra. The rate of increase in current in the 220-ohm setup was much faster as it was mediated by ferricyanide. Recent reports of current production by cyanobacteria during dark aerobic and anaerobic conditions in presence of glucose further support this inference (Tanaka et al. 2021).

The power profile of setups was then compared after photosynthetic recovery when the profiles started receding due to oxygen accumulation. It was observed that the power magnitude of the MFC setup under 10 kilo-ohm resistor was highest and somewhat comparable to 330 kilo-ohms on day 2 with a magnitude closer to120 $\mu W/m^2$ **(Fig. 3.44)**.

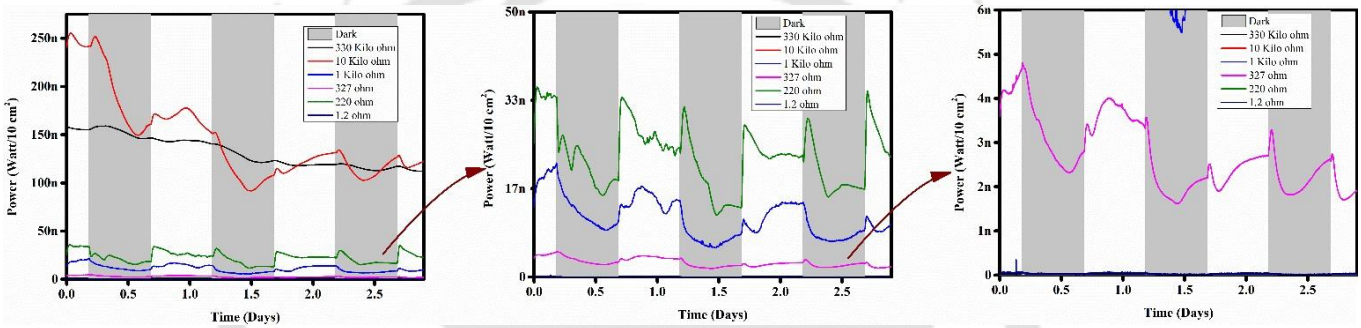

Figure 3. 44. Power generation in MFC setups in 12-12-hour light-dark cycle.

Interestingly, an increase in power density was not observed during 12 h dark phases in the 330 kilo-ohm MFC setup unlike what we expected. Rather, a complex pattern of modulations in the power density profile was observed in both light-dark transition phases in MFC setups under 10 kilo-ohm resistors and below it. These complex features are typical of a cyanobacterial amperogram as reported earlier (Zhang et al. 2018). One interesting addition to earlier reports was that we also observed this as the biofilm transitioned into the 12 h dark phase. Similar features have been reported recently by Hatano and coworkers by who did not explain them in physiological terms (Hatano et al. 2022). Additionally, no modulations were observed in MFC setups under a load of 1.2 ohms during light-dark transitions. Laura et al and coworkers showed such features to be associated with the peptidoglycan cell wall layer (Wey et al. 2021). Thus, based on experimental observations, we hypothesize that these features correspond to some gated ion channels present on cyanobacterial cell walls or redox processes in biofilm matrix influenced by these ion channels whose electrochemical response is elicited in response to a polarized electrode in an optimum potential range. As a small concentration of ferricyanide was detected in the setup under 220 ohm, it can be clearly observed that the power magnitude of this setup was higher than 327 and 1000 ohm, demonstrating the effect played by

the ferricyanide as a redox mediator (**Fig. 3.44**). The modulation patterns in this setup were also significantly pronounced, indicating that the rate of reduction of ferricyanide by biomass is much higher than its accessibility to anode and oxidation over it.

The next experiment involved the operation of seven MFC setups corresponding to the fixed resistors: 330 kilo-ohms, 200 kilo-ohms, 145 kilo-ohms, 77.8 kilo-ohms, 10 kilo-ohms, 1 kilo-ohms, and a OCP setup. The setups were operated with a regime similar to that described in open-circuit operation earlier and in methods. The intent was to generate a continuous current-voltage-power profile during abiotic operation, biofilm formation, and dark metabolism sequentially. Due to the inherent drawback of catholyte cross-over which varied in extent and timing between setups, the results varied and biofilm had to be replaced due to the toxic effect of ferricyanide in a few setups (**Fig. 3.45**).

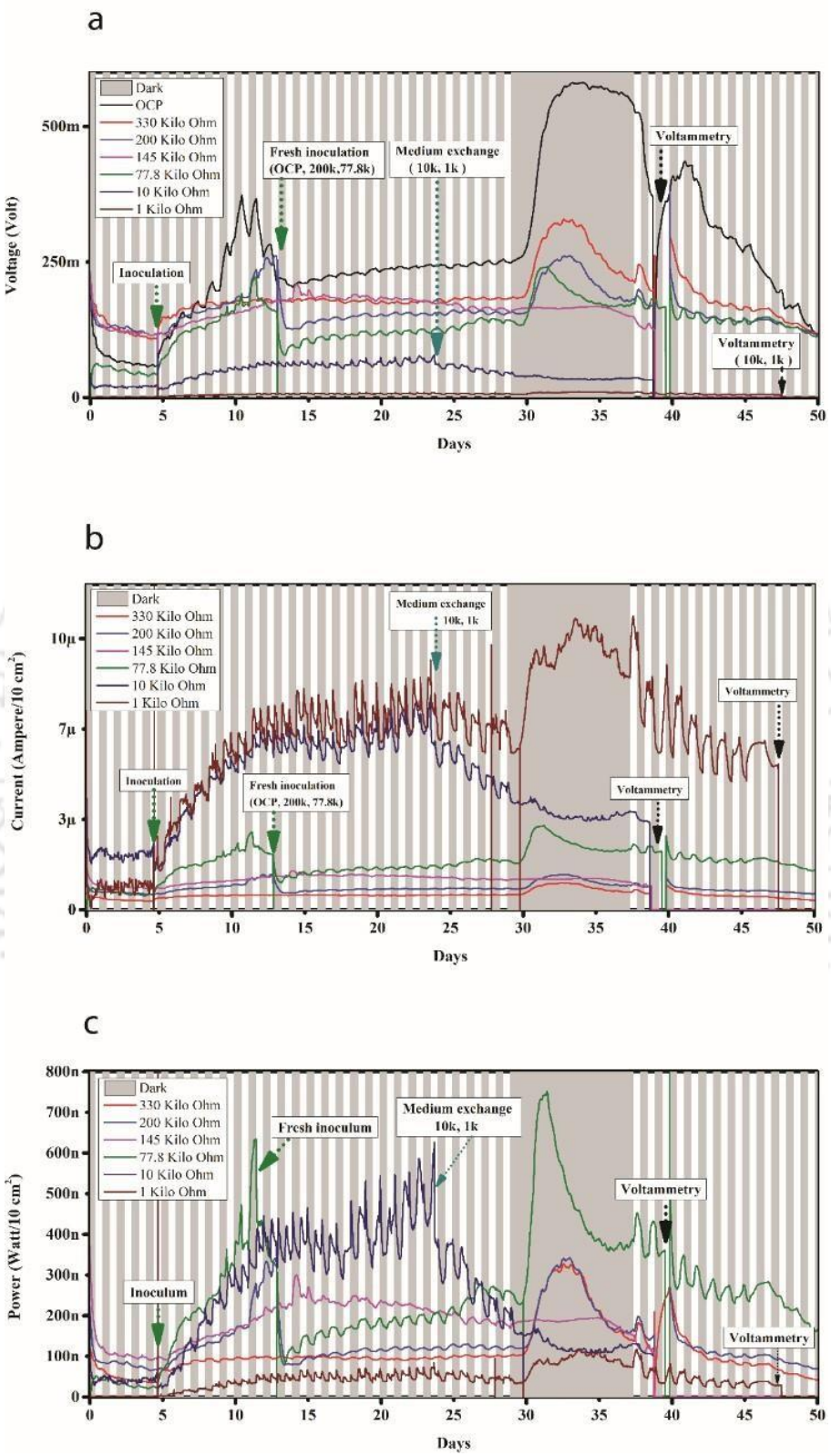

Figure 3. 45. (a) Complete voltage profile obtained for seven MFC setups operated under different loads and corresponding (b) current and (c) power profile.

The transition from active photosynthetic metabolism to cell death was judged by a combination of decrease in dissolved oxygen concentration, a sudden dip in electrochemical performance after rapid increase and visual browning of biofilm or either one of these. Thus, we only draw qualitative inferences from the observations we made as it was difficult to compare the setups in a quantitative manner. Another factor that may have contributed to variability between setups is difference in the extent and thickness of biofilm formation between setups, which must have influenced the local ferricyanide concentration within the biofilm microenvironment.

The biofilms were replaced in MFC setups under resistor values of OCP, 200 kilo-ohms, and 77.8 kilo-ohms on day 13th. The setup under 145 kilo-ohm was left unchanged as a sudden increase in voltage on day 14 was not accompanied by an immediate decrease in dissolved oxygen concentration. Though, dissolved oxygen was found to be reduced on later days. A marginal decrease in dissolved oxygen concentration upto 187% saturation was observed in MFC setups under resistor values of 10 kilo-ohms and 1 kilo-ohm on day 24. Thus, attempts were made to replace the inorganic medium on this day causing unintentional detachment of biofilms due to convection. The trade-off between electrochemical performance and mediator toxicity could not be maintained for a long time period evenly across setups in this experiment unlike previous experiments described. The first 13 days of voltage readings were without interruptions (**Fig. 3.46**). During this phase, the readings can be the net effect of simultaneous processes of biofilm formation, ferricyanide-mediated redox activity, mediator toxicity, and anode potential regulation by resistors**.** It was again observed that the setups in OCP and higher resistance ranges from 330 kilo-ohms to 77 kilo-ohms exhibited an increase in voltage/power density on each 12 h dark phase and a reduction in the 12 h light phase. This pattern sharply increased as more ferricyanide entered the anode causing a reduction in magnitude by day 13th in setups OCP with 200 kilo-ohm and 77.8 kilo-ohm due to toxicity. This also occurred in setup 145 kilo-ohm on day 14**.** In setup 330 kilo-ohm, even though the pattern of change in voltage was similar to others during this period, the magnitude was very less and features were poorly resolved. Oxygen concentration in this setup was however above 200%. In contrast to this, the setups under the load of 10 kilo-ohms and 1 kilo-ohm showed an incremental increase in voltage on each 12 h light phase. In addition, a sharp increase in voltage at the beginning of each 12 h dark phase was also observed that lasted for approximately 45 minutes. This feature became prominent from day 8 (day 3 after inoculation of biomass) which indicates that this feature was associated with an extracellular biofilm matrix that accumulated gradually. This pattern of increase in voltage is reminiscent of an increase in biofilm wet biomass, dissolved oxygen concentration, and stages of biofilm formation described in the biofilm characterization section.

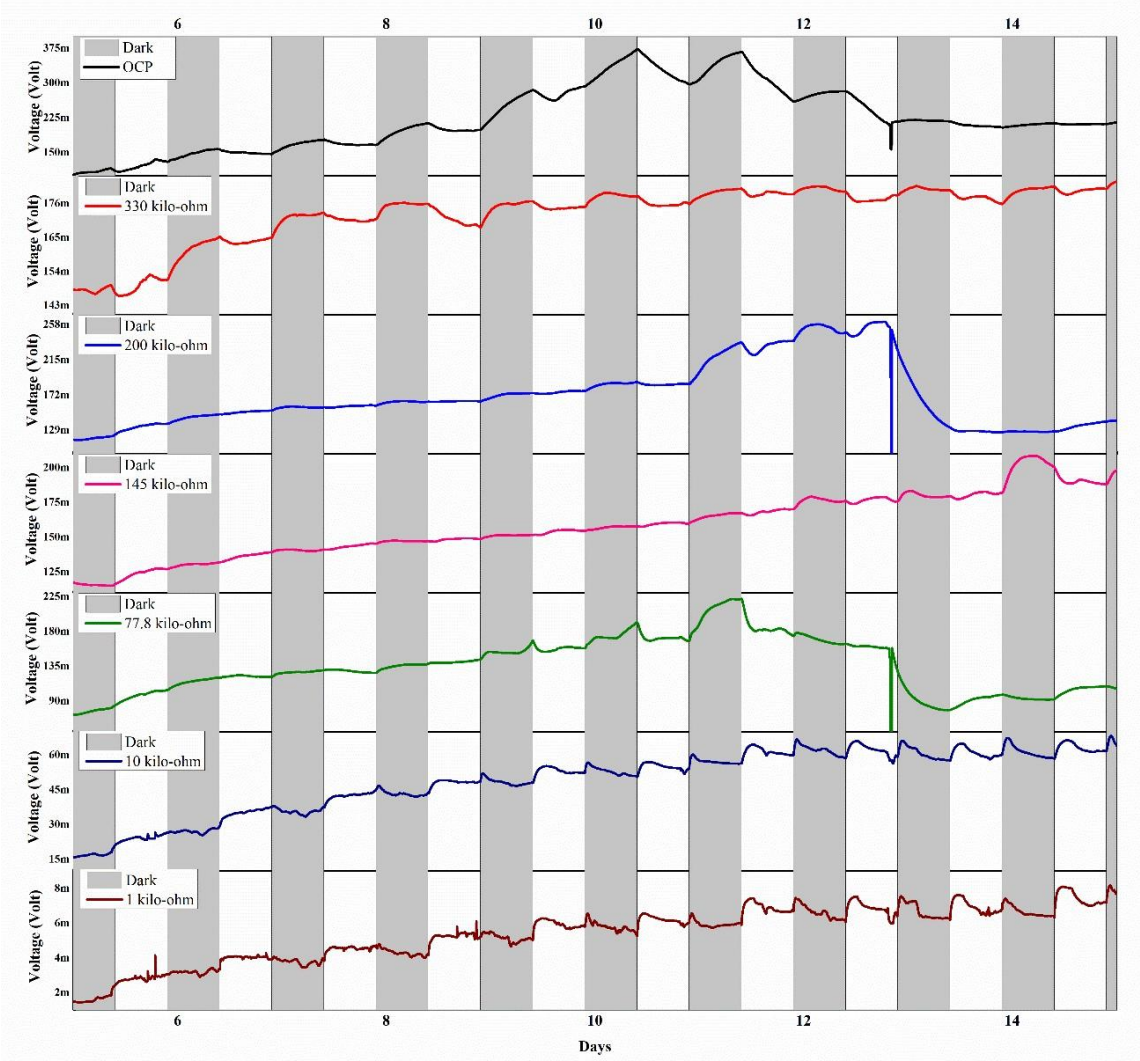

Figure 3. 46. OCP and closed circuit operation of MFC setups before cross-over (**INSET of Figure 3.45 from day 6 to 14**).

Thereafter, from day 12, the characteristic pattern of change in voltage was same and stabilized in magnitude to a certain extent. It again gradually increased in magnitude between day 17 and day 23 (**Fig. 3.47**). On this day, the dissolved oxygen concentration in the setup was found to be 193 %. Thus, to minimize the toxic effect of ferricyanide, an attempt of replacing the inorganic media was made. This led to partial detachment of the biofilms which was obvious in the 10 kilo-ohm setup, leading to a sharp reduction in voltage magnitude. This difference in the modulation patterns in current-voltage-power profiles of setups above and below 10 kilo-ohms is a reproduction of the earlier observation described above. This reaffirms the presence of redox processes on the cell walls and in the biofilm matrix that is elicited in response to a polarized electrode.

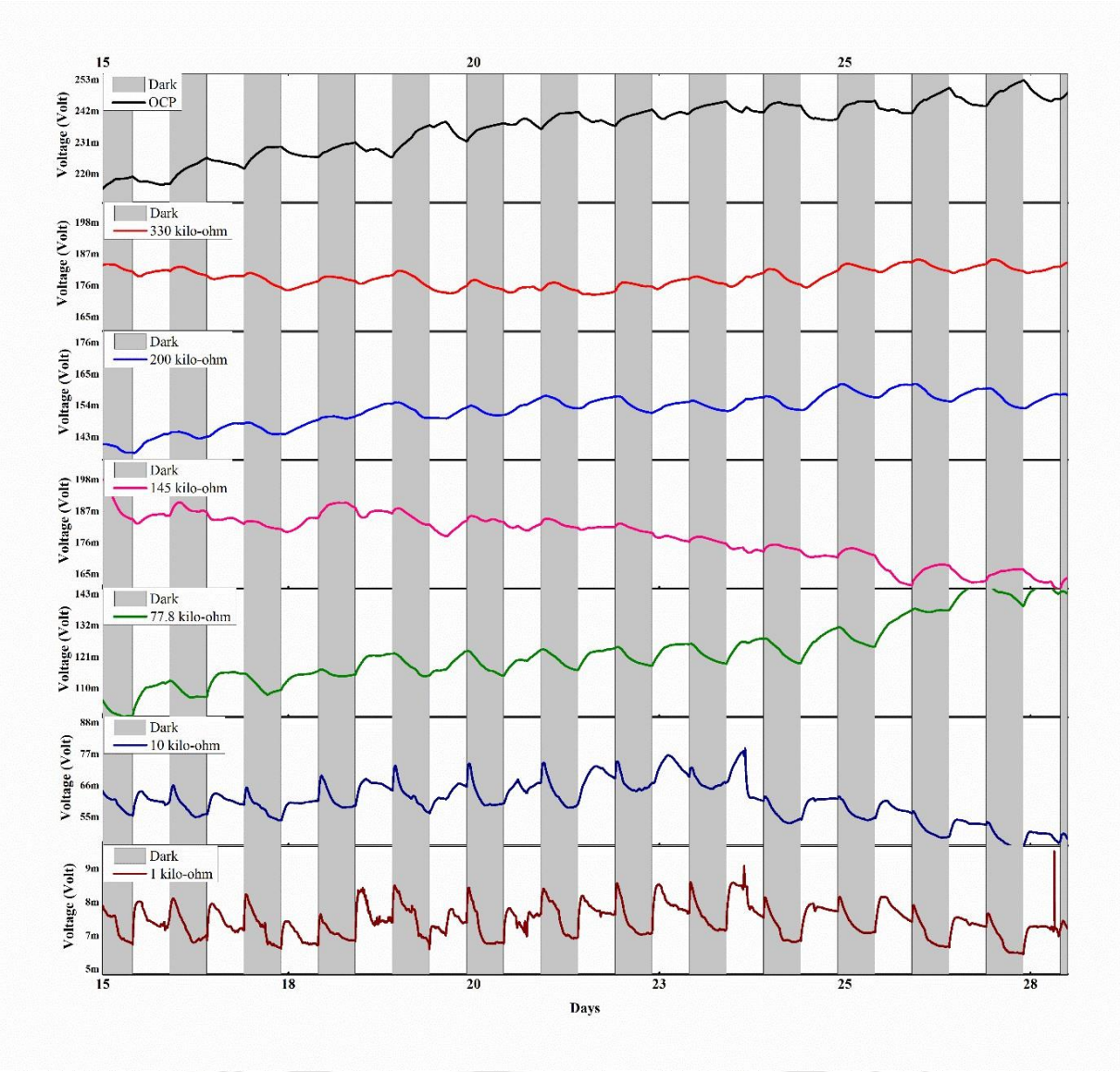

Figure 3. 47. MFC operation after fresh biomass replacement. (Media replaced in 10 kilo-ohms and I kilo-ohm on day 24).(**INSET of Figure 3.45 from day 15 to 28**).

The period after fresh biomass replenishment in the setups OCP, 200 kilo-ohms and 77.8 kilo-ohms showed a marked reduction in the magnitude of voltage response which had very poor resolution. We believe that this was because of the fouling of the electrode surface by remnants of previously formed biofilms and their debris. We realized that the poorly resolved pattern of change in voltage modulations with light-dark cycles, was different for the OCP setup and closed-circuit setups between days 13 and 29 (**Fig. 3.47**). Moreover, the pattern of voltage modulations also differed for the same setups before and after biofilm removal (day 13). Due to the removal of biofilm and reintroduction of biomass with continuous prolonged exposure to low

concentration ferricyanide, the redox molecule must have redistributed uniformly inside the biofilm matrix getting access to the anode surface. Thus, in closed circuit conditions, the photosynthetically reduced molecules must have oxidized over anodes causing a light-dependent increase in power density. In contrast to this, in the OCP setup, the reduced ferricyanide accumulated in the matrix with no path for electron release. Thus, we infer that factors like biomass-mediator concentration ratio in the biofilm microenvironment, the extent of its distribution inside the matrix, and anode potential together influence the pattern of current-voltage-power modulations.

On day 29, dark metabolism was induced in all the setups for 9 days (**Fig. 3.48**). As ferricyanide was found to be present in all the setups upon voltammetry at the end of operation, we consider the readings of this period to be redox-mediated (**Fig.3.49**). The rate of increase in voltage readings did not span the whole dark period, rather the onset started from 2nd day itself after partial anaerobiosis. As the absolute concentration of ferricyanide could not be inferred with accuracy due to the biofilm coverage of electrodes, we refrain from making a quantitative comparison of voltage and power densities between setups as all of them might be having different ferricyanide concentrations in the biofilm microenvironment influencing the power density to a different extent. However, the effect of resistor magnitude was quite evident by the difference in the time of decline in power magnitude between 330 kilo-ohms, 200 kilo-ohms, and 77.8 kilo-ohms. The decline was earlier in lower magnitude of 77.8 kilo-ohm than 330 and 200 kilo-ohms. A minor decline in voltage was observed after day 36 in the OCP setup, which is much later than that of 330 kilo-ohms. No increase in voltage/power density of 145 kilo-ohms was observed during this period as the biofilm formation was not complete. The dissolved oxygen started declining gradually after day 14 in this setup, possibly due to higher mediator concentration in the microenvironment such that the concentration of oxygen was only 43% before dark induction. Additionally, the effect of biofilm detachment on the performance of 10 kilo-ohms and 1 kilo-ohm setups was quite evident. Even though the power density of the 10 kilo-ohm setup was much higher in the photosynthetic phase before the detachment of biofilm, no increase in power density during the dark phase was observed due to it. Contrary to this, an increase in power magnitude was observed in a 1 kilo-ohm setup, which also underwent biofilm detachment to a lesser extent (**Fig.3.46**). These inferences were further confirmed by the pulse voltammetry results (**Fig.3.49**), where the value of differential current beyond 0.65 V declined due to higher baseline current on account of organic matter irreversible oxidation on high surface area electrodes. The setups which did not show a proper increase in power density during the dark phase due to incomplete biofilm formation or physical detachment, showed a lesser decline in differential current magnitude beyond 0.65 V.

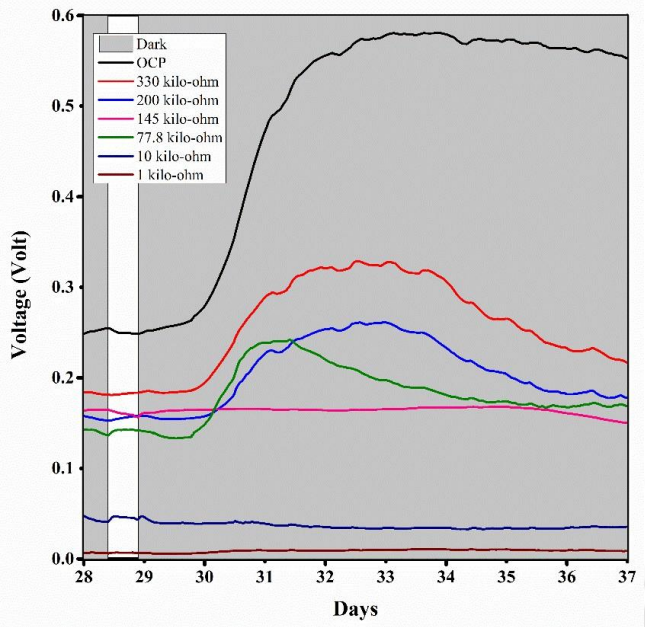

Figure 3. 48. MFC operation for 9 days in dark condition from day 29 to day 37. (INSET of Figure 3.45 from day 28 to 37).

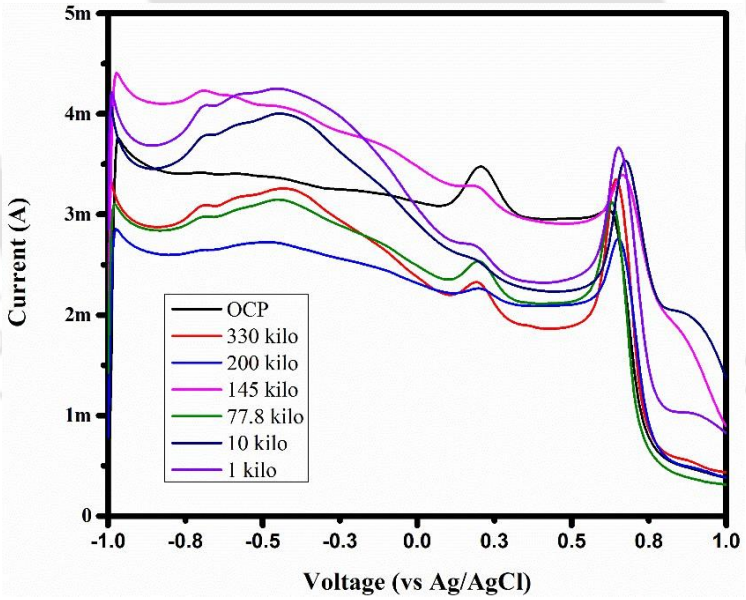

Figure 3. 49. Pulse voltammograms of MFC setups at the end of operation.

A final experiment was run under a resistor magnitude of 10 kilo-ohms with two setups, MFC-1 and 2. It was clearly observed that a light dependent modulation was present only in setups with biofilms in direct contact with the electrodes. This confirmed that redox processes in the biofilm matrix were responsible for those voltage modulations in light-to-dark transition phases (**Fig. 3.50**).

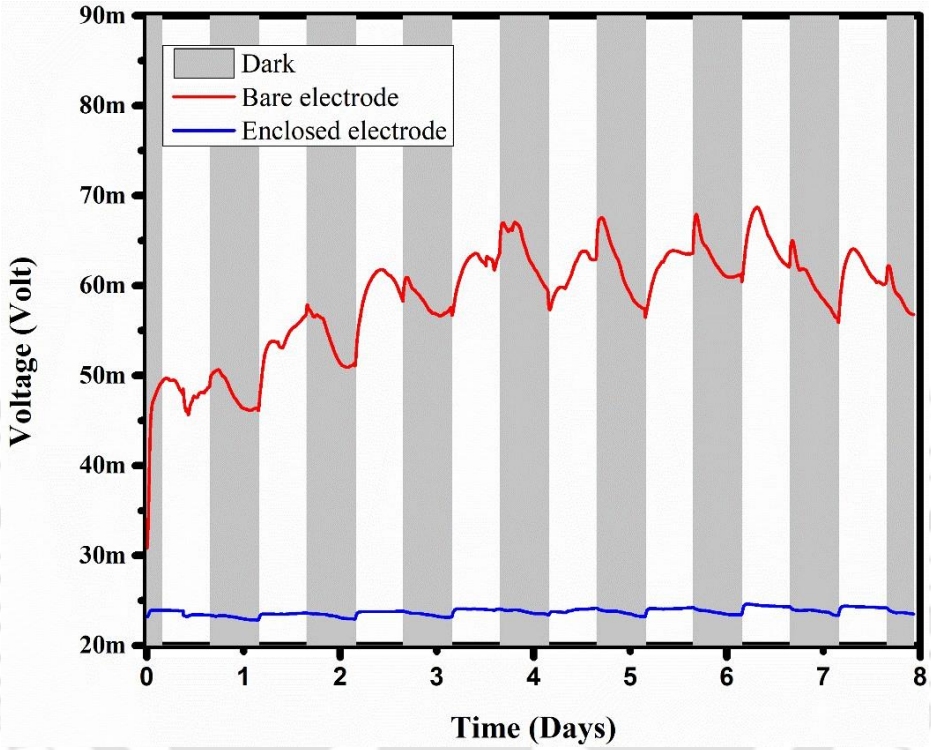

Figure 3. 50. Closed circuit MFC operation under 10 kilo-ohm resistors for a biofilm formed over bare anode (red color MFC-2) and biofilm not in direct contact with anode (blue color MFC-1).

CHAPTER 4

Conclusions and Future prospects

4.1 Conclusions

Our study reports fundamentally distinct open-circuit electrochemical behaviour of a *Spirulina* biofilm than that of a typical cyanobacteria-based biophotovoltaic anode, which reduces in magnitude during dark phase instead of light phase. *Ex-situ* electrochemical investigations revealed the presence of unidentified redox entities in the secreted organic matter bound to cell walls coupled with the presence of fluorescent moieties having putative redox activity accruing in the extracellular space. This extracellular space constituted the bulk of the biofilm volume and was the major biofilm component interacting physically with an electrode at interface. This biofilm exposed to gradually accruing ferricyanide redox mediator was found to be preserving metabolically active motile cells within the matrix. Further, it was observed that biotic activity was enhanced during prolonged dark conditions due to the respiratory and fermentative metabolism of cyanobacteria and associated symbionts at the expense of carbon reserves stored intracellularly and extracellularly which permanently altered the redox milieu. As the photosynthetic metabolism could be resumed upon illumination, this biofilm system was deemed suitable for performing time-dependent *in- situ* electrochemical investigations under versatile metabolic conditions. Direct and contiguous physical contact of the biofilm extracellular matrix with the electrode is necessary for potentiometric or amperometric sensing of the intrabiofilm redox process. The magnitude dark-dependent increase (more –ve) in anode potential was greatly influenced by dissolved oxygen and redox mediator concentrations in the biofilm matrix as determined by Tafel analysis. While the former attenuated the signals, the latter enhanced the signals. The presence of ferricyanide or anaerobic conditions made the reductive reactions in the extracellular matrix more dominant causing accumulation of electrons emanating from cellular metabolism into it. Whereas the absence of mediator with the presence of oxygen-saturated conditions in the matrix made oxidative reactions more dominant leading to the electron quenching by oxygen.

Moreover, the mediator concentration in the biofilm matrix was not uniform as most of it gets trapped and reduced inside the biofilm matrix itself. As a result of this, the redox conduction occurred only over a short distance and could be sensed over the electrode only when the biofilm was in direct contact or when the biofilm components were released into the dialysis bag after polysaccharide degradation in the biofilm during prolonged dark period. This tendency of mediator trapping inside biofilm was also responsible for the prolonged viability of cells within the bulk of biofilm as it preserved them from sudden exposure to high mediator concentration and acute toxicity. The influence of mediator concentration hangs

perilously between enhanced electrochemical performance and mediator toxicity at each coordinate and depends on its relative position with respect to the biofilm surface and electrode surface. Voltammetry results also indicated that ferricyanide exposure leads to an increase of irreversibly oxidizable and reducible species in the biofilm that might be released as a biological response to ferricyanide exposure.

In response to the closed circuit current drawn by a resistor magnitude of 10 kilo-ohms and below, the voltage profile showed two inflections during dark-to-light and light-to-dark transitions. While the former istypical of cyanobacteria chronoamperograms, the latter is an unexplained observation reported recently (Hatano et al. 2022). The gradual increase in magnitude for the first 12 to 13 days with superimposed light-dark transition inflections is reminiscent of the early stages of *Spirulina* biofilm formation. Contrary to this,at resistors higher than 10 kilo-ohms, the voltage profiles were similar to the open-circuit voltage profiles. Thus, we infer that in response to resistor-influenced current demand, redox gradients were established at the electrode interface. This gradient influenced the pattern and magnitude along with other additional factors like (i) mediator concentration, (ii) extent of biofilm formation, (iii) distribution of mediator inside abiofilm, (iv) mediator concentration at each coordinate, which were beyond operators control in this experiment.

While the biotic activity during prolonged dark conditions inside the biofilm alters it biochemically, in an electrochemical context the anode potential was gradually reduced. This could be due to a combination of anaerobiosis and exoelectrogenicity, which lead to electron accumulation in extracellular space. Upon closed circuit operations, we observed that the rate of increase in current was much faster in presence of redox mediators. Disintegration of extracellular matrix components during this phase and the presence of bulky molecules must have reduced the rate of electron transfer, whereas in the presence of highly diffusible redox molecules, it was observed that electron mediation was much faster. The voltage magnitude declined quickly indicating the eventual depletion of carbon reserves influenced by resistor magnitude. Even though in BPV research we focus on sustainable power production derived from water lysis, the electrochemical performance in phototrophic mats during prolonged dark conditions has an important implication for BPV device functionality during storage or minimal light access affecting its shelf life.

The results of our study demonstrate the role and associated pros and cons of biofilm extracellular matrix on the electrochemical performance of cyanobacterial biofilm based biophotovoltaic devices. Firstly, the extracellular matrix provides nourishment to cyanobacteria for surviving prolonged dark conditions and harbors symbionts that make the biotic component of BPV resilient and durable for real-time application. Secondly, it provides safety to the cells within it from stressful high mediator concentrations and toxic substances. Thirdly, it may act as a reservoir of endogenously produced or artificially introduced redox

molecules enhancing electrochemical performance. On the other side, it is difficult to achieve uniform mediator concentration and predictable control over reaction dynamics within the biofilm matrix causing unpredictable variations that influence the viability and performance of the BPV system. Moreover, the reaction dynamics within this matrix also change with time and metabolic conditions that persist within the biofilm. These insights gained by this work may guide researchers who aim to rationally engineer a monospecies or multispecies-based phototrophic biofilm specialized for ideal biophotovoltaic applications.

4.2 Future prospects

Biophotovoltaics is a field with immense scope of both fundamental and applicative research. In this study, we have shown the steady-state redox behavior of a cyanobacterial biofilm in the context of a biofilm organization. Further, we also did an experiment in closed-circuit drawing current through a resistor. The results indicate that the redox processes occurring in the biofilm matrix also influence the current profile. However, several investigations need to be carried out for further development and improvement of BPV technology.

1. Identification of specific redox processes occurring in the extracellular biofilm matrix.

2. Identification of the cell surface ion channels/proteins responsible for generating current production in cyanobacteria based MFC devices.

3. Studying the effect of electrochemical bias on the physiology of individual cyanobacterial cells and the associated self-produced matrix through advanced omics technology.

4. Identification of genes and metabolic pathways to be targeted for synthetic biology-based development of cyanobacterial strains for application in BPV technology.

5. Electrochemical analysis of cyanobacterial symbionts for their evaluation in the context of BPV technology.

6. Design of synthetic cyanobacteria-dominated microbial consortia for application in BPV technology.

7. Power management systems for enhancing the performance of BPV technology.

8. Design of a cell-electrode interface for enhanced electron extraction from cyanobacterial cells.

REFERENCES

Abed, Raeid M.M., Burhanuddin Zein, Assad Al-Thukair, and Dirk de Beer. 2007. "Phylogenetic Diversity and Activity of Aerobic Heterotrophic Bacteria from a Hypersaline Oil-Polluted Microbial Mat." *Systematic and Applied Microbiology* 30 (4): 319–30. https://doi.org/10.1016/j.syapm.2006.09.001.

Aeschbacher, Michael, Michael Sander, and René P. Schwarzenbach. 2010. "Novel Electrochemical Approach to Assess the Redox Properties of Humic Substances." *Environmental Science and Technology* 44 (1): 87–93. https://doi.org/10.1021/es902627p.

Aiyer, Kartik, and Lucinda E. Doyle. 2022. "Capturing the Signal of Weak Electricigens: A Worthy Endeavour." *Trends in Biotechnology* 40 (5): 564–75. https://doi.org/10.1016/j.tibtech.2021.10.002.

Ananyev, Gennady, Damian Carrieri, and G. Charles Dismukes. 2008. "Optimization of Metabolic Capacity and Flux through Environmental Cues to Maximize Hydrogen Production by the Cyanobacterium 'Arthrospira (Spirulina) Maxima.'" *Applied and Environmental Microbiology* 74 (19): 6102–13. https://doi.org/10.1128/AEM.01078-08.

Ananyev, Gennady M., Nicholas J. Skizim, and G. Charles Dismukes. 2012. "Enhancing Biological Hydrogen Production from Cyanobacteria by Removal of Excreted Products." *Journal of Biotechnology* 162 (1): 97–104. https://doi.org/10.1016/j.jbiotec.2012.03.026.

Argandoña, Montserrat, Fernando Martínez-Checa, Inmaculada Llamas, Yolanda Arco, Emilia Quesada, and Ana Del Moral. 2006. "A Membrane-Bound Nitrate Reductase Encoded by the NarGHJI Operon Is Responsible for Anaerobic Respiration in Halomonas Maura." *Extremophiles* 10 (5): 411–19. https://doi.org/10.1007/s00792-006-0515-2.

Artuso, Irene, Paolo Turrini, Mattia Pirolo, Gabriele Andrea Lugli, Marco Ventura, and Paolo Visca. 2021. "Phylogenomic Reconstruction and Metabolic Potential of the Genus Aminobacter." *Microorganisms* 9 (6). https://doi.org/10.3390/microorganisms9061332.

Ataeian, Maryam, Yihua Liu, Angela Kouris, Alyse K. Hawley, and Marc Strous. 2022. "Ecological Interactions of Cyanobacteria and Heterotrophs Enhances the Robustness of Cyanobacterial Consortium for Carbon Sequestration." *Frontiers in Microbiology* 13 (February): 1–16. https://doi.org/10.3389/fmicb.2022.780346.

Babauta, Jerome, Ryan Renslow, Zbigniew Lewandowski, and Haluk Beyenal. 2012. "Electrochemically Active Biofilms: Facts and Fiction. A Review." *Biofouling* 28 (8): 789–812. https://doi.org/10.1080/08927014.2012.710324.

Babauta, Jerome T., and Haluk Beyenal. 2014. "Mass Transfer Studies of Geobacter Sulfurreducens Biofilms on Rotating Disk Electrodes." *Biotechnology and Bioengineering* 111 (2): 285–94. https://doi.org/10.1002/bit.25105.

Béjar, Victoria, In Mac Ulada Llamas, Concepción Calvo, and Emilia Quesada. 1998. "Characterization of Exopolysaccharides Produced by 19 Halophilic Strains of the Species Halomonas Eurihalina." *Journal of Biotechnology* 61 (2): 135–41. https://doi.org/10.1016/S0168-1656(98)00024-8.

Beygmoradi, Azadeh, and Ahmad Homaei. 2017. "Marine Microbes as a Valuable Resource for Brand New Industrial Biocatalysts." *Biocatalysis and Agricultural Biotechnology* 11 (June): 131–52. https://doi.org/10.1016/j.bcab.2017.06.013.

Bhakar, R. N., R. Kumar, and Sunil Pabbi. 2013. "Total Lipids and Fatty Acid Profile of Different Spirulina Strains as Affected by Salinity and Incubation Time." *Vegetos* 26 (January): 148–54. https://doi.org/10.5958/j.2229-4473.26.2s.133.

Bombelli, P., A. Savanth, A. Scarampi, S. J. L. Rowden, D. H. Green, A. Erbe, E. Årstøl, et al. 2022. "Powering a Microprocessor by Photosynthesis." *Energy & Environmental Science*. https://doi.org/10.1039/d2ee00233g.

Bombelli, Paolo, Robert W. Bradley, Amanda M. Scott, Alexander J. Philips, Alistair J. McCormick, Sonia M. Cruz, Alexander Anderson, et al. 2011. "Quantitative Analysis of the Factors Limiting Solar Power Transduction by Synechocystis Sp. PCC 6803 in Biological Photovoltaic Devices." *Energy and Environmental Science* 4 (11): 4690–98. https://doi.org/10.1039/c1ee02531g.

Bombelli, Paolo, Thomas Müller, Therese W. Herling, Christopher J. Howe, and Tuomas P.J. Knowles. 2015. "A High Power-Density, Mediator-Free, Microfluidic Biophotovoltaic Device for Cyanobacterial Cells." *Advanced Energy Materials* 5 (2). https://doi.org/10.1002/aenm.201401299.

Bombelli, Paolo, Marie Zarrouati, Rebecca J. Thorne, Kenneth Schneider, Stephen J.L. Rowden, Akin Ali, Kamran Yunus, et al. 2012. "Surface Morphology and Surface Energy of Anode Materials Influence Power Outputs in a Multi-Channel Mediatorless Bio-Photovoltaic (BPV) System." *Physical Chemistry Chemical Physics* 14 (35): 12221–29. https://doi.org/10.1039/c2cp42526b.

Bond, Daniel R., and Derek R. Lovley. 2003. "Electricity Production by Geobacter Sulfurreducens Attached to Electrodes." *Applied and Environmental Microbiology* 69 (3): 1548–55. https://doi.org/10.1128/AEM.69.3.1548-1555.2003.

Bradley, Robert W., Paolo Bombelli, David J. Lea-Smith, and Christopher J. Howe. 2013. "Terminal Oxidase Mutants of the Cyanobacterium Synechocystis Sp. PCC 6803 Show Increased Electrogenic Activity in Biological Photo-Voltaic Systems." *Physical Chemistry Chemical Physics* 15 (32): 13611–18. https://doi.org/10.1039/c3cp52438h.

Bruce E. Logan, Bert Hamelers, René Rozendal, Uwe Shroder, Jurg Keller, Stefano Freguia, Peter Aelterman, Willy Verstraete and Korneel Rabaey. 2006. "Critical Review Microbial Fuel Cells : Methodology and Technology." *Environmental Science & Technology* 40 (17): 5181–92. http://pubs.acs.org/doi/abs/10.1021/es0605016.

Buchan, Alison, Gary R. LeCleir, Christopher A. Gulvik, and José M. González. 2014. "Master Recyclers: Features and Functions of Bacteria Associated with Phytoplankton Blooms." *Nature Reviews. Microbiology* 12 (10): 686–98. https://doi.org/10.1038/nrmicro3326.

Carrieri, Damian, Dariya Momot, Ian A. Brasg, Gennady Ananyev, Oliver Lenz, Donald A. Bryant, and G. Charles Dismukes. 2010. "Boosting Autofermentation Rates and Product Yields with Sodium Stress Cycling: Application to Production of Renewable Fuels by Cyanobacteria." *Applied and Environmental Microbiology* 76 (19): 6455–62. https://doi.org/10.1128/AEM.00975-10.

Castenholz, Richard W., Rosmarie Rippka, Michael Herdman, and Annick Wilmotte. 2015. " Form-Spirulina ." *Bergey's Manual of Systematics of Archaea and Bacteria*, 1–4. https://doi.org/10.1002/9781118960608.gbm00445.

Cereda, Angelo, Andrew Hitchcock, Mark D. Symes, Leroy Cronin, Thomas S. Bibby, and Anne K. Jones. 2014. "A Bioelectrochemical Approach to Characterize Extracellular Electron Transfer by Synechocystis Sp. PCC6803." *PLoS ONE* 9 (3): 1–8. https://doi.org/10.1371/journal.pone.0091484.

Chakraborty, Tania, A K Sen, and R Pal. 2015. "Stress Induced Extra Cellular Polysaccharide of Spirulina Subsalsa Stress Induced Enhancement in Exo-Polysaccharide Production in Spirulina

Subsalsa and Its Chemical Characterization." *J. Algal Biomass Utln* 6 (3): 24–38. http://jalgalbiomass.com/paper5vol6no3.pdf.

Chen, Wen, Paul Westerhoff, Jerry A. Leenheer, and Karl Booksh. 2003. "Fluorescence Excitation-Emission Matrix Regional Integration to Quantify Spectra for Dissolved Organic Matter." *Environmental Science and Technology* 37 (24): 5701–10. https://doi.org/10.1021/es034354c.

Chen, Xiaolong, Joshua M. Lawrence, Laura T. Wey, Lukas Schertel, Qingshen Jing, Silvia Vignolini, Christopher J. Howe, Sohini Kar-Narayan, and Jenny Z. Zhang. 2022. "3D-Printed Hierarchical Pillar Array Electrodes for High-Performance Semi-Artificial Photosynthesis." *Nature Materials*. https://doi.org/10.1038/s41563-022-01205-5.

Choi, Gang Guk, Myong Sook Bae, Chi Yong Ahn, and Hee Mock Oh. 2008. "Induction of Axenic Culture of Arthrospira (Spirulina) Platensis Based on Antibiotic Sensitivity of Contaminating Bacteria." *Biotechnology Letters* 30 (1): 87–92. https://doi.org/10.1007/s10529-007-9523-2.

Christie-Oleza, Joseph A., Jean Armengaud, Philippe Guerin, and David J. Scanlan. 2015. "Functional Distinctness in the Exoproteomes of Marine Synechococcus." *Environmental Microbiology* 17 (10): 3781–94. https://doi.org/10.1111/1462-2920.12822.

Chu, Steven, Yi Cui, and Nian Liu. 2016. "The Path towards Sustainable Energy." *Nature Materials* 16 (1): 16–22. https://doi.org/10.1038/nmat4834.

Clifford, Eleanor R., Robert W. Bradley, Laura T. Wey, Joshua M. Lawrence, Xiaolong Chen, Christopher J. Howe, and Jenny Z. Zhang. 2021. "Phenazines as Model Low-Midpoint Potential Electron Shuttles for Photosynthetic Bioelectrochemical Systems." *Chemical Science* 12 (9): 3328–38. https://doi.org/10.1039/d0sc05655c.

Coble, Paula G. 1996. "Characterization of Marine and Terrestrial DOM in Seawater Using Excitation-Emission Matrix Spectroscopy." *Marine Chemistry* 51 (4): 325–46. https://doi.org/10.1016/0304-4203(95)00062-3.

Conde, Tiago A., Bruna F. Neves, Daniela Couto, Tânia Melo, Bruno Neves, Margarida Costa, Joana Silva, Pedro Domingues, and M. Rosário Domingues. 2021. "Microalgae as Sustainable Bio-Factories of Healthy Lipids: Evaluating Fatty Acid Content and Antioxidant Activity." *Marine Drugs* 19 (7): 1–20. https://doi.org/10.3390/md19070357.

Coulon, Frédéric, Panagiota Myrsini Chronopoulou, Anne Fahy, Sandrine Païssé, Marisol Goñi-Urriza, Louis Peperzak, Laura Acuña Alvarez, et al. 2012. "Central Role of Dynamic Tidal Biofilms Dominated by Aerobic Hydrocarbonoclastic Bacteria and Diatoms in the Biodegradation of Hydrocarbons in Coastal Mudflats." *Applied and Environmental Microbiology* 78 (10): 3638–48. https://doi.org/10.1128/AEM.00072-12.

Darus, Libertus, Yang Lu, Pablo Ledezma, Jürg Keller, and Stefano Freguia. 2015. "Fully Reversible Current Driven by a Dual Marine Photosynthetic Microbial Community." *Bioresource Technology* 195: 248–53. https://doi.org/10.1016/j.biortech.2015.06.055.

Darus, Libertus, Takuya Sadakane, Pablo Ledezma, Seiya Tsujimura, Isioma Osadebe, Dónal Leech, Lo Gorton, and Stefano Freguia. 2017. "Redox-Polymers Enable Uninterrupted Day/Night Photo-Driven Electricity Generation in Biophotovoltaic Devices." *Journal of The Electrochemical Society* 164 (3): H3037–40. https://doi.org/10.1149/2.0091703jes.

David, Christian, Rohan Karande, and Katja Bühler. 2021. "Cyanobacterial Biofilms in Natural and Synthetic Environments." *Cyanobacteria Biotechnology*, 477–503. https://doi.org/10.1002/9783527824908.ch15.

Deschoenmaeker, Frédéric, Raphaël Facchini, Juan Carlos Cabrera Pino, Guillaume Bayon-Vicente, Neha Sachdeva, Patrick Flammang, and Ruddy Wattiez. 2016. "Nitrogen Depletion in Arthrospira Sp. PCC 8005, an Ultrastructural Point of View." *Journal of Structural Biology* 196 (3): 385–93. https://doi.org/10.1016/j.jsb.2016.08.007.

Deschoenmaeker, Frédéric, Raphaël Facchini, Baptiste Leroy, Hanène Badri, C. C. Zhang, and Ruddy Wattiez. 2014. "Proteomic and Cellular Views of Arthrospira Sp. PCC 8005 Adaptation to Nitrogen Depletion." *Microbiology (United Kingdom)* 160 (PART 6): 1224–36. https://doi.org/10.1099/mic.0.074641-0.

Diamond, Spencer, Benjamin E. Rubin, Ryan K. Shultzaberger, You Chen, Chase D. Barber, and Susan S. Golden. 2017. "Redox Crisis Underlies Conditional Light-Dark Lethality in Cyanobacterial Mutants That Lack the Circadian Regulator, RpaA." *Proceedings of the National Academy of Sciences of the United States of America* 114 (4): E580–89. https://doi.org/10.1073/pnas.1613078114.

Doyle, Lucinda E., and Enrico Marsili. 2018. "Weak Electricigens: A New Avenue for Bioelectrochemical Research." *Bioresource Technology* 258 (February): 354–64. https://doi.org/10.1016/j.biortech.2018.02.073.

Doyle, Lucinda Elizabeth, and Enrico Marsili. 2015. "Methods for Enrichment of Novel Electrochemically-Active Microorganisms." *Bioresource Technology* 195: 273–82. https://doi.org/10.1016/j.biortech.2015.07.025.

Elgrishi, Noémie, Kelley J. Rountree, Brian D. McCarthy, Eric S. Rountree, Thomas T. Eisenhart, and Jillian L. Dempsey. 2018. "A Practical Beginner's Guide to Cyclic Voltammetry." *Journal of Chemical Education* 95 (2): 197–206. https://doi.org/10.1021/acs.jchemed.7b00361.

Ferris, M. J., and C. F. Hirsch. 1991. "Method for Isolation and Purification of Cyanobacteria." *Applied and Environmental Microbiology* 57 (5): 1448–52. https://doi.org/10.1128/aem.57.5.1448-1452.1991.

Filali Mouhim, R., J. F. Cornet, T. Fontane, B. Fournet, and G. Dubertret. 1993. "Production, Isolation and Preliminary Characterization of the Exopolysaccharide of the Cyanobacterium Spirulina Platensis." *Biotechnology Letters* 15 (6): 567–72. https://doi.org/10.1007/BF00138541.

Finkelstein, David A., Leonard M. Tender, and J. Gregory Zeikus. 2006. "Effect of Electrode Potential on Electrode-Reducing Microbiota." *Environmental Science and Technology* 40 (22): 6990–95. https://doi.org/10.1021/es061146m.

Flemming, Hans Curt, Eric D. van Hullebusch, Thomas R. Neu, Per H. Nielsen, Thomas Seviour, Paul Stoodley, Jost Wingender, and Stefan Wuertz. 2022. "The Biofilm Matrix: Multitasking in a Shared Space." *Nature Reviews Microbiology* 0123456789. https://doi.org/10.1038/s41579-022-00791-0.

Fu, Chun Chong, Tien Chieh Hung, Wen Teng Wu, Ten Chin Wen, and Chia Hung Su. 2010. "Current and Voltage Responses in Instant Photosynthetic Microbial Cells with Spirulina Platensis." *Biochemical Engineering Journal* 52 (2–3): 175–80. https://doi.org/10.1016/j.bej.2010.08.004.

Fu, Chun Chong, Chia Hung Su, Tien Chieh Hung, Chih Hung Hsieh, Devi Suryani, and Wen Teng Wu. 2009. "Effects of Biomass Weight and Light Intensity on the Performance of Photosynthetic Microbial Fuel Cells with Spirulina Platensis." *Bioresource Technology* 100 (18): 4183–86. https://doi.org/10.1016/j.biortech.2009.03.059.

Gacitua, Manuel, Catalina Urrejola, Javiera Carrasco, Rafael Vicuña, Benjamín M. Srain, Silvio Pantoja-Gutiérrez, Donal Leech, Riccarda Antiochia, and Federico Tasca. 2020. "Use of a Thermophile

Desiccation-Tolerant Cyanobacterial Culture and Os Redox Polymer for the Preparation of Photocurrent Producing Anodes." *Frontiers in Bioengineering and Biotechnology* 8 (August): 1–11. https://doi.org/10.3389/fbioe.2020.00900.

Gan, Longzhan, Xiufeng Long, Heming Zhang, Yanyan Hou, Jiewei Tian, Yuqin Zhang, and Yongqiang Tian. 2018. "Halomonas Saliphila Sp. Nov., a Moderately Halophilic Bacterium Isolated from a Saline Soil." *International Journal of Systematic and Evolutionary Microbiology* 68 (4): 1153–59. https://doi.org/10.1099/ijsem.0.002644.

Gao, Pin, Benru Song, Rui Xu, Xiaoxu Sun, Hanzhi Lin, Fuqing Xu, Baoqin Li, and Weimin Sun. 2021. "Structure and Variation of Root-Associated Bacterial Communities of Cyperus Rotundus L. in the Contaminated Soils around Pb/Zn Mine Sites." *Environmental Science and Pollution Research* 28 (41): 58523–35. https://doi.org/10.1007/s11356-021-14595-x.

Giner-Lamia, Joaquín, Sara B. Pereira, Miquel Bovea-Marco, Matthias E. Futschik, Paula Tamagnini, and Paulo Oliveira. 2016. "Extracellular Proteins: Novel Key Components of Metal Resistance in Cyanobacteria?" *Frontiers in Microbiology* 7 (JUN): 1–8. https://doi.org/10.3389/fmicb.2016.00878.

Gonzalez-Aravena, A. C., K. Yunus, L. Zhang, B. Norling, and A. C. Fisher. 2018. "Tapping into Cyanobacteria Electron Transfer for Higher Exoelectrogenic Activity by Imposing Iron Limited Growth." *RSC Advances* 8 (36): 20263–74. https://doi.org/10.1039/c8ra00951a.

Goyal, Rajendra N., Vinod K. Gupta, Munetaka Oyama, and Neeta Bachheti. 2006. "Differential Pulse Voltammetric Determination of Atenolol in Pharmaceutical Formulations and Urine Using Nanogold Modified Indium Tin Oxide Electrode." *Electrochemistry Communications* 8 (1): 65–70. https://doi.org/10.1016/j.elecom.2005.10.011.

Graef, Mark R. De, Svetlana Alexeeva, Jacky L. Snoep, and M. Joost Teixeira De Mattos. 1999. "The Steady-State Internal Redox State (NADH/NAD) Reflects the External Redox State and Is Correlated with Catabolic Adaptation in Escherichia Coli." *Journal of Bacteriology* 181 (8): 2351–57. https://doi.org/10.1128/jb.181.8.2351-2357.1999.

Guzman, Michael S., Karthikeyan Rengasamy, Michael M. Binkley, Clive Jones, Tahina Onina Ranaivoarisoa, Rajesh Singh, David A. Fike, J. Mark Meacham, and Arpita Bose. 2019. "Phototrophic Extracellular Electron Uptake Is Linked to Carbon Dioxide Fixation in the Bacterium Rhodopseudomonas Palustris." *Nature Communications* 10 (1): 1–13. https://doi.org/10.1038/s41467-019-09377-6.

Halary, Sébastien, Sébastien Duperron, Justine Demay, Charlotte Duval, Sahima Hamlaoui, Bérénice Piquet, Anita Reinhart, Cécile Bernard, and Benjamin Marie. 2022. "Metagenome-Based Exploration of Bacterial Communities Associated with Cyanobacteria Strains Isolated from Thermal Muds," no. September. https://doi.org/10.20944/preprints202209.0219.v1.

Hatano, Jiro, Shoko Kusama, Kenya Tanaka, Ayaka Kohara, Chikahiro Miyake, Shuji Nakanishi, and Ginga Shimakawa. 2022. "NADPH Production in Dark Stages Is Critical for Cyanobacterial Photocurrent Generation: A Study Using Mutants Deficient in Oxidative Pentose Phosphate Pathway." *Photosynthesis Research*, no. 0123456789. https://doi.org/10.1007/s11120-022-00903-0.

Helburn, Robin S., and Patrick MacCarthy. 1994. "Determination of Some Redox Properties of Humic Acid by Alkaline Ferricyanide Titration." *Analytica Chimica Acta* 295 (3): 263–72. https://doi.org/10.1016/0003-2670(94)80231-9.

Howley, Ethan, Rosa Krajmalnik-brown, and César I. Torres. 2022. "Cytochrome Expression Shifts in Geobacter Sulfurreducens to Maximize Energy Conservation in Response to Changes in Redox

Conditions." *BioRxiv*, 1–34. https://www.biorxiv.org/content/10.1101/2022.05.22.492868v1%0Ahttps://www.biorxiv.org/content/10.1101/2022.05.22.492868v1.abstract.

Huisman, Jef, Geoffrey A. Codd, Hans W. Paerl, Bas W. Ibelings, Jolanda M.H. Verspagen, and Petra M. Visser. 2018. "Cyanobacterial Blooms." *Nature Reviews Microbiology* 16 (8): 471–83. https://doi.org/10.1038/s41579-018-0040-1.

Ichihashi, Osamu, Chika Tada, and Yutaka Nakai. 2011. "Power Generation from Animal Wastewater Using Microbial Fuel Cell." *Journal of Integrated Field Science* 8 (November): 13–20. http://ir.library.tohoku.ac.jp/re/bitstream/10097/50392/1/AA12005506-2011-8-13.pdf.

Jeon, Hyeon Jin, Yong Keun Choi, Kyung Guen Song, Sang Hyun Lee, Yung Hun Yang, Hyungsup Kim, Sunghyun Kim, Rangarajulu Kumaran, Seok Won Hong, and Hyung Joo Kim. 2013. "Development of a Photoelectrochemical Sensor for Monitoring Algal Biomass (Chlorella Vulgaris)." *Sensors and Actuators, B: Chemical* 185: 405–10. https://doi.org/10.1016/j.snb.2013.05.026.

Jiang, Liqun, Jiongming Sun, Changliang Nie, Yizhen Li, Jackson Jenkins, and Haiyan Pei. 2019. "Filamentous Cyanobacteria Triples Oil Production in Seawater-Based Medium Supplemented with Industrial Waste: Monosodium Glutamate Residue." *Biotechnology for Biofuels* 12 (1): 1–16. https://doi.org/10.1186/s13068-019-1391-1.

Jodlbauer, Julia, Thomas Rohr, Oliver Spadiut, Marko D. Mihovilovic, and Florian Rudroff. 2021. "Biocatalysis in Green and Blue: Cyanobacteria." *Trends in Biotechnology* 39 (9): 875–89. https://doi.org/10.1016/j.tibtech.2020.12.009.

Kaushik, Sharbani, and Pranab Goswami. 2018. "Bacterial Membrane Depolarization-Linked Fuel Cell Potential Burst as Signal for Selective Detection of Alcohol." *ACS Applied Materials and Interfaces* 10 (22): 18630–40. https://doi.org/10.1021/acsami.8b01838.

Kern, Suzanne E, Alexa Price-whelan, and Dianne K Newman. n.d. *Chapter 26 Extraction and Measurement of NAD (P) + and NAD (P) H*. Vol. 1149. https://doi.org/10.1007/978-1-4939-0473-0.

Kimura, Motoo. 1980. "A Simple Method for Estimating Evolutionary Rates of Base Substitutions through Comparative Studies of Nucleotide Sequences." *Journal of Molecular Evolution* 16 (2): 111–20. https://doi.org/10.1007/BF01731581.

Klanchui, Amornpan, Supapon Cheevadhanarak, Peerada Prommeenate, and Asawin Meechai. 2017. "Exploring Components of the CO2-Concentrating Mechanism in Alkaliphilic Cyanobacteria Through Genome-Based Analysis." *Computational and Structural Biotechnology Journal* 15: 340–50. https://doi.org/10.1016/j.csbj.2017.05.001.

Klüpfel, Laura, Annette Piepenbrock, Andreas Kappler, and Michael Sander. 2014. "Humic Substances as Fully Regenerable Electron Acceptors in Recurrently Anoxic Environments." *Nature Geoscience* 7 (3): 195–200. https://doi.org/10.1038/ngeo2084.

Koch, Christin, and Falk Harnisch. 2016. "What Is the Essence of Microbial Electroactivity?" *Frontiers in Microbiology* 7 (NOV): 1–5. https://doi.org/10.3389/fmicb.2016.01890.

Korak, Julie A., Eric C. Wert, and Fernando L. Rosario-Ortiz. 2015. "Evaluating Fluorescence Spectroscopy as a Tool to Characterize Cyanobacteria Intracellular Organic Matter upon Simulated Release and Oxidation in Natural Water." *Water Research* 68: 432–43. https://doi.org/10.1016/j.watres.2014.09.046.

Kretzschmar, Jörg, and Falk Harnisch. 2021. "Electrochemical Impedance Spectroscopy on Biofilm

Electrodes – Conclusive or Euphonious?" *Current Opinion in Electrochemistry* 29 (April): 100757. https://doi.org/10.1016/j.coelec.2021.100757.

Kumar, Mrinal, Mohd Golam, Abdul Quadir, Rupam Bhaduri, and Sharbani Kaushik. 2018. "Biosensors and Bioelectronics Composite Polymer Coated Magnetic Nanoparticles Based Anode Enhances Dye Degradation and Power Production in Microbial Fuel Cells." *Biosensors and Bioelectronic* 119 (July): 94–102. https://doi.org/10.1016/j.bios.2018.07.065.

Kusama, Shoko, Seiji Kojima, Ginga Shimakawa, Chikahiro Miyake, Kenya Tanaka, Yasuaki Okumura, and Shuji Nakanishi. 2021a. "A 35-Fold Enhancement in Photocurrent Generation of Synechocystis Sp. PCC 6803 by Outer Membrane Deprivation," 1–16.

Ladkau, Nadine, Andreas Schmid, and Bruno Bühler. 2014. "The Microbial Cell-Functional Unit for Energy Dependent Multistep Biocatalysis." *Current Opinion in Biotechnology* 30: 178–89. https://doi.org/10.1016/j.copbio.2014.06.003.

Lai, Bin, Hans Schneider, Jenny Tschörtner, Andreas Schmid, and Jens O. Krömer. 2021. "Technical-Scale Biophotovoltaics for Long-Term Photo-Current Generation from Synechocystis Sp. PCC6803." *Biotechnology and Bioengineering* 118 (7): 2637–48. https://doi.org/10.1002/bit.27784.

Lai, Qiliang, and Zongze Shao. 2012. "Genome Sequence of an Alkane-Degrading Bacterium, Alcanivorax Pacificus Type Strain W11-5, Isolated from Deep Sea Sediment." *Journal of Bacteriology* 194 (24): 6936–6936. https://doi.org/10.1128/JB.01845-12.

Lee, Yuan-Kun, and Hui Shen. 2004. "Chapter 3 - Basic Culturing Techniques." *Handbook of Microalgal Culture: Biotechnology and Applied Phycology*, 40–56.

Li, Feng, Yuan Xiu Li, Ying Xiu Cao, Lei Wang, Chen Guang Liu, Liang Shi, and Hao Song. 2018. "Modular Engineering to Increase Intracellular NAD(H/+) Promotes Rate of Extracellular Electron Transfer of Shewanella Oneidensis." *Nature Communications* 9 (1): 1–13. https://doi.org/10.1038/s41467-018-05995-8.

Li, Xiaomin, Tongxu Liu, Kai Wang, and T. David Waite. 2015. "Light-Induced Extracellular Electron Transport by the Marine Raphidophyte Chattonella Marina." *Environmental Science and Technology* 49 (3): 1392–99. https://doi.org/10.1021/es503511m.

Liu, Lin, and Seokheun Choi. 2021. "Enhanced Biophotoelectricity Generation in Cyanobacterial Biophotovoltaics with Intracellularly Biosynthesized Gold Nanoparticles." *Journal of Power Sources* 506 (May): 230251. https://doi.org/10.1016/j.jpowsour.2021.230251.

Liyan, Gao, Yuanya , Xiahe Huang , Haitao Ge, Zhang, Yu Kang, Kehui Liu and , Longfa Fang, and Yingchun Wang. 2014. "Profiling and Compositional Analysis of the Exoproteome of Synechocystis Sp. PCC 6803." *Journal of Metabolomics & Systems Biology* 1 (1). https://doi.org/10.13188/2329-1583.1000004.

Lu, Yue, Koichi Nishio, Shoichi Matsuda, Yuki Toshima, Hiroshi Ito, Tomohiro Konno, Kazuhiko Ishihara, Souichiro Kato, Kazuhito Hashimoto, and Shuji Nakanishi. 2014. "Regulation of the Cyanobacterial Circadian Clock by Electrochemically Controlled Extracellular Electron Transfer." *Angewandte Chemie - International Edition* 53 (8): 2208–11. https://doi.org/10.1002/anie.201309560.

Marin, Irma, and David Ruiz Arahal. 2014. *The Family Beijerinckiaceae*. *The Prokaryotes*.

Marquez, Facundo J., Ken Sasaki, Toshihide Kakizono, Naomichi Nishio, and Shiro Nagai. 1993. "Growth Characteristics of Spirulina Platensis in Mixotrophic and Heterotrophic Conditions." *Journal of Fermentation and Bioengineering* 76 (5): 408–10. https://doi.org/10.1016/0922-

338X(93)90034-6.

Marsili, Enrico, Daniel B. Baron, Indraneel D. Shikhare, Dan Coursolle, Jeffrey A. Gralnick, and Daniel R. Bond. 2008. “Shewanella Secretes Flavins That Mediate Extracellular Electron Transfer.” *Proceedings of the National Academy of Sciences of the United States of America* 105 (10): 3968–73. https://doi.org/10.1073/pnas.0710525105.

Marsili, Enrico, Janet B. Rollefson, Daniel B. Baron, Raymond M. Hozalski, and Daniel R. Bond. 2008. “Microbial Biofilm Voltammetry: Direct Electrochemical Characterization of Catalytic Electrode-Attached Biofilms.” *Applied and Environmental Microbiology* 74 (23): 7329–37. https://doi.org/10.1128/AEM.00177-08.

Marsili, Enrico, Jian Sun, and Daniel R. Bond. 2010. “Voltammetry and Growth Physiology of Geobacter Sulfurreducens Biofilms as a Function of Growth Stage and Imposed Electrode Potential.” *Electroanalysis* 22 (7–8): 865–74. https://doi.org/10.1002/elan.200800007.

McCormick, Alistair J., Paolo Bombelli, Robert W. Bradley, Rebecca Thorne, Tobias Wenzel, and Christopher J. Howe. 2015. “Biophotovoltaics: Oxygenic Photosynthetic Organisms in the World of Bioelectrochemical Systems.” *Energy and Environmental Science* 8 (4): 1092–1109. https://doi.org/10.1039/c4ee03875d.

McCormick, Alistair J., Paolo Bombelli, David J. Lea-Smith, Robert W. Bradley, Amanda M. Scott, Adrian C. Fisher, Alison G. Smith, and Christopher J. Howe. 2013. “Hydrogen Production through Oxygenic Photosynthesis Using the Cyanobacterium Synechocystis Sp. PCC 6803 in a Bio-Photoelectrolysis Cell (BPE) System.” *Energy and Environmental Science* 6 (9): 2682–90. https://doi.org/10.1039/c3ee40491a.

McCormick, Alistair J., Paolo Bombelli, Amanda M. Scott, Alexander J. Philips, Alison G. Smith, Adrian C. Fisher, and Christopher J. Howe. 2011. “Photosynthetic Biofilms in Pure Culture Harness Solar Energy in a Mediatorless Bio-Photovoltaic Cell (BPV) System.” *Energy and Environmental Science* 4 (11): 4699–4709. https://doi.org/10.1039/c1ee01965a.

Menicucci, Joseph, Haluk Beyenal, Enrico Marsili, Raajaraajan Angathevar Veluchamy, Goksel Demir, and Zbigniew Lewandowski. 2006. “Procedure for Determining Maximum Sustainable Power Generated by Microbial Fuel Cells.” *Environmental Science and Technology* 40 (3): 1062–68. https://doi.org/10.1021/es051180l.

Meyer, Julie L., Sarath P. Gunasekera, Raymond M. Scott, Valerie J. Paul, and Max Teplitski. 2016. “Microbiome Shifts and the Inhibition of Quorum Sensing by Black Band Disease Cyanobacteria.” *ISME Journal* 10 (5): 1204–16. https://doi.org/10.1038/ismej.2015.184.

Modestra, J. Annie, and S. Venkata Mohan. 2014. “Bio-Electrocatalyzed Electron Efflux in Gram Positive and Gram Negative Bacteria: An Insight into Disparity in Electron Transfer Kinetics.” *RSC Advances* 4 (64): 34045–55. https://doi.org/10.1039/c4ra03489a.

Moezelaar, Roy, Saskia M. Bijvank, and Lucas J. Stal. 1996. “Fermentation and Sulfur Reduction in the Mat-Building Cyanobacterium Microcoleus Chthonoplastes.” *Applied and Environmental Microbiology* 62 (5): 1752–58. https://doi.org/10.1128/aem.62.5.1752-1758.1996.

Monk, Paul. 2001. *Electro- Analytical*.

Mukherjee, Manisha, and Bin Cao. 2021. “Engineering Controllable Biofilms for Biotechnological Applications.” *Microbial Biotechnology* 14 (1): 74–78. https://doi.org/10.1111/1751-7915.13715.

Nair, Shailesh, Zenghu Zhang, Hongmei Li, Hanshuang Zhao, Hui Shen, Shuh-Ji Kao, Nianzhi Jiao, and Yongyu Zhang. 2022. “ Inherent Tendency of Synechococcus and Heterotrophic Bacteria for

Mutualism on Long-Term Coexistence despite Environmental Interference .” *Science Advances* 8 (39). https://doi.org/10.1126/sciadv.abf4792.

Ng, Fong Lee, Siew Moi Phang, Mitsumasa Iwamoto, Takaaki Manaka, Cheng Han Thong, Keito Shimosawa, Vengadesh Periasamy, G. Gnana Kumar, Kamran Yunus, and Adrian C. Fisher. 2020. “Algal Biophotovoltaic Devices: Surface Potential Studies.” *ACS Sustainable Chemistry and Engineering* 8 (28): 10511–20. https://doi.org/10.1021/acssuschemeng.0c02831.

Nishio, Koichi, Tunanunkul Pornpitra, Seiichiro Izawa, Taeko Nishiwaki-Ohkawa, Souichiro Kato, Kazuhito Hashimoto, and Shuji Nakanishi. 2014. “Electrochemical Detection of Circadian Redox Rhythm in Cyanobacterial Cells via Extracellular Electron Transfer.” *Plant and Cell Physiology* 56 (6): 1053–58. https://doi.org/10.1093/pcp/pcv066.

Nübel, Ulrich, Ferran Garcia-Pichel, and Gerard Muyzer. 1997. “PCR Primers to Amplify 16S RRNA Genes from Cyanobacteria.” *Applied and Environmental Microbiology* 63 (8): 3327–32. https://doi.org/10.1128/aem.63.8.3327-3332.1997.

Oliveira, Paulo, Nuno M. Martins, Marina Santos, Narciso A.S. Couto, Phillip C. Wright, and Paula Tamagnini. 2015. “The Anabaena Sp. PCC 7120 Exoproteome: Taking a Peek Outside the Box.” *Life* 5 (1): 130–63. https://doi.org/10.3390/life5010130.

Parada, José L., Gloria Zulpa De Caire, María C.Zaccaro De Mulé, and Mónica M.Storni De Cano. 1998. “Lactic Acid Bacteria Growth Promoters from Spirulina Platensis.” *International Journal of Food Microbiology* 45 (3): 225–28. https://doi.org/10.1016/S0168-1605(98)00151-2.

Parlanti, E., K. Wörz, L. Geoffroy, and M. Lamotte. 2000. “Dissolved Organic Matter Fluorescence Spectroscopy as a Tool to Estimate Biological Activity in a Coastal Zone Submitted to Anthropogenic Inputs.” *Organic Geochemistry* 31 (12): 1765–81. https://doi.org/10.1016/S0146-6380(00)00124-8.

Parveen, Bushra, Viviane Ravet, Chakib Djediat, Isabelle Mary, Catherine Quiblier, Didier Debroas, and Jean François Humbert. 2013. “Bacterial Communities Associated with Microcystis Colonies Differ from Free-Living Communities Living in the Same Ecosystem.” *Environmental Microbiology Reports* 5 (5): 716–24. https://doi.org/10.1111/1758-2229.12071.

Pavitt, Ania S., and Paul G. Tratnyek. 2019. “Electrochemical Characterization of Natural Organic Matter by Direct Voltammetry in an Aprotic Solvent.” *Environmental Science: Processes and Impacts* 21 (10): 1664–83. https://doi.org/10.1039/c9em00313d.

Penteado, Eduardo D., Carmen Maria Fernandez-Marchante, Marcelo Zaiat, Ernesto Rafael Gonzalez, and Manuel Andrés Rodrigo. 2017. “On the Effects of Ferricyanide as Cathodic Mediator on the Performance of Microbial Fuel Cells.” *Electrocatalysis* 8 (1): 59–66. https://doi.org/10.1007/s12678-016-0334-x.

Pereira, Sara, Andrea Zille, Ernesto Micheletti, Pedro Moradas-Ferreira, Roberto De Philippis, and Paula Tamagnini. 2009. “Complexity of Cyanobacterial Exopolysaccharides: Composition, Structures, Inducing Factors and Putative Genes Involved in Their Biosynthesis and Assembly.” *FEMS Microbiology Reviews* 33 (5): 917–41. https://doi.org/10.1111/j.1574-6976.2009.00183.x.

Pisciotta, John M., Yongjin Zou, and Ilia V. Baskakov. 2010. “Light-Dependent Electrogenic Activity of Cyanobacteria.” *PLoS ONE* 5 (5). https://doi.org/10.1371/journal.pone.0010821.

Porcellinis, Alice De, Niels Ulrik Frigaard, and Yumiko Sakuragi. 2017. “Determination of the Glycogen Content in Cyanobacteria.” *Journal of Visualized Experiments* 2017 (125): 1–6. https://doi.org/10.3791/56068.

Prasad, Rout Nutan, Khandual Sanghamitra, Gutierrez-Mora Antonia, Gallardo-Valdéz Juan, Rodriguez-Garay Benjamin, Ibarra-Montoya J. Luis, and Vega-Valero Guillermo. 2013. "Isolation, Identification and Germplasm Preservation of Different Native <I>Spirulina</I> Species from Western Mexico." *American Journal of Plant Sciences* 04 (12): 65–71. https://doi.org/10.4236/ajps.2013.412a2009.

Qiang, Hu, Hugo Guterman, and Amos Richmond. 1996. "Physiological Characteristics of Spirulina Platensis (Cyanobacteria) Cultured at Ultrahigh Cell Densities." *Journal of Phycology* 32 (6): 1066–73. https://doi.org/10.1111/j.0022-3646.1996.01066.x.

Quadir, Mohd Golam Abdul, Pranab Goswami, and Mrinal Kumar Sarma. 2020. "Photoelectrochemical and Photosynthetic Material-Based Biosensors." *Advanced Materials and Techniques for Biosensors and Bioanalytical Applications*, 183–210. https://doi.org/10.1201/9781003083856-9.

Rabaey, Korneel, and Willy Verstraete. 2005. "Microbial Fuel Cells: Novel Biotechnology for Energy Generation." *Trends in Biotechnology* 23 (6): 291–98. https://doi.org/10.1016/j.tibtech.2005.04.008.

Ramanan, Rishiram, Byung Hyuk Kim, Dae Hyun Cho, Hee Mock Oh, and Hee Sik Kim. 2016. "Algae-Bacteria Interactions: Evolution, Ecology and Emerging Applications." *Biotechnology Advances* 34 (1): 14–29. https://doi.org/10.1016/j.biotechadv.2015.12.003.

Rivas, Raúl, Anne Willems, Nanjappa S. Subba-Rao, Pedro F. Mateos, Frank B. Dazzo, Reiner M. Kroppenstedt, Eustoquio Martínez-Molina, Monique Gillis, and Encarna Velázquez. 2003. "Description of Devosia Neptuniae Sp. Nov. That Nodulates and Fixes Nitrogen in Symbiosis with Neptunia Natans, an Aquatic Legume from India." *Systematic and Applied Microbiology* 26 (1): 47–53. https://doi.org/10.1078/072320203322337308.

Romera-Castillo, Cristina, Hugo Sarmento, Xosé Antón Álvarez-Salgado, Josep M. Gasol, and Celia Marrasé. 2010. "Production of Chromophoric Dissolved Organic Matter by Marine Phytoplankton." *Limnology and Oceanography* 55 (1): 446–54. https://doi.org/10.4319/lo.2010.55.1.0446.

Rossi, Federico, and Roberto De Philippis. 2015. "Role of Cyanobacterial Exopolysaccharides in Phototrophic Biofilms and in Complex Microbial Mats." *Life* 5 (2): 1218–38. https://doi.org/10.3390/life5021218.

Ryabushko, Larisa, Ekaterina Miroshnichenko, Anastasia Blaginina, Armine Shiroyan, and Denis Lishaev. 2021. "Diatom and Cyanobacteria Communities on Artificial Polymer Substrates in the Crimean Coastal Waters of the Black Sea." *Marine Pollution Bulletin* 169: 112521. https://doi.org/10.1016/j.marpolbul.2021.112521.

Saar, Kadi L., Paolo Bombelli, David J. Lea-Smith, Toby Call, Eva Mari Aro, Thomas Müller, Christopher J. Howe, and Tuomas P.J. Knowles. 2018a. "Enhancing Power Density of Biophotovoltaics by Decoupling Storage and Power Delivery." *Nature Energy* 3 (1): 75–81. https://doi.org/10.1038/s41560-017-0073-0.

Saitou, N., and M. Nei. 1987. "The Neighbor-Joining Method: A New Method for Reconstructing Phylogenetic Trees." *Molecular Biology and Evolution* 4 (4): 406–25. https://doi.org/10.1093/oxfordjournals.molbev.a040454.

Saper, Gadiel, Dan Kallmann, Felipe Conzuelo, Fangyuan Zhao, Tünde N. Tóth, Varda Liveanu, Sagit Meir, et al. 2018. "Live Cyanobacteria Produce Photocurrent and Hydrogen Using Both the Respiratory and Photosynthetic Systems." *Nature Communications* 9 (1): 1–9. https://doi.org/10.1038/s41467-018-04613-x.

Sauer, Karin, Paul Stoodley, Darla M. Goeres, Luanne Hall-Stoodley, Mette Burmølle, Philip S. Stewart,

and Thomas Bjarnsholt. 2022. “The Biofilm Life Cycle: Expanding the Conceptual Model of Biofilm Formation.” *Nature Reviews Microbiology* 20 (10): 608–20. https://doi.org/10.1038/s41579-022-00767-0.

Sawa, Marin, Andrea Fantuzzi, Paolo Bombelli, Christopher J. Howe, Klaus Hellgardt, and Peter J. Nixon. 2017. “Electricity Generation from Digitally Printed Cyanobacteria.” *Nature Communications* 8 (1): 1–9. https://doi.org/10.1038/s41467-017-01084-4.

Schröder, Uwe, Falk Harnisch, and Largus T. Angenent. 2015. “Microbial Electrochemistry and Technology: Terminology and Classification.” *Energy and Environmental Science* 8 (2): 513–19. https://doi.org/10.1039/c4ee03359k.

Schuurmans, R. M., J. C.P. Matthijs, and K. J. Hellingwerf. 2017. “Transition from Exponential to Linear Photoautotrophic Growth Changes the Physiology of Synechocystis Sp. PCC 6803.” *Photosynthesis Research* 132 (1): 69–82. https://doi.org/10.1007/s11120-016-0329-8.

Sekar, Narendran, Rachit Jain, Yajun Yan, and Ramaraja P. Ramasamy. 2016. “Enhanced Photo-Bioelectrochemical Energy Conversion by Genetically Engineered Cyanobacteria.” *Biotechnology and Bioengineering* 113 (3): 675–79. https://doi.org/10.1002/bit.25829.

Sekar, Narendran, Yogeswaran Umasankar, and Ramaraja P. Ramasamy. 2014. “Photocurrent Generation by Immobilized Cyanobacteria via Direct Electron Transport in Photo-Bioelectrochemical Cells.” *Physical Chemistry Chemical Physics* 16 (17): 7862–71. https://doi.org/10.1039/c4cp00494a.

Sekar, Narendran, Jian Wang, Yan Zhou, Yi Fang, Yajun Yan, and Ramaraja P. Ramasamy. 2018. “Role of Respiratory Terminal Oxidases in the Extracellular Electron Transfer Ability of Cyanobacteria.” *Biotechnology and Bioengineering* 115 (5): 1361–66. https://doi.org/10.1002/bit.26542.

Sena, Lucia, Diego Rojas, Edie Montiel, Héctor González, Josnell Moret, and Leopoldo Naranjo. 2011. “A Strategy to Obtain Axenic Cultures of Arthrospira Spp. Cyanobacteria.” *World Journal of Microbiology and Biotechnology* 27 (5): 1045–53. https://doi.org/10.1007/s11274-010-0549-6.

Shlosberg, Yaniv, Benjamin Eichenbaum, Tünde N. Tóth, Guy Levin, Varda Liveanu, Gadi Schuster, and Noam Adir. 2021. “NADPH Performs Mediated Electron Transfer in Cyanobacterial-Driven Bio-Photoelectrochemical Cells.” *IScience* 24 (1). https://doi.org/10.1016/j.isci.2020.101892.

Stal, L J, and W E Krumbein. 1984. “Metabolism of Cyanobacteria in Anaerobic Marine Sediments.” *Actes de Colloques* 3: 301–9.

Stief, Peter, Anja Kamp, Bo Thamdrup, and Ronnie N. Glud. 2016. “Anaerobic Nitrogen Turnover by Sinking Diatom Aggregates at Varying Ambient Oxygen Levels.” *Frontiers in Microbiology* 7 (FEB): 1–11. https://doi.org/10.3389/fmicb.2016.00098.

Stuart, Rhona K., Xavier Mayali, Amy A. Boaro, Adam Zemla, R. Craig Everroad, Daniel Nilson, Peter K. Weber, et al. 2016. “Light Regimes Shape Utilization of Extracellular Organic C and N in a Cyanobacterial Biofilm.” *MBio* 7 (3): 1–14. https://doi.org/10.1128/mBio.00650-16.

Stuart, Rhona K, Xavier Mayali, Jackson Z Lee, R Craig Everroad, Mona Hwang, Brad Bebout, Peter K Weber, Jennifer Pett-ridge, and Michael P Thelen. 2014. “Cyanobacterial Recycling of the Extracellular Matrix in Microbial Mats” 1: 1–14.

Talwar, Chandni, Shekhar Nagar, Roshan Kumar, Joy Scaria, Rup Lal, and Ram Krishan Negi. 2020. “Defining the Environmental Adaptations of Genus Devosia: Insights into Its Expansive Short Peptide Transport System and Positively Selected Genes.” *Scientific Reports* 10 (1): 1–18. https://doi.org/10.1038/s41598-020-58163-8.

Tanaka, Kenya, Ginga Shimakawa, Shoko Kusama, Takashi Harada, Souichiro Kato, and Shuji Nakanishi. 2021. "Ferrihydrite Reduction by Photosynthetic Synechocystis Sp. PCC 6803 and Its Correlation With Electricity Generation." *Frontiers in Microbiology* 12 (March): 1–8. https://doi.org/10.3389/fmicb.2021.650832.

Thirumurthy, Miyuki A., Andrew Hitchcock, Angelo Cereda, Jiawei Liu, Marko S. Chavez, Bryant L. Doss, Robert Ros, et al. 2020. "Type IV Pili-Independent Photocurrent Production by the Cyanobacterium Synechocystis Sp. PCC 6803." *Frontiers in Microbiology* 11 (June): 1–11. https://doi.org/10.3389/fmicb.2020.01344.

Thorne, Rebecca J., Kenneth Schneider, Huaining Hu, and Petra J. Cameron. 2015. "Iron Reduction by the Cyanobacterium Synechocystis Sp. PCC 6803." *Bioelectrochemistry* 105: 103–9. https://doi.org/10.1016/j.bioelechem.2015.05.015.

Tschörtner, Jenny, Bin Lai, and Jens O. Krömer. 2019. "Biophotovoltaics: Green Power Generation from Sunlight and Water." *Frontiers in Microbiology* 10 (APR). https://doi.org/10.3389/fmicb.2019.00866.

Vaara, T., M. Vaara, and S. Niemela. 1979. "Two Improved Methods for Obtaining Axenic Cultures of Cyanobacteria." *Applied and Environmental Microbiology* 38 (5): 1011–14. https://doi.org/10.1128/aem.38.5.1011-1014.1979.

Vieira Lemos, Rita, Seiya Tsujimura, Pablo Ledezma, Yoshihide Tokunou, Akihiro Okamoto, and Stefano Freguia. 2021a. "Extracellular Electron Transfer by Microcystis Aeruginosa Is Solely Driven by High PH." *Bioelectrochemistry* 137. https://doi.org/10.1016/j.bioelechem.2020.107637.

Vilhauer, Laura, Judith Jervis, W. Keith Ray, and Richard F. Helm. 2014. "The Exo-Proteome and Exo-Metabolome of Nostoc Punctiforme (Cyanobacteria) in the Presence and Absence of Nitrate." *Archives of Microbiology* 196 (5): 357–67. https://doi.org/10.1007/s00203-014-0974-2.

Wang, Di, Anming Xu, Claudine Elmerich, and Luyan Z. Ma. 2017. "Biofilm Formation Enables Free-Living Nitrogen-Fixing Rhizobacteria to Fix Nitrogen under Aerobic Conditions." *ISME Journal* 11 (7): 1602–13. https://doi.org/10.1038/ismej.2017.30.

Wang, Guanghua, Kefu Yu, Yinghui Wang, Hongfei Su, Hualian Wu, Tao Li, Jiayuan Liang, Wen Huang, and Wenzhou Xiang. 2017. "Pelagibacterium Lentulum Sp. Nov., a Marine Bacterium from the Culture Broth of Picochlorum Sp. 122." *International Journal of Systematic and Evolutionary Microbiology* 67 (9): 3182–85. https://doi.org/10.1099/ijsem.0.002054.

Wang, Kai, Shikha Garg, and T. David Waite. 2017. "Redox Transformations of Iron in the Presence of Exudate from the Cyanobacterium Microcystis Aeruginosa under Conditions Typical of Natural Waters." *Environmental Science and Technology* 51 (6): 3287–97. https://doi.org/10.1021/acs.est.7b00396.

Wang, Liping, Lin Lin, and Baoxian Ye. 2006. "Electrochemical Studies of the Interaction of the Anticancer Herbal Drug Emodin with DNA." *Journal of Pharmaceutical and Biomedical Analysis* 42 (5): 625–29. https://doi.org/10.1016/j.jpba.2006.05.017.

Watson, Valerie J., and Bruce E. Logan. 2011. "Analysis of Polarization Methods for Elimination of Power Overshoot in Microbial Fuel Cells." *Electrochemistry Communications* 13 (1): 54–56. https://doi.org/10.1016/j.elecom.2010.11.011.

Weldmichael, T. G., D. Márton, B. Simon, E. Michéli, G. T. Reda, F. Adiyah, and M. Cserháti. 2021. "Bacterial Community Characterization and Microbial Respiration of Selected Arable Soils of Ethiopia." *Eurasian Soil Science* 54 (12): 1921–34. https://doi.org/10.1134/S1064229321120140.

Welkie, David G., Benjamin E. Rubin, Spencer Diamond, Rachel D. Hood, David F. Savage, and Susan S. Golden. 2019. “A Hard Day’s Night: Cyanobacteria in Diel Cycles.” *Trends in Microbiology* 27 (3): 231–42. https://doi.org/10.1016/j.tim.2018.11.002.

Wenzel, Tobias, Daniel Härtter, Paolo Bombelli, Christopher J. Howe, and Ullrich Steiner. 2018a. “Porous Translucent Electrodes Enhance Current Generation from Photosynthetic Biofilms.” *Nature Communications* 9 (1): 1–9. https://doi.org/10.1038/s41467-018-03320-x.

Wey, Laura T., Joshua M. Lawrence, Xiaolong Chen, Robert Clark, David J. Lea-Smith, Jenny Z. Zhang, and Christopher J. Howe. 2021. “A Biophotoelectrochemical Approach to Unravelling the Role of Cyanobacterial Cell Structures in Exoelectrogenesis.” *Electrochimica Acta* 395: 1–40. https://doi.org/10.1016/j.electacta.2021.139214.

Włodarska-Kowalczuk, Maria. 2014. “Large Red Cyanobacterial Mats (Spirulina Subsalsa Oersted Ex Gomont) in the Shallow Sublittoral of the Southern Baltic.” *Oceanologia* 56 (3): 661–66. https://doi.org/10.5697/oc.56-3.661.

Wohlgemuth, Roland. 2010. “Asymmetric Biocatalysis with Microbial Enzymes and Cells.” *Current Opinion in Microbiology* 13 (3): 283–92. https://doi.org/10.1016/j.mib.2010.04.001.

Wu, Yicheng, Kai Guan, Zejie Wang, Bing Xu, and Feng Zhao. 2013. “Isolation, Identification and Characterization of an Electrogenic Microalgae Strain.” *PLoS ONE* 8 (9). https://doi.org/10.1371/journal.pone.0073442.

Yagishita, Tatsuo, Takashi Horigome, and Kazuko Tanaka. 1993. “Effects of Light, CO2 and Inhibitors on the Current Output of Biofuel Cells Containing the Photosynthetic Organism Synechococcus Sp.” *Journal of Chemical Technology & Biotechnology* 56 (4): 393–99. https://doi.org/10.1002/jctb.280560411.

Yagishita, Tatsuo, Shigeki Sawayama, Ken Ichiro Tsukahara, and Tomoko Ogi. 1997. “Behavior of Glucose Degradation in Synechocystis Sp. M-203 in Bioelectrochemical Fuel Cells.” *Bioelectrochemistry and Bioenergetics* 43 (1): 177–80. https://doi.org/10.1016/S0302-4598(96)05145-8.

Yagishita, Tatsuo, Shigeki Sawayama, Kenichiro Tsukahara, and Tomoko Ogi. 1999. “Effects of Glucose Addition and Light on Current Outputs in Photosynthetic Electrochemical Cells Using Synechocystis Sp. PCC6714.” *Journal of Bioscience and Bioengineering* 88 (2): 210–14. https://doi.org/10.1016/S1389-1723(99)80204-7.

Yong, Xiao Yu, Jiao Feng, Yi Lu Chen, Dong Yan Shi, Yu Shang Xu, Jun Zhou, Shu Ya Wang, et al. 2014. “Enhancement of Bioelectricity Generation by Cofactor Manipulation in Microbial Fuel Cell.” *Biosensors and Bioelectronics* 56: 19–25. https://doi.org/10.1016/j.bios.2013.12.058.

Yongjin, Zou, John Pisciotta, R. Blake Billmyre, and Ilia V. Baskakov. 2009. “Photosynthetic Microbial Fuel Cells with Positive Light Response.” *Biotechnology and Bioengineering* 104 (5): 939–46. https://doi.org/10.1002/bit.22466.

Zhang, Jenny Z., Paolo Bombelli, Katarzyna P. Sokol, Andrea Fantuzzi, A. William Rutherford, Christopher J. Howe, and Erwin Reisner. 2018. “Photoelectrochemistry of Photosystem II in Vitro vs in Vivo.” *Journal of the American Chemical Society* 140 (1): 6–9. https://doi.org/10.1021/jacs.7b08563.

Zhang, Zenghu, Shailesh Nair, Lili Tang, Hanshuang Zhao, Zhenzhen Hu, Mingming Chen, Yao Zhang, Shuh Ji Kao, Nianzhi Jiao, and Yongyu Zhang. 2021. “Long-Term Survival of Synechococcus and Heterotrophic Bacteria without External Nutrient Supply after Changes in Their Relationship from

Antagonism to Mutualism." *MBio* 12 (4): 1–15. https://doi.org/10.1128/mBio.01614-21.

Zhou, Hui, Xin Gan, Jin Wang, Xiaoli Zhu, and Genxi Li. 2005. "Hemoglobin-Based Hydrogen Peroxide Biosensor Tuned by the Photovoltaic Effect of Nano Titanium Dioxide." *Analytical Chemistry* 77 (18): 6102–4. https://doi.org/10.1021/ac050924a.

Zhu, Huawei, Hengkai Meng, Wei Zhang, Haichun Gao, Jie Zhou, Yanping Zhang, and Yin Li. 2019. "Development of a Longevous Two-Species Biophotovoltaics with Constrained Electron Flow." *Nature Communications* 10 (1). https://doi.org/10.1038/s41467-019-12190-w.

Zhu, Lin, Anouk Zancarini, Imen Louati, Silvia De Cesare, Charlotte Duval, Kevin Tambosco, Cécile Bernard, et al. 2016. "Bacterial Communities Associated with Four Cyanobacterial Genera Display Structural and Functional Differences: Evidence from an Experimental Approach." *Frontiers in Microbiology* 7 (OCT): 1–11. https://doi.org/10.3389/fmicb.2016.01662.

Zou, Yongjin, John Pisciotta, and Ilia V. Baskakov. 2010. "Nanostructured Polypyrrole-Coated Anode for Sun-Powered Microbial Fuel Cells." *Bioelectrochemistry* 79 (1): 50–56. https://doi.org/10.1016/j.bioelechem.2009.11.001.

PUBLICATIONS AND CONFERENCES

Publications

1. Mrinal Kumar Sarma, M.G. Abdul Quadir, Rupam Bhaduri, Sharbani Kaushik, Pranab Goswami. Composite polymer coated magnetic nanoparticles based anode enhances dye degradation and power production in microbial fuel cells. Biosens Bioelectron 2018 Nov 15;119:94-102. doi: 10.1016/j.bios.2018.07.065.
2. M.G. Abdul Quadir, Pranab Goswami, Mrinal Kumar Sarma. Photoelectrochemical and Photosynthetic Material-Based Biosensors. Advanced Materials and Techniques for Biosensors and Bioanalytical Applications, Editor: Pranab Goswami, CRC Press Tailor& Francis, Boca Raton, New York, London, Page 183-210 (2020) ISBN: 9780367539658 (hbk) ISBN: 9780367539672 (pbk) ISBN: 9781003083856 (ebk).
3. Electrochemical investigations of cyanobacterial biofilms under versatile metabolic modes. (Manuscript submitted)

Conferences

1. Oral presentation " Transducing light to current: Cyanobacteria as anodic biocatalyst in biofuel cell setup" in 4th Asia Pacific - International Society of Microbial Electrochemistry and Technology (AP-ISMET) Meeting
2. Presented poster "Synechococcus pevalaki BDU140432 as potential anodic biocatalyst for biofuel cell applications" in International Conference of Young Researchers on Advanced Materials (IUMRS-ICYRAM 2016) held at IISc Bangalore from 11-15 December
3. Presented poster "Synechococcus sp BDU140432 as anodic biocatalyst on polyaniline-polypyrole copolymer coated electrodes for biofuel cell applications " in Cell Factories held at IIT Bombay from 18-20 March
4. Participated in Frontier energy research with industry academia partnership, March 2015

Workshops

1. Participated in "Integrated OMICS II" (Genomics, Proteomics, Metabolomics, Bioinformatics), National Centre for biological sciences, Bangalore. December 16-20, 2019